INTERNAL FRICTION STUDIES IN NICKEL CRYSTALS FROM 77°K-298°K

Peruvemba S. Venkatesan

Columbia University
New York, New York

10 January 1968

INTERNAL FRICTION STUDIES IN NICKEL CRYSTALS FROM 77°K - 298°K.

BY

P. S. VENKATESAN

Submitted in partial fulfillment of the requirements
for the degree of Doctor of Engineering Science
in the School of Engineering and Applied Science
Columbia University
1967

ABSTRACT

INTERNAL FRICTION STUDIES IN NICKEL CRYSTALS FROM 77°K - 298°K.

by

Peruvemba Swaminatha Venkatesan

The internal friction spectrum in nickel single crystals has been studied near 20 kHz from 77°K to 298°K as a function of the stages of deformation, crystal orientation, temperature of deformation, magnetic field and state of annealing. Plastic deformation produces two major peaks centered at 230°K (peak X) and 130°K (peak Y). Peak X grows throughout stages I and II and falls in stage III. Peak Y occurs only in stage III. The height of peak X when plotted against the flow stress resolved on the primary glide system is approximately a straight line in each of stages I and II, with the slope in stage I probably higher than the slope in stage II. The variation in the height of peak X with crystal orientation is consistent with the hypothesis that dislocations in the primary glide system are responsible for it. Peak Y shows a different dependence, for which there is no immediate explanation. Isochronal annealing (1/2 hour) in steps of 100°C showed two recovery stages, one between 25°C and 100°C, and the other between 320°C and 430°C. Peak X is not removed till recrystallization and peak Y is removed between 320°C and 430°C.

TABLE OF CONTENTS

I. INTRODUCTION

In 1949 Bordoni[1] observed that a large peak in the graph of internal friction against temperature occurs at low temperatures in plastically deformed copper and other f.c.c. metals. Since then this peak, commonly named after its first observer, has been studied extensively. The interest in such studies stems from the generally accepted belief that this peak arises from the thermally activated displacement of dislocations in the crystal lattice and that such experiments may permit a determination of the Peierls potential[2] or other fundamental quantities related to dislocation motion. Some of the theories that have been proposed to explain the nature of this peak are given in Appendix A. A recent study of polycrystalline nickel by A. W. Sommer[3,4] gave results which were not in agreement with some of the conclusions reached by previous workers using other f.c.c. metals. The present work is a further investigation of these disagreements in high purity nickel crystals after carefully controlled plastic deformation.

The experimental work done in this area prior to 1963 has been reviewed by Niblett[5] who summarizes the principal results of these investigations and gives eight criteria for a Bordoni peak:

(a) Measurements on single crystals and polycrystalline specimens are substantially similar.

(b) The Bordoni peak is not observed in fully annealed specimens but appears as a result of cold work.

(c) The height of the peak increases rapidly with increasing amount of cold work for deformation up to about 3% but for greater deformations it remains fairly constant.

(d) The height of the peak is reduced by the presence of impurities.

(e) The temperature at which the peak occurs increases when the frequency of vibration is increased.

(f) The temperature at which the peak occurs is not strongly affected by either the amount of cold work or the impurity content of the material.

(g) The height of the peak and the temperature at which it occurs are almost independent of the amplitude of vibrations.

(h) In addition to the main Bordoni peak, a smaller subsidiary peak (Niblett-Wilks peak) is usually observed at a lower temperature. This peak appears to be closely related to the Bordoni peak.

These specifications apply generally to f.c.c. metals[6,7,8,9] at low deformation levels. But recent studies on the deformation behaviour of polycrystalline nickel[3,4] and silver single crystals[10] among f.c.c. metals and Ta, Mo and W among b.c.c. metals[5] indicated that the peak height when plotted against

the amount of deformation does not obey criterion (c) but goes through a maximum and decreases. Furtner in nickel, large peak shifts with deformation were observed in contrast to criterion (f). In the light of these observations the criteria (c) and (f) given by Niblett[5] need to be altered.

The previous work[4] in polycrystalline nickel reported two major peaks centered at -20 C (peak X) and -140 C (peak Y) which were identified as the Bordoni peak and the Niblett-Wilks peak respectively. Chambers[11] expressed doubts about this interpretation on the basis of an empirical plot of W_B versus Gb^3 for the Bordoni peak in f.c.c. metals, where W_B is the activation energy for the Bordoni peak, G the shear modulus and b the burgers vector. He found peak Y on a line determined by the Bordoni peaks in other f.c.c. metals, while peak X was close to a grouping of b.c.c. metals.

There was a complementary relation between the peaks X and Y in nickel which is not found in any other f.c.c. metal. Peak X was present only in light to moderately deformed (tensile flow stress $\sigma_f < 17$ Kg/mm^2) nickel which showed little peak Y and was absent in heavily deformed nickel ($\sigma_f > 17$ Kg/mm^2) where peak Y was prominent. The height of peak X when plotted as a function of flow stress showed a maximum at $\sigma_f = 10$ Kg/mm^2 and then decreased to zero. The position of peak X shifted

to lower temperatures by as much as 70° C with deformation. Peak Y was present only in heavily deformed nickel ($\sigma_f > 13$ Kg/mm^2) and its height reached a constant saturation value with increasing tensile stress. The temperature of this peak was fairly constant with deformation.

Values of activation parameters for these two peaks were obtained from a study of the shifts in peak temperature when the frequency was changed from the kHz range to MHz range. Peak Y was found to split into 2 peaks in the MHz range. The values were found as below:-

	Q ev/atom	$-\log_{10} 2\pi\tau_o$
Peak X	.4	11.7
Peak Y	.16, .22	12, 11.1

where Q = activation energy and $\frac{1}{2\pi\tau_o}$ = attempt frequency.

The following questions remained unanswered:

1. Is either of the peaks X or Y associated with grain boundaries?
2. Can one observe such large peak shifts in a single crystal?
3. How do the heights of peaks X and Y vary with (a) the stages of deformation of a single crystal? (b) deformation temperature? (c) the crystal orientation?

Questions (1) and (2) are related to Niblett's criteria of the Bordoni peak and need clarification in nickel. Question (3) does not pertain to Niblett's criteria but is of fundamental

significance in understanding the nature of these relaxation peaks. The present study was undertaken partly to find answers to the above questions.

OBJECTIVES OF THE PRESENT WORK:

The major part of this work is a study of peaks X and Y in nickel crystals of different orientations following controlled deformation in the various stages of strain hardening (stages of strain hardening is described in Appendix B). The heights and positions of peaks X and Y were determined as a function of τ, the resolved shear stress on the primary glide system to see (a) whether the curve of the height of peak X versus resolved shear stress goes through a maximum and if so, at what stage does the peak height grow to its maximum and at what stage does it start decreasing? (b) at what stage of strain hardening does peak Y appear? (c) how do the temperatures of peaks X and Y shift with deformation?

The orientation dependence of peak X is of particular interest to see whether its height is in anyway related to the hypothesis[12] that dislocations in the primary slip system are responsible for it.

The effect of temperature of deformation on the peaks X and Y was studied by observing the variation of the peak heights with resolved shear stress in two crystals of the

same orientation, one deformed at room temperature and the other at liquid nitrogen temperature.

Isochronal annealing ($\frac{1}{2}$ hour) to a temperature of 510° C in steps of 100° C was done on a deformed crystal which showed both peaks X and Y to study the effect of recovery on the peak heights and the resonant frequency profiles.

II. EXPERIMENTAL PROCEDURE

A. MEASUREMENT TECHNIQUES:

Internal friction measurements were made in the kiloHertz frequency range in the temperature interval 77° K to 298° K using a resonant bar technique. A schematic of the specimen used for these measurements is shown in Fig. 3(a). The lay out of the apparatus is shown in Fig. 1., and the equivalent detection circuit shown in Fig. 2. The apparatus is described below.[13]

1. SPECIMEN EXCITATION:

The specimen is excited into longitudinal oscillation by means of an electromagnet.[13,14,15,16] The windings on one leg of the electromagnet are connected to the A.C. drive voltage obtained after amplification of the sinusoidal voltage output of an oscillator. The frequency at the oscillator output is measured by means of an electronic counter. The A.C. drive voltage across the windings is measured by means of a voltmeter. The D.C. voltage from a 12 volt battery is connected to the windings on the other leg of the magnet. The purpose of this D.C. field is to increase the driving force many times over that produced by an unaided A.C. field.[17] The magnet can be raised or lowered from outside the evacuated specimen chamber to position it at the optimum distance from the top of the specimen.

2. GRIPPING DEVICE:

The specimen is gripped at its center by means of steel pins mounted in oversized holes by means of soft solder. This is found to decouple the specimen adequately from the support rods.

3. DETECTION:

The end of the specimen opposite the magnet along with another plate forms a capacitor. A D.C. voltage is applied across this capacitor and small variations in its gap caused by specimen vibration produce an A.C. voltage of the same frequency as that of the vibrating specimen superposed on the D.C. voltage. The D.C. voltage is blocked by means of a capacitor and the A.C. voltage is amplified and read on a voltmeter and/or oscilloscope. The RMS value of this voltage VO_1 can be shown[13] to be proportional to the amplitude of vibration of the specimen and given by the following expression:

$$VO_1 = BV_{DC} \frac{\omega K' A Z_1}{\sqrt{2}} \frac{\delta d_o}{d_c}_2 \qquad (1)$$

where B = amplification of signal

V_{DC} = the D.C. voltage applied to the pickup capacitor.

ω = circular frequency

K' = dielectric constant of vacuum

A = area of the capacitance plate

Z_i = impedance faced by the generated voltage including the grid leak resistance of the amplifier.

δd_o = amplitude of vibration of the specimen or the change in the gap of the pickup capacitor.

d_o = gap width of the pickup capacitor.

This expression can be rewritten in terms of the strain amplitude when the following substitutions are made:

$$\varepsilon_o = 2\frac{\delta d_o}{L} \qquad \text{where L = length of the specimen}$$

$$\varepsilon_o = \frac{2\sqrt{2}\, d_o^2 VO_1}{\gamma V_{DC} L} \qquad \text{and } \gamma = BZ_i K' A\omega \qquad (2)$$

In this expression γ is constant for any specific set up and determined by the following calibration procedure.

A known A.C. signal from the oscillator-power amplifier is connected across the pickup capacitor and the output VO_2 measured. It is given by $VO_2 = BV_{ac}\frac{Z_i}{Z_i+X_c}$ (see Fig. 2.)

Making substitutions for X_c we get $VO_2 = \frac{\gamma V_{ac}}{d_o}$

Allowing for any stray capacitance couplings we can rewrite

$$VO_2 = \left(\frac{\gamma}{d_o} + \beta\right) V_{ac}$$

The constants γ, β are determined by measuring VO_2 at different values of d_o for a certain known input signal V_{ac}. The gap width can then be determined at any temperature by measuring

VO_2 and V_{ac}. The strain amplitude is then obtained using the formula (2).

4. MEASUREMENT OF DECREMENT:

The logarithmic decrement is directly related to the width of the resonance response curve[18] when the specimen damping is independent of strain amplitude. It is given by the relation:

$$\Delta = \pi \frac{(\omega_2 - \omega_1)}{\omega_r}$$

where ω_r = resonant frequency, Δ = log decrement

$\omega_2 - \omega_1$ = width of the resonant response curve, where ω_2 and ω_1 refer to frequencies at .707 x maximum amplitude.

To measure the damping at high strain amplitudes, we use the relation[18] that in a specimen vibrating at resonance, the amplitude of vibration is directly proportional to the driving force and inversely proportional to the damping.

$$\Delta = \frac{CF}{\epsilon_o}$$

The constant C is determined by measuring Δ, drive voltage V_D, and VO_1 at a low level of strain amplitude. Once C is known, Δ at any high strain amplitudes is obtained by measuring VO_1 and V_D'

5. EXTERNAL MAGNETIC FIELD:

A solenoid to give a maximum magnetic field of 300 oersteds parallel to the specimen axis is wound around the

outside of the specimen chamber. This was calibrated by means of a differential gaussmeter.

B. SPECIMEN MATERIAL AND SINGLE CRYSTAL GROWTH:

Ni 270 was obtained from the International Nickel Co. in the form of 1/2" rods. It contains 99.7% Ni, .005% C, and traces of Mn, Fe, Cu, Cr, S, Si, Mg, Ti, and Co. These were annealed in evacuated quartz capsules at 800°C, swaged into .23 inch diameter rods, approximately 18 inches long, and then electron-beam zone-refined by 4 passes at 10^{-6} mm Hg vacuum, at a speed of 2" per hour. Crystals with random orientations were grown from this rod. A few crystals corresponding to easy glide orientation were grown using seed crystals supplied by M.R.C. Corp., Orangeburg, New York. Chemical analysis of zone refined Ni 270 was found by Sommer[3] to be similar to Wesley's nickel,[19] and the electrical resistivity ratio was determined to be $\frac{R_{298°K}}{R_{4.2°K}} = 600$.

1. PREPARATION OF CRYSTAL SPECIMEN AND ELECTRON BEAM WELDING OF GRIPS:

Fig. 3(a) shows the single crystal specimen with welded polycrystalline grips that is used for the present investigation. Grips were necessary in order to deform the crystal to different stages of deformation and subsequently obtain damping measurements. Appendix D gives a theoretical justification

for the use of such a specimen configuration.

The crystals as grown showed nonuniformity in the diameter. These were ground in a bench post tool grinder, taking .0005" of radius at a time and allowing enough time between grindings to avoid any heating of the specimen. Surface preparation of one crystal to achieve a uniform diameter took about 20 hours. The ends were ground after mounting the crystal in Wood's metal. These were then etched in a solution of 40% acetic acid, 40% nitric acid and 20% water to remove 4 mils of the radius. Back reflection Laue photographs were taken to determine the orientation. There was no asterism seen in the patterns indicating no surface deformation after etching. The crystals were vacuum annealed in quartz capsules by slowly heating to a temperature of 800°C and holding it for 2 hours and subsequent slow cooling. Subsequent etching and Laue patterns indicated they were still single crystals of the same orientation.

The grips, made of polycrystalline Ni 270 were then electron-beam-welded to the crystals. The crystals with the grips were vacuum annealed at 800° C, etched and chemically polished in a solution consisting of

50 ml glacial acetic acid

30 ml nitric acid

10 ml phosphoric acid and

10 ml sulfuric acid

C. DEFORMATION OF SINGLE CRYSTALS:

The crystals were deformed in an Instron tensile testing machine. The deformation was done intermittently in that after a crystal was stressed to a certain stress representative of stage I (Fig. 3 (b)), it was unloaded and damping measurements taken. The crystal was then reloaded and the above procedure was repeated for representative points in stages of deformation of the stress-strain curve.

Knowing the cross-sectional area, gauge length, orientation of the crystal and the load-extension curve, the curve of resolved shear stress versus resolved shear strain can be plotted[20] as in Fig. 4. After various amounts of deformation the slip bands on the surface were observed by optical microscopy.

III. EXPERIMENTAL RESULTS

We shall consider first the results of plastic deformation in nickel crystals of different orientations following which the results of damping measurements in each crystal are given.

A. RESULTS OF PLASTIC DEFORMATION:

Figures 4(a) and 4(b) show for each crystal, the orientation and the curve of resolved shear stress versus resolved shear strain. The various strain hardening parameters defined in Fig. 3(b) are given in Table I. These results are in general agreement with those obtained by Haasen[28] for nickel crystals and the stress strain curves in Figs. 4(a) and 4(b) show behaviour similar to other F.C.C. crystals.[22]

Crystals 5, 11, 13, 14 and 18 were deformed at room temperature with halts to make damping measurements. Crystal 16 was deformed at liquid nitrogen temperature in a similar manner. Crystal 17 was strained continuously at liquid nitrogen temperature to the same terminal flow stress in stage III as that of crystal 16 and then the internal friction measurement taken. The strain rate used varied between 2×10^{-3} and $.5\times10^{-3}$ due to different gauge lengths of crystals. The cross-head speed was constant for all the crystals and equalled .002 inches per minute.

B. RESULTS OF DAMPING MEASUREMENTS:

1. OBSERVATIONS IN CRYSTAL NO. 5

The orientation of this crystal is near the (100) pole and stage III shows a strong dynamic recovery (Fig. 4(a)).

a. Variation of peaks X and Y with deformation:

Fig. 5 shows the anelastic behaviour of an annealed crystal and after deformation to a resolved shear stress = 1.1 Kg/mm^2. Most of the high background damping observed can be eliminated by the application of a magnetic field of 200 Oe and is attributable to magnetic domain wall motion. If the solenoid is not perfectly aligned, the application of a magnetic field places a force on the specimen which deforms the soft crystal in the vicinity of the pins, thereby loosening them and making it quite difficult to obtain damping measurements. Curve B (Fig. 5) shows a small peak X superposed on a large background damping. No peak Y is observed. Fig. 6 (curve A) shows peak X is fully developed after deformation to the end of stage II (= 4.8 Kg/mm^2). Curves B, C and D (Fig. 6) show the decay of peak X and rise of peak Y after deformation in stage III corresponding to τ = 6.7, 7.8, and 8.8 Kg/mm^2 respectively. Fig. 7 gives the resonant frequency profiles corresponding to Fig. 6. Fig. 8 summarizes the variation of heights of peaks X and Y with resolved shear stress. Table III gives the temperatures T_X and T_y for peaks X and Y for various values of τ.

The temperature at which peak X appears shifts from -20° C to -40° C with increasing deformation from $\tau = 4.8$ to 7.8 Kg/mm^2 and then rises to -30° C at $\tau = 8.8$ Kg/mm^2 (Fig. 6). The temperature of peak Y shifts from -150 to -135° C.

The ratio of modulus defect/ 2 peak height is greater than 1 indicating that both peaks X and Y are broader than a single relaxation.

b. Slip line observations:

An electron-microscopic study of slip line patterns in deformed Ni crystals has been undertaken by J.P. Guth.[23] Low magnification pictures of slip lines were taken during this study. The main observation pertains to the appearance of slip bands and fragmented slip line bundles in stage III whereby segments of slip bands on the primary slip plane are interlinked with slip lines on the cross slip system. Though this interlinking is most predominant in stage III, the same occurs to a less extent in stage II. Similar observations by others[24,25,26] have been interpreted to mean that stage III begins when the applied stress has reached a level sufficient to allow dislocations to cross slip around obstacles in their path.[26,27]

c. Effects due to recovery annealing:

Successive runs on 2 single crystals demonstrated that the heights and positions of peaks X and Y are retained indefinitely at room temperature. Recovery studies at higher temperatures were carried out isochronally up to 510° C. Figs. 9, 10 and 11 are a summary of the results obtained after a series of 30 minute anneals. There is a major reduction in the heights of peaks X and Y after the anneal at 100° C. Peak Y anneals out between 320 and 430° C, after which peak X starts to grow and shifts to higher temperatures.

The modulus defect, as determined from resonant frequency profiles, decreases during the reduction in peak heights of X and Y upto 320° C and then increases on further annealing at higher temperatures.

2. OBSERVATIONS IN CRYSTAL NO. 11:

Fig. 12 (curves A, A') shows the damping and resonant frequency profiles for the annealed crystal with and without a saturating magnetic field. The following points are immediately apparent. First a large positive magnetic damping component (defined as log dec(H=0)-log dec(H=200)) exists at all temperatures. The effect of the magnetic field application on a demagnetized and annealed nickel crystal at 22 kHz is to cause a monotonous decrease in log.dec to saturation

and a corresponding increase in ν_r. Second a correspondingly large change in ν_r occurs with the magnetic field application indicating that the specimen is stiffer at saturation than at zero field. This behavior is known as the "ΔE" effect (defined quantitatively here as $\nu_r(H = 200\ Oe) - \nu_r(H = 0)$).

a. Effects of cold work on the "ΔE" effect and magnetic damping components:

Fig. 12 (curve B) shows the internal friction data after a resolved shear stress $\tau = 1.3\ Kg/mm^2$. It is apparent that the magnetic damping has reduced considerably in comparison to the annealed crystal. In contrast to the "ΔE" effect which merely decreases with increasing cold work, the magnetic damping component decreases sharply with cold work. We also see that the application of a magnetic field merely changes the background damping and that there are no large effects on the peak heights or their temperatures (Figs. 13 and 15).

b. Variation of peak heights with deformation:

Figs. 12, 13 and 14 show the damping and resonant frequency profiles after the crystal is deformed to various values of resolved shear stresses. Fig. 16 summarizes the variation of heights of peaks X and Y with τ. The peak heights could not be determined accurately when less than $5x10^{-4}$ because for $\Delta_X \leq 5x10^{-4}$ at low flow stresses the magnetic background is large and for $\Delta_y \leq 5x10^{-4}$ the tail of peak X is large. There was less difficulty with small Δ_X at high τ. As in crystal 5, we see peak X appears small during stage I, grows to a maximum

during stage II and drops during stage III. Peak Y appears near the start of stage III. It is observed that peak X in crystal 11 is much larger and peak Y smaller than in crystal 5.

c. Justification for specimen configuration:

As seen from Fig. 3(a), the specimen used in all internal friction measurements has polycrystalline grips welded to the single crystal. In order to be sure that almost all of the damping comes from the single crystal portion of the specimen, internal friction data was taken with the sample with and without the polycrystalline grips. The results are shown in Fig. 17. It can be seen that the damping profiles are similar except for a shift in peak temperatures which is due to the higher resonant frequency of the crystal without the grips.

3. OBSERVATIONS IN CRYSTALS 16, 17, 18:

All these crystals have the same orientation.

a. Correlation of the heights of peaks X and Y with the deformation stages in crystal 16:

Figs. 18, 19 and 20 show the damping and resonant frequency profiles at various values of τ. As in crystals 5, 11, 13 and 14 peak X is small in stage I, reaches a maximum at the end of stage II and drops during stage III. Peak Y appears near the start of stage III.

b. Effect of interrupted testing on damping measurements:

As stated before, the deformation of crystal 16 was

carried out at liquid nitrogen temperature to a certain resolved shear stress, the crystal warmed to room temperature and the internal friction data taken subsequently. By this interrupted method the entire stress-strain curve was covered. To study the recovery that takes place at room temperature by this interrupted procedure, another crystal 17 was pulled continuously at liquid nitrogen temperature to a resolved shear stress $\tau = 9.13$ Kg/mm^2 which is the same as the terminal stress of crystal 16. Damping and resonant frequency profiles were measured on this and compared with that of crystal 16. The results are shown in Fig. 22. It is seen that the warm up of crystal 16 to room temperature had little effect on the damping.

c. Effect of deformation temperature on heights of peaks X and Y:

Crystal 18 which has the same orientation as 16 and 17 was deformed at room temperature and the internal friction spectrum studied at various resolved shear stress levels. The results are shown in Figs. 23, 24 and 25. It is apparent as in crystal 16, peak X is small in stage I, is large at the end of stage II and decreases in stage III. Peak Y appears only in stage III. Comparing Figs. 25 and 21 we see peak Y in crystal 18 is much larger than in crystal 16. This shows that the peak Y is strongly affected by the temperature of deformation.

4. OBSERVATIONS IN CRYSTAL 13:

a. Variation of peaks X and Y with deformation in crystal 13:

Figs. 26, 27, 28 and 29 show the damping and resonant frequency profiles after the crystal is deformed to various values of resolved shear stresses. It is seen the temperature of peak X shifts from -12° C to -52° C for deformation up to $\tau = 6$ Kg/mm^2 and then increases to -40° C when $\tau = 7.3$ Kg/mm^2. The temperature of peak Y is fairly constant. Fig. 30 summarizes the variation of heights of peaks X and Y with τ.

5. OBSERVATIONS IN CRYSTAL 14:

a. Variation of peaks X and Y with deformation in crystal 14:

Figs. 31, 32, 33 and 34 give the internal friction data in crystal 14 after deformation to various values of τ. The temperature of peak X shifts from -20° C to -32° C as τ is first increased from 1 to 5 Kg/mm^2 and then rises to -18° C when τ is further increased from 5 to 8 Kg/mm^2. The temperature of peak Y is fairly constant. Peak Y appears near the start of stage III when peak X drops. Fig. 35 gives the summary of variation of the heights of peaks X and Y with τ.

IV. DISCUSSION OF RESULTS

The significant results of this work are, first those on plastic deformation, because relatively little work has been done on deformation of nickel single crystals, and second, the observations of the damping spectrum during changes in plastic deformation. The discussion will take up in turn (A) the work hardening curves of nickel single crystals; (B) the phenomenological characterization of peak X; (C) the phenomenological characterization of peak Y; both (B) and (C) in terms of (1) effect of deformation, (2) annealing, (3) peak temperature shift with deformation, (4) strain amplitude dependence, (5) application of a saturating magnetic field, (6) deformation temperature, (7) crystal orientation, (8) activation energy; and (D) comparison of the results with predictions of current theories (Appendix A) of deformation induced damping peaks.

A. WORK HARDENING OF NICKEL CRYSTALS

Figs. 4(a) and 4(b) show the work hardening curves for crystals of orientations given in the stereographic triangle. Table I lists the work hardening parameters defined in Fig. 3(b). Our crystals do not show a discontinuity of the work hardening rate in stage II and give larger values for a_{II}, a_{III}, τ_o, τ_{II}, and τ_{III}, than those reported by Mader et al [21]. The

work hardening parameters obtained in the present investigation are similar to the ones reported by Haasen.[28]

A number of points previously known for other f.c.c. metals[22] are now confirmed for nickel. These include the variation of a_{II}, θ_{II} and of dynamic recovery with crystal orientation and temperature of deformation. The variation of a_{II} with crystal orientation and temperature of deformation is similar to those reported for other f.c.c. metals.[22] Crystals 5 and 14 near the (100) pole and 11 near the (111) pole of the stereographic triangle show an appreciably higher value for θ_{II} than those for crystals 13, 16, 17 and 18 closer to (110). This is consistent with the observations of Rosi[29] and Diehl[30] on the rates of hardening for copper crystals in stage II. Crystals 5 and 14 near the (100) pole show a larger dynamic recovery than the other crystals. Similar observations have been made in aluminium crystals by Lange and Lücke.[31] This indicates that in nickel crystals the orientation dependence of dynamic recovery in stage III is different from that of stage I and stage II strain hardening.

The ratio of θ_{II} in crystal 16 and 18 due to change in deformation temperature from 77° K to 298° K is equal to 1.08 and is approximately the same as that of the elastic modulii at these temperatures (1.07). This is consistent with the

findings of Diehl and Berner[32]. Comparison of curves for crystal 16 deformed at 77° K and 18 at 298° K (Fig. 4(a)) shows that with rising temperature the stress for the onset of stage III drops and the amount of dynamic recovery increases. This is observed in other f.c.c. crystals[22].

B. PHENOMENOLOGICAL CHARACTERIZATION OF PEAK X.

1. Effect of deformation

Peak X is absent in annealed crystals with no static stress applied, and is introduced and augmented by deformation. The height of peak X denoted by Δ_X, shows a maximum and not saturation when plotted against τ, confirming Sommer's results[4] in polycrystals. We also observe that the maximum height of peak X is reached at the end of stage II i.e. $\frac{d\,\Delta_X}{d\tau} = 0$ and the peak height drops in stage III i.e. $\frac{d\,\Delta_X}{d\tau} < 0$. The width of peak X is nearly a constant during stages I and II and decreases during stage III.

2. Annealing behaviour of peak X.

The isochronal annealing behaviour of peak X is shown in Figs. 9, 10, and 11. It is seen that the height of peak X first decreases and then rises and is not removed until full recrystallization takes place. We observe that the simultaneous decrease in peak height and temperature on low temperature

annealing up to 320° C are similar to the observation mentioned for the Bordoni peak in copper by Mecs and Nowick.[33] The large loss in peak height after 30 minutes at 100° C can be related to the low temperature recovery stage III reported by Clarebrough et al[34], Sosin and Brinkman[35], and Wuttig and Birnbaum[36]. Although the former two authors observed a recovery stage at 270° C, the peaks X and Y underwent no significant change during isochronal annealing near this temperature.

We believe the decrease in the height of peak X upto 320° C is due to the pinning of dislocations by point defects migrating in recovery stages III and IV in nickel because this drop is accompanied by an increase in resonant frequency; if both the in-phase and out-of-phase components of the dislocation strain are smaller, then less dislocation motion is occurring. The rise of the height of peak X, accompanied by a drop in ν_r on annealing at higher temperatures (450° C and 510° C), implies that more dislocation motion is taking place. A similar observation has been made for the Bordoni peak in copper[37,38]. We attribute the increased motion to depinning of dislocations and/or dislocation rearrangement during stages of recovery.

3. Shift in temperature of peak X.

Table III lists the temperature of peak X for various values of τ. For crystal 13, for example, it is seen that the temperature of peak X (i) first decreases from -12° C to -52° C when τ is increased from .93 to 6 Kg/mm^2 and (ii) then rises to -40° C when τ is further raised to 7.3 Kg/mm^2. The latter rise may be due to a reduction in the internal stress due to dynamic recovery in stage III of deformation of the crystal. A similar behaviour is exhibited by other crystals. Sommer observed at 30 kHz a shift in the temperature of peak X from -6° C to -65° C as the flow stress was increased from 5.3 Kg/mm^2 (8000 psi) to 20.7 Kg/mm^2 (31000 psi) which is a larger shift than we observed in single crystals.

4. Dependence of peak X on strain amplitude and magnetic field.

A variation of strain amplitude by a factor of 20 from 1.5×10^{-7} to 3×10^{-6} does not affect the resonant frequency or damping profiles as seen in Figs. 6 and 7. Alefeld[39] pointed out that the amplitude dependence of the Bordoni peak is not expected for strain amplitudes smaller than 10^{-5}.

It is seen from Fig. 15 that the height and position of peak X is relatively insensitive to the application of a saturating magnetic field of 200 Oe. The effect of the field is to reduce the background damping and the maximum of

the peak but the height of the peak measured with reference to the background remains the same.

5. Effect of deformation temperature on peak X.

As seen in Figs. 21 and 25, there is no marked effect on the height of peak X by changing the deformation temperature from 77° K to 298° K. The maximum height of peak X is larger in the sample deformed at 77° K only to the extent that the flow stress is affected by the deformation temperature.

The temperature of peak T_x seems at a lower value in crystal 18 deformed at 298° K compared to that in crystal 16 deformed at 77° K. It is also observed that the width of peak X in crystal 18 is larger than in crystal 16.

6. Effect of crystal orientation on peak X.

To compare the results of the variation of Δ_x with τ in different crystals it is necessary to have a hypothesis concerning the origin of the peak. The hypothesis advanced here is that peak X arises from the motion of dislocations belonging to the primary slip system. It is then necessary to take into account that (1) the alternating applied stress (measuring stress) gives rise to different resolved shear stresses in differently oriented crystals (2) the dislocation strain is different in different crystals and (3) Young's

modulus along the axis of the crystal is different for different orientations. Appendix E considers these factors and in order to compare the variation of log. dec. with τ in crystals of different orientations, it is necessary to divide log. dec. by $E \sin^2\chi_o \cos^2\lambda_o$ where χ_o is the angle between the tensile axis and the slip plane and λ_o the angle between the tensile axis and the slip direction. Table II gives the values of $E \sin^2\chi_o \cos^2\lambda_o$ for the crystals of various orientations and Fig. 36 is a plot of $\frac{\Delta_x}{E \sin^2\chi_o \cos^2\lambda_o}$ versus τ for values of τ to the end of stage II. A single curve represents the points for all crystals fairly well, consistent with the hypothesis that dislocations on the primary slip plane are responsible for peak X. The curve in Fig. 36 is adequately described as two straight lines through stages I and II. It indicates that the rate of change of the height of peak X with τ in stage I is at least equal to and possibly greater than that in stage II. These results may be summarized symbolically $\left.\frac{d\Delta_x}{d\tau}\right|_I = K_1 \geq \left.\frac{d\Delta_x}{d\tau}\right|_{II} = K_2 > 0$

7. Activation energy for peak X.

The 10° shift in the temperature of peak X (Fig. 17) is somewhat lower than the shift of 15° predicted from the

activation energy of 0.4 e.v. reported by Sommer[3] for the peak in polycrystalline nickel, implying an activation energy $Q \geq .4$ e.v. The value of the frequency factor obtained from Fig. 17 is unreasonable ($-\log_{10} 2\pi\tau_o = 15.7$) and larger than the value reported by Sommer, ($-\log_{10} 2\pi\tau_o = 11.7$). This could be due to the large error (± 20°C) in measuring the peak temperature but there may also be an effect of the grips entering here. If so, the contribution from material within the grips did not affect the peak temperature more than ±2°C or the peak height by more than 5%.

C. PHENOMENOLOGICAL CHARACTERIZATION OF PEAK Y.

1. Effect of deformation.

Peak Y is present near the start of stage III of deformation of a single crystal (Figs. 8, 25, 30, 35) when peak X starts to drop. With increasing deformation this peak increases in height (Figs. 21, 35). There is no obvious correlation between the rate of fall of peak X and the rate of rise of peak Y in crystals of different orientations.

2. Annealing behavior.

Figs. 9 and 10 show the isochronal annealing behavior of peak Y. The large loss of peak height and increase in ν_r after annealing at 100°C for 30 minutes is believed to be caused by defects migrating in recovery stage III. The peak underwent no significant change around 270°C, the temperature reported by Clarebrough et al[34], and Sosin and Brinkman[35] for recovery stage IV in nickel. The peak is removed around 375°C,

when peak X begins its regrowth. It is interesting to point out here that Sommer[3] observed in polycrystalline nickel that the annealing behaviour of peak Y was found to depend on the amount of prior deformation, the larger the prior deformation, the more refractory was the peak to annealing at recovery temperatures.

3. Shift in peak temperature with τ.

Table III lists the peak temperature at various values of τ for all crystals. It can be seen that the peak temperature is approximately a constant and there is no obvious correlation between τ and the slight shift in the peak temperature.

4. Dependence on strain amplitude and magnetic field.

As in the case of peak X, a variation of strain amplitude by a factor of 20 does not affect the resonant frequency or damping profiles as seen in Figs. 6 and 7. Fig. 15 shows that the relative height and position of peak Y is unaffected by the application of a saturating magnetic field of 200 Oe. The precision in peak temperature measurement is $\pm$ 2° C and in the peak height $\pm$ 5%.

5. Effect of deformation temperature.

Figs. 21 and 25 show the variation of peak Y with τ in crystals of the same orientation deformed at liquid nitrogen and room temperature respectively. It is apparent that

the height of peak Y in crystal 18 deformed at room temperature is almost twice that in crystal 16 deformed at liquid nitrogen temperature. Since peak Y occurs only in stage III and stage III is thermally activated it is reasonable to conclude that the strong dependence of the height of peak Y on the deformation temperature is related to the dependence of stage III on the deformation temperature.

6. Effect of crystal orientation.

There is no obvious correlation between the heights of peak Y and crystal orientations.

7. Activation energy.

The 10^{o} shift in the temperature of peak Y (Fig. 17) is consistent with the shift of 12^{o} estimated from the average activation energy of .19 e.. reported by Sommer[3] for the peak in polycrystalline nickel.

D. A COMPARISON OF THE PROPERTIES OF PEAKS X AND Y WITH CURRENT THEORIES OF DEFORMATION INDUCED DAMPING PEAKS

1. Peak X.

Before discussing which of the theories listed in Appendix A describes peak X the best, we shall enumerate some of the important experimental results related to peak X. Peak X in nickel single crystals obeys the Niblett's criteria

(see Introduction) (b), (g), (e) and criterion (a) in so far that the measurements relating to criteria (b), (c), (e), (f), (g) and (h) in single and polycrystals are in agreement. The observed behaviour of peak X in single crystals and polycrystalline specimens is not in accordance with (c) and (f) in that the peak height (Δ_X) does not saturate with flow stress τ and the peak temperature (T_X) shifts with τ. This is similar to the results obtained in polycrystalline nickel[4] except that (i) the maximum ratio of shift in peak temperature in single crystals is $\frac{\Delta T_X}{T_X} = .16$ compared to .29 in polycrystals, and (ii) the maximum Δ_X observed with deformation is 10 times smaller in single crystals than in polycrystals. We believe the hump seen in curve B, Fig. 14 at -80°C on the low temperature side of peak X is to be identified as the Niblett-Wilks peak rather than peak Y which has been previously so identified[4], as its behaviour is closely related to peak X as demanded by criterion (h) and its appearance is somewhat similar to that observed in copper. On the other hand, peak Y does not seem to be related to peak X regarding its behavior with deformation and crystal orientation. The earlier work reports peak Y as the Niblett-Wilks peak because the older Niblett-Wilks criterion[40] required only that the N-W peak should occur on the low temperature side of peak X and does not demand

that its behavior should be closely related to peak X unlike the recent Niblett's criterion[5] which we are considering here.

The following results (1) to (6) are a brief summary of the phenomenological characterization of peak X. Results (1) to (4) parallel those for polycrystals but the additional correlation between the observed variables and the stages I, II and III of deformation is new. Observations (5) and (6) are new.

(1) Δ_X when plotted against τ is approximately a straight line in each of the stages I and II, with the slope in stage I probably higher than the slope in stage II. It drops in stage III. The maximum Δ_X observed is approximately 10 times smaller than that in polycrystals.

(2) The width of peak X (ΔW_X) is nearly a constant with τ in stages I and II and decreases during stage III. ΔW_X observed in single crystals is smaller than in polycrystals.

(3) T_X decreases with τ in stages I and II and the early part of III and then increases for higher values of τ during stage III. The maximum ratio of the shift in peak temperature observed in single crystals is $\frac{\Delta T_X}{T_X} = .16$ and is smaller than .29 observed in polycrystals.

(4) Isochronal annealing behavior of peak X in single crystals shows results similar to that in polycrystals in that Δ_X and T_X decrease during annealing up to 320°C. Annealing at higher temperatures results in an increase of Δ_X and T_X and a decrease in ΔW_X.

(5) The variation of Δ_X with τ in stages I and II in crystals of different orientations is consistent with the hypothesis that dislocations in the principal glide system are responsible for peak X and inconsistent with dislocations in the cross-glide and conjugate glide systems.

(6) Δ_X in single crystals varies with deformation temperature only to the extent that the flow stress is affected by such a change.

Our observations (1) and (4) are similar to Sommer's observations in polycrystalline nickel[4] that peak X was important only at low to moderate dislocation densities and grew during the first stages of recrystallization. He discards the dipole model for peak X on the basis that dislocation debris should continually increase with plastic deformation and anneal out during recovery. We might interpret our observation on the drop of Δ_X in stage III against the dipole mechanism for peak X as follows. Johnston and Gilman[41] have shown

with an etch pit technique that moving screw dislocations leave numerous edge dislocation dipoles in their wakes and electron microscopic evidence[42] seems to confirm this. Also as reported in Appendix B, in stage I of deformation, those dipoles which are present are seen at the intersection of sub-boundaries and the cross-glide plane, indicating the possibility that moving screw dislocations on the cross glide plane may have originated these dipoles. From observation (5), we see that dislocations in the cross-glide plane are inconsistent with peak X. If moving screw dislocations produce these dipoles one would expect the dipole density to increase enormously in stage III which is attributed to cross-slip of screw dislocations around obstacles (Appendix B). As there are no reliable experimental measurements on dipole density, it is not possible to subject the Gilman model[43] to close scrutiny, but we speculate that if dipoles are responsible for peak X, one would expect a rise in peak X in stage III, while our observation (1) is that peak X drops, while peak Y rises. Further the dipole hypothesis[43] predicts a Q in Ni of .2 e.v./atom which again fits better with peak Y than with peak X.

Brailsford's original model[44] is unacceptable for reasons given in Appendix A, and the later model[45] does not

predict a shift in the peak temperature of the Bordoni peak with deformation contrary to observation (3), probably because the treatment neglects the effect of internal stress on double kink generation.

This leaves us with the Seeger mechanism of double kink generation as modified by Pare to be responsible for the relaxation process of peak X. We shall rationalize the observed experimental results on the basis of this theory. According to this theory[6], the Bordoni peak is caused by only those dislocations in Peierls valleys which are acted upon by an internal stress $\sigma_i \geq \frac{2W_k}{abl}$ .....(1) where W_k is the kink energy; a, the distance between Peierls valleys; l, the loop length along Peierls valley and b, the burgers vector. The maximum peak height is given by $\delta_{max} \propto \rho_p l$ .....(2) where ρ_p is the dislocation density along Peierls valleys. In order to calculate the effect of cold work on peak temperature and peak width, Pare assumes a normal distribution of internal stress with mean zero and standard deviation S and obtains an activation energy distribution by use of the following equation taken from Seeger and Donth[47] for the activation energy W, for double kink pair formation.

$$W = 4.56\, W_k \left[1 - .785 \left(\frac{\sigma_i}{\tau_p^{o}} \right)^{.592} \right] \qquad (3)$$

where τ_p^{o} = Peierls stress.

The most probable activation energy and the width at half maximum of this distribution is then related to the peak temperature and peak width respectively. The most probable activation energy W_m, is given by

$$W_m = W_o \left[1 - .6 \left(\frac{S}{\tau_p}_o\right)^{.592}\right] \qquad (4)$$

where $W_o = 4.56\ W_k$

Equation (4) predicts a decrease in the activation energy W_m and therefore the peak temperature with increase in S caused by cold work.

What Paré's theory[6] does not make explicit is to relate the changes in W_m due to changes in l caused for example by dislocation pinning with little change in the internal stress distribution. If l decreases, it means that dislocations which give rise to the Bordoni peak are those which are under the influence of a greater internal stress as required by (1) and hence the peak temperature decreases because W_m decreases according to (4). Also the δ_{max} is lower when l decreases as demanded by (2) and also from the argument that if l decreases when the internal stress distribution is invariant, fewer dislocations will be under the influence of the internal stress required by (1).

Accordingly, we can relate simply variations in Δ_x,

T_x and ΔW_x to variations in ρ_p, l and S. An increase in Δ_x implies an increase in the product $\rho_p l$; an increase in T_x is due to a decrease in S and/or an increase in l; a decrease in T_x is due to an increase in S and/or a decrease in l; and an increase in ΔW_x is due to an increase in S.

Our observation (1) is rationalized on the Seeger-Pare theory as follows. A peak in Δ_x vs τ is a peak in the product $\rho_p l$ vs τ. In stage I, long loops of dislocations lying along the Peierls valley are observed[48]. Since the probability of double kink generation according to Seeger's theory depends on the loop length and the number of dislocations lying along Peierls valleys, the rate of increase of Δ_x with τ is larger at low amounts of deformation. For larger amounts of deformation the number of dislocations will continue to increase, but their mutual interactions will result in a decrease in both the average loop length and the fraction of the dislocations which lie along the close packed directions. This results in a decreased rate of increase of Δ_x with τ, even though the magnitude of Δ_x is large in stage II because of the higher value of the product $\rho_p l$.

The product $\rho_p l$ may decrease at very large deformations because either factor decreases or both do. A decrease in ρ_p

may be due to increased dislocation interactions in stage III evidenced by electron microscopic observations[49,50,51,52] of the growth of cell walls together with a drop in dislocations in the interior of the cells (appendix B). A decrease in ρ_p is also expected under Gilman's microdynamical theory of plasticity[53] which gives the mobile dislocation density ρ_m as a function of plastic strain and shows that it goes through a maximum and then decreases whereas the total dislocation density keeps increasing with plastic strain. One plausible hypothesis is that ρ_m and ρ_p are related. To have a large value for ρ_p it is necessary to have long loops of dislocations lying along Peierls valleys with very little dislocation interactions. ρ_p is reduced by dislocation interactions because the Peierls energy which causes the dislocations to lie along the Peierls valley remains the same whereas the forces which push the dislocations from the close packed directions into some other configurations increase with dislocation interactions. ρ_m is also reduced by dislocation interactions due to the formation of tangles and cell walls. A decrease in loop length might be caused by the pinning of dislocations by point defects produced in large numbers in stage III[54].

Our observation of a smaller peak X in single crystals (compared to polycrystals) is probably because ρ_p is lower

in single crystals than in polycrystals.

Our observations (2) and (3) are explained on the basis of Seeger-Pare theory as follows. Since ΔW_x does not change appreciably during stages I and II, the width of the internal stress distribution does not change either. The observed decrease in T_x during stages I and II is therefore attributed to a decrease in loop length l. An increase in l to account for rise in T_x in stage III seems unlikely on the basis of electron microscopic observations (Appendix B). The rise of T_x and decrease in ΔW_x during stage III is due to decrease in S on the dislocations giving rise to peak X. The peak shift observed with deformation in polycrystalline nickel by Sommer[4] which is larger than we observed in single crystals is believed to be due to the higher value of S in polycrystals. Observation (4) is rationalized as follows. Since the change in ΔW_x for annealing temperatures $T < 320^{\circ}C$ is small, S does not change much. Therefore the simultaneous decrease in Δ_x and T_x for annealing temperatures $T < 320^{\circ}C$ is interpretable as a shortening of the loop length participating in the Bordoni relaxation.

The increase in Δ_x and T_x on further annealing at temperatures $> 320^{\circ}C$ is due to the depinning of dislocations resulting in an increase in loop length and possibly changes in ρ_p caused by dislocation rearrangement. The slight decrease in ΔW_x may be associated with the decrease in S caused by dislocation rearrangement after depinning.

All our observations in single crystals confirm Sommer's identification of peak X in polycrystals as the Bordoni peak and the Seeger-Pare theory[6,12] of the double kink generation provides a basis for the qualitative understanding of our results.

2. Peak Y

The significant results relating to peak Y are:

(1) The behavior of peak Y in single crystals with deformation and isochronal annealing is substantially similar to the results reported for polycrystals[3,4], with the new additional observation that peak Y appears predominantly in stage III at a smaller flow stress than in polycrystals, before or after τ_{III}. Also, the maximum height of peak Y observed in single crystals is approximately 5 times smaller than that in polycrystalline specimens.

(2) The observed variation in Δ_y with crystal orientations could not be explained under the assumption that dislocations in the primary, cross or conjugate slip systems are respon-

sible for it. Further from the observation in crystals of different orientations that there is no correlation between the drop of peak X and the rise of peak Y in stage III, we might conclude that the mechanism for the generation of peak Y is not necessarily the one for the removal of peak X.
(3) A change in the deformation temperature affects the height of peak Y markedly and this might be associated with the temperature dependence of stage III.
(4) In crystals of different orientations, T_y is higher for those which show larger Δ_y.

Observation (1) indicates that the long loops of dislocations one normally considers for the Bordoni peak are not applicable here. As mentioned earlier, the dipole hypothesis may apply to peak Y on the basis that moving screw dislocations create edge dislocation dipoles and a good agreement between the Q observed for peak Y and the Q calculated assuming the dipole model[43]. It is well known that stage III shows large cross slip of screw dislocations (Appendix B). Johnston and Gilman[41] have shown that moving screw dislocations leave numerous edge dislocation dipoles in their wakes and this has been observed in a broad variety of crystals including Al[42], Zn[52], Fe (3% Si)[55], LiF[41], MgO[56], NaCl[57], and Si[58]. Even though stage III is not studied very well through electron microscopy,

numerous dislocation debris dipoles have been observed during this stage (Appendix B). On the basis of this observation, the dipole model, which has been rejected for peak X may apply to peak Y. The explanation why peak Y is not seen in stages I and II could be that the dipoles that are observed in these stages are too widely separated to give rise to relaxation under Gilman's dipole model[43]. Observation (3) can be reconciled with the dipole hypothesis as follows. If we assume that the number of dipoles created by cross slip of screw dislocations in stage III is dependent on the deformation temperature, then so is the height of peak Y which depends on the relaxation of these dipoles. We associate the annealing out of peak Y between 320° C and 430° C under (1) with the recovery of dislocation debris dipoles created during stage III of deformation of the single crystal. Our observation (1) also eliminates grain boundaries as responsible for peak Y.

We cannot unequivocably assign a mechanism for peak Y but the important findings are that peak Y is created by an entirely different mechanism from the one for peak X, the former involving the relaxation of some sort of dislocation debris configuration created in stage III, possibly dipoles.

SUMMARY AND CONCLUSIONS

A. SUMMARY

(1) The internal friction spectrum in nickel single crystals of different orientations has been studied near 20 kHz from 77°K to 298°K after prestrain to values correponding to the 3 stages of strain hardening, and located the peaks X and Y reported earlier for polycrystals around -40°C and -140°C respectively. The magnitude of peak X in single crystals was found to be approximately 10 times smaller and peak Y approximately 5 times smaller than in polycrystals.

(2) The variations in the heights, positions and widths of peaks X and Y in single crystals with deformation and isochronal annealing, are substantially similar to those reported for polycrystals. The present work relates these variations to the stages of strain hardening of the crystals.

(3) With plastic deformation in single crystals, peak X grows throughout stages I and II and falls in stage III. The height of peak X when plotted against the flow stress resolved on the primary glide system follows a straight line in each of the stages I and II, with the slope in stage I probably higher than in stage II.

(4) The drop in T_X with deformation in stages I, II and rise of T_X and decrease of ΔW_X in stage III are similar to previous

results in polycrystals except the magnitude of variations in T_x and ΔW_x reported are larger in polycrystals probably due to higher internal stress caused by the grain boundaries.

(5) In crystals of different orientations, the changes in the height of peak X with τ in stages I and II can be accounted for on the assumption that dislocations in the primary glide system are responsible for peak X. Such changes are not consistent with dislocations in the crossglide or conjugate glide systems.

(6) Peak Y appears near the start of stage III of strain hardening at a smaller flow stress than in polycrystals, and increases in height with further deformation in stage III as in polycrystals.

(7) Changes in the height of peak Y with crystal orientations are not related to dislocations in the primary, conjugate or critical glide systems. The orientation dependence of peak Y is not understood.

(8) A variation in the deformation temperature affects the height of peak Y markedly and the height of peak X only to the extent that the flow stress is affected by such a change.

(9) Peak X obeys the Niblett's criteria (a), (b), (e), (g) and (h) of the Bordoni peak given in Chapter I, and criteria

(c) and (f) with certain modifications. Deviations from criteria (c) and (f) and other experimental observations have been rationalized on the basis of the Seeger-Paré theory of the Bordoni peak. The experimental results on peak Y suggest it is associated with the structural characteristic of stage III and may be due to the relaxation of dipoles created in stage III.

B. CONCLUSIONS

The major points of the summary are:

(a) Peak X grows throughout stages I and II and drops in stage III. The height of peak X when plotted against the flow stress resolved on the primary glide system is approximately a straight line in each of the stages I and II, with the slope in stage I probably higher than the slope in stage II.

(b) The variation in the height of peak X with crystal orientation is consistent with the hypothesis that dislocations in the primary glide system are responsible for it.

(c) Peak Y appears near the start of stage III and increases in height with further deformation.

(d) A variation in the deformation temperature affects the height of peak Y markedly and the height of peak X only to the extent that the flow stress is affected by such a change.

APPENDIX A

THEORIES OF THE BORDONI PEAK

1. Seeger's theory:

The essential feature of Seeger's theory[12,46,47,59] is that the observed internal friction peaks are due to intrinsic properties of individual dislocations lying along a close packed direction. At moderately high temperature a dislocation, which on an average lies parallel to a close packed crystallographic direction contains a certain number of kinks.[60] The formation of the kinks is thermally activated and can give rise to a relaxation phenomenon under the action of an applied stress which tends to move the kinks sideways (i.e. parallel to the close packed direction). The internal friction due to this process reaches its maximum when the frequency of the applied stress is equal to the frequency of the kink generation. The activation energy E is an intrinsic property of the dislocation line and is independent of the dislocation density or the impurity content of the material. According to Seeger's theory, the relaxation peaks in F.C.C. metals are caused by the motions of dislocation lines with burgers vector $(a/2)\langle 110\rangle$ lying in $\{111\}$ glide planes along one of the close packed directions. A $\{111\}$ plane contains three $\langle 110\rangle$ directions, thus allowing two different configurations: the burger's vector may be either parallel to or form an angle of $\pm$ 60 degrees with the direction of the dislocation line. Due to the two configurations,

two types of relaxation peaks, the Bordoni peak and the Niblett-Wilks peak, are observed with different relaxation times. In certain material it is possible they may coincide. Those dislocation lines which on an average do not run approximately parallel to a close packed direction do not contribute to the internal friction mechanism. Therefore one expects that only a small fraction of the total number of dislocations participate in the relaxation phenomena.

This interpretation has won considerable support but some features are not explained: (1) the measured width of the peaks is two to three times larger than predicted by Seeger's theory[61] and (2) the Bordoni peak shifts to lower temperature after deformation[4].

2. Pare's modification of Seeger's theory:

Pare[6] modified Seeger's theory by taking into account the effect of internal stresses σ_i produced by plastic deformation. He shows that $\sigma_i \neq 0$ is necessary to create two stable positions for a dislocation line of length L pinned at its ends, and lying parallel to the potential minima of the lattice[62]; (1) straight in which the entire loop lies in the same valley as the pinning points and (2) deformed, in which the entire loop is in the adjacent valley except for a kink at each end, where it is held in the original valley by the pinning points.

Either an internal stress or an externally applied "measuring stress" will tend to move the dislocation toward the deformed position.

Pare's detailed calculation based on the above assumptions and using the theory of absolute reaction rates gives

$$\delta = \frac{\pi L a^2 b^2 G \rho}{4kT} \frac{(\omega/\omega_o)}{1 + (\omega/\omega_o)^2}$$

where L is loop length, ρ the dislocation density, a the distance between valleys, b the burger's vector, G the shear modulus, ω the applied anguiar frequency and ω_o the relaxation frequency.

He further derives (1) the lowering in the temperature of the peak with increasing internal stress (2) the increase in width of the peak with internal stress of deformation.

3. Brailsford's theory:

Brailsford[63] presents a different model of the dislocation relaxation process. He describes the behaviour of a dislocation in the presence of an applied stress in terms of a redistribution of kinks along its length. In contrast with the Seeger-Pare model,[6,12] in which the kink is envisaged as a smooth step extending over many lattice spacings, he supposes that the kink is abrupt. Most dislocations contain kinks because of the constraints imposed on them by the presence of other dislocations and by other lattice imperfections. Only a few

dislocations will lie along the close packed direction.

The kinks are supposed to be independent and kink diffusion at any finite temperature is a thermally activated process with the relaxation time of $\tau = L^2 D^{-1} \pi^{-2}$ where L = dislocation line length and D the diffusion coefficient of the kinks. In his theory the thermal generation of kinks is negligible at low temperatures. Dislocations which lie along close packed directions do not contribute to internal friction. This is in contrast to Seeger's theory. In Brailsford's model therefore dislocations will not respond to dynamic stresses at temperatures below the temperature of Bordoni peak. This conclusion is against the observation of a modulus defect in F.C.C. metals at 4° K.[44]

In order to meet the above objections, Brailsford[45] in a later paper proposes a model based on thermally activated kink motion taking into account the effect of internal stresses upon dislocation motion. In this model interactions among kinks play an important part. This model is similar to the Seeger-Pare model except for the fact that the kinks are abrupt.

4. Gilman's theory:

Gilman[43] proposes a theory entirely different from the others. He attributes the Bordoni peak to dislocation dipoles, which are parallel dislocation segments having opposite sign.

In this theory, the peak is presumed to be connected with thermally activated flip-flopping of edge dislocation dipoles between their two energetically stable positions. The flipping of a small segment of a dipole is a thermally activated process which results in the formation of dipole junctions. According to this picture the redistribution of the junctions under the influence of an applied stress gives rise to the Bordoni peak. For the effective occurrence of flipping, the dipole width must be small so that no correlated atom movement is required. The activation energy is determined by the height of the barrier separating the two stable orientations, and the relaxation strength is proportional to ρW where ρ = dipole density in cm/cm^3 and W = average dipole width.

APPENDIX B

STRAIN HARDENING OF F.C.C. CRYSTALS

As seen in Fig. 3(b), the deformation curve of F.C.C. single crystals shows 3 stages.

Stage I or the easy glide region shows a small work hardening $\theta_I = \frac{d\tau}{da}$; the extent of this region depends on the orientation, purity and size of crystals and deformation temperature[65,66] and consequently values of G/θ_I can be very large ($> 10^4$) and will have as a lower limit $\frac{G}{\theta_{II}}$ when stages I and II become indistinguishable. Stage I is associated with slip on only one set of planes. The slip distance is large (of the order of specimen diameter). As soon as slip commences on another set of planes, a strong interaction between dislocations on the primary and secondary slip systems arises and this gives rise to a steep increase in work hardening and is related to the transition from stage I to II.

The dislocation pattern has been studied by thin film electron transmission microscopy, X-ray techniques and etch pit methods.[68] The dislocation density in a single crystal prepared with normal care is of the order of $10^6/cm.^2$ Young and Livingston's[68] studies of etch pits show pile-up of dislocations at sub-boundaries is enhanced when stage I begins. The distribution of dislocations in primary glide plane is

much more isotropic than that observed on the cross glide plane where etch pits are aligned roughly along the intersection with the primary and sometimes the critical and conjugate planes.

The most striking electron micrographs are those of sections which include the [12$\bar{1}$]direction.[49,69,70] A large number of dipoles are seen in the immediate vicinity of sub-boundaries which agrees with the increase of etch pit density near sub-boundaries on the cross-glide plane. There are invariably a few forest dislocations associated with groups of dipoles. It appears likely[70] that long dipoles are originally formed but are continuously cut during subsequent deformation. The dislocation density is non-uniform, clusters of dislocations surrounding regions of low dislocation densities.[71]

Electron micrographs in the transition region show considerable activity on the conjugate and critical slip system resulting in the formation of immobile tangles of dislocations of these two systems and of their reaction products. The number of dipole segments increased during this transition.[69]

Stage II

The density of forest dislocations increases until by end of stage II they are as abundant as primary dislocations.[72,73] However primary dislocations pile up at sub-boundaries while forest dislocations do not. This implies primary dislocations

have a mean free path large compared with the width of a subgrain, while the mean free path of a forest dislocation is much less. The fact that the lattice rotation corresponds to that calculated on the assumption that slip occurs solely on the primary glide system is explained by the short mean free path of forest dislocations. Lomer-Cottrell locks are formed during this stage.

The slip bands in stage II are broad diffuse bundles[25] and the lengths of individual slip lines are inversely proportional to strain in stage II.[74] Diehl and Berner[32] found that the slope of stage II depended on temperature in approximately the same way as the elastic modulus. The dipole density increases slowly in stage II.[69]

Stage III

Stage III has not been studied as carefully by electron microscopy as have the earlier stages, because it can hardly be understood before there is a firm understanding of stage II. The slip bands are coarse and fragmented, with abundant cross slip and continual growth of individual bands.[25] This cross slip probably occurs by the contraction of screw dislocations originally extended on the primary glide plane, followed by their extension on the cross slip plane.[27] It is to be distinguished from the motion of dislocations originally generated on

the cross slip plane which can occur under much lower stresses. As a result of this cross slip, screw dislocations can circumvent the obstacles and the stress-strain curve falls below the straight line of stage II. Obstacles are presumably dislocation tangles. Lomer-Cottrell locks have often been considered but they have not been observed in copper.[68] The slip lines show directly that the stress relieving process is the cross slip of screw dislocations and not the collapse of Lomer-Cottrell locks.[27] Cross slip in stage III is thermally activated which explains why the onset of stage III and its slope depends on deformation temperature.

During stage III, a three dimensional cell structure develops[50,51] involving a high dislocation density in the cell boundaries surrounding regions with low dislocation density.[49,52] The cell wall thickness increases.[50] Since screw dislocations suddenly cross slip in this stage, it is conceivable that a large number of vacancies and edge dislocation dipoles are formed. This debris has been observed in Al[69], Zn[52], and other materials.[75]

APPENDIX C

A NOTE ON THE STACKING FAULT ENERGY OF NICKEL.

The stacking fault energy of nickel has been estimated (1) by the study of extended nodes using electron microscopy[76] and (2) by studying the variation of τ_{111} as a function of temperature.[77,78]

Howie and Swann[76] obtained estimates of stacking fault energy by the use of extended nodes seen in the electron microscope. They obtain a value of 150 ergs/cm^2 by extrapolation of values obtained in Ni-Cu and Ni-Co alloys. This extrapolation may not be justifiable because of a large change in the Fermi surface of the pure metal on alloying.[79] Their method is based on the measurement of the radius of curvature of the extended node and the assumption that the partials in the node are independent. The equilibrium curvature is then determined by the balance between the line tension which can be taken as $\frac{\mu b}{2R}$ and the effective shear stress due to the stacking fault which is given by $\frac{\gamma}{b}$. The equilibrium radius of curvature can then be equated $R = \frac{\mu b^2}{2\gamma}$.

Seeger et al[77,78] measured γ based on a study of τ_{111} with temperature. Their theory is based on the thermally activated formation of a constriction in the leading extended dislocation in a pile up resulting in cross slip. The value of γ obtained is 200 ergs/cm^2. The criticism of their method[76] is that for

silver it does not give a value which is similar to the one obtained by direct observation of nodes using electron transmission microscopy.

APPENDIX D

JUSTIFICATION FOR THE SPECIMEN CONFIGURATION

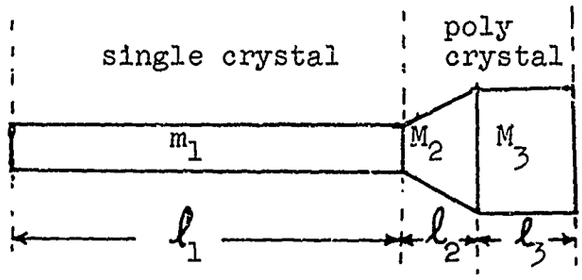

Fig. 39

Consider Fig. 39. It is assumed that the polycrystalline masses M_2, M_3 move as a single mass with no elastic strain. The Lagrangian L for the motion of a crystal with polycrystalline mass at its end is given by

$$L = T - V$$

$$= \int_0^{\ell_1} \frac{1}{2} \rho A_1 \dot{u}^2 dx + \frac{1}{2} M \dot{u}_{\ell_1}^2 - \frac{1}{2} \int_0^{\ell_1} E_1 A_1 \left(\frac{\partial u}{\partial x}\right)^2 dx \qquad (1)$$

where $M = M_2 + M_3$

u = displacement at any point x

A_1 = cross-sectional area of m_1

ρ = density

E_1 = elastic modulus of single crystal

It is assumed $u = u_{\ell_1}(t)\frac{x}{\ell_1}$ (2)

Substitution of (2) in (1) and integration yields

$$L = \frac{1}{2}\left[\frac{1}{3}\rho A_1 \ell_1 + M\right] \dot{u}_{\ell_1}^2 - \frac{1}{2} \frac{E_1 A_1}{\ell_1} u_{\ell_1}^2 \qquad (3)$$

The equation of motion $\frac{d}{dt}\left(\frac{\partial L}{\partial \dot{q}}\right) - \frac{\partial L}{\partial q} = 0$ is obtained from (3) and is given by:

$$\left(\frac{1}{3}\rho A_1 \ell_1 + M\right)\ddot{u}_{\ell_1} - \frac{E_1 A_1}{\ell_1} u_{\ell_1} = 0 \qquad (4)$$

$u_{\ell_1} = A \sin \omega t$ where $\omega^2 = \frac{3E_1 A_1}{\ell_1(\rho A_1 \ell_1 + 3M)}$ is a solution to (4) and

$$\omega = \sqrt{\frac{3E_1 A_1}{\ell_1(\rho A_1 \ell_1 + 3M)}} \qquad (5)$$

For crystal 11, substitution of appropriate values in (5) yields ω = 126·3 kHz

ν = 20·05 kHz

The observed resonant frequency was 19.35 kHz which is almost the same as the calculated resonant frequency. This calculation shows that if it is assumed that the vibrating strain is all in the specimen, the resonant frequency is predicted correctly. This calculation together with the experimental observation shown in Fig. 17 justifies the use of a specimen configuration given in Fig. 3(a) for our measurements.

APPENDIX E

ORIENTATION DEPENDENCE OF DISLOCATION DAMPING.

If a periodic stress $\sigma = \sigma_o e^{i\omega t}$ is applied to an anelastic solid, the strain lags behind the stress by an angle ϕ where

$$\tan\phi = \frac{\text{log decrement}}{\pi} = \frac{\Delta W}{2W\pi} = \frac{\text{energy lost per cycle}}{2 \times \text{elastic energy stored per cycle}} \times \pi.$$

$$= \frac{\epsilon_2}{\epsilon_1} \quad \text{where} \quad \frac{\epsilon_2}{\epsilon_1} = \frac{\text{strain } 90^\circ \text{ out of phase with stress}}{\text{strain in phase with stress.}}$$

It is assumed that the energy loss comes from the oscillations of dislocations in <110> direction lying in (111) plane. Consider Fig. 37, which shows the stress and strain relations in the complex plane used to represent periodic phenomena.

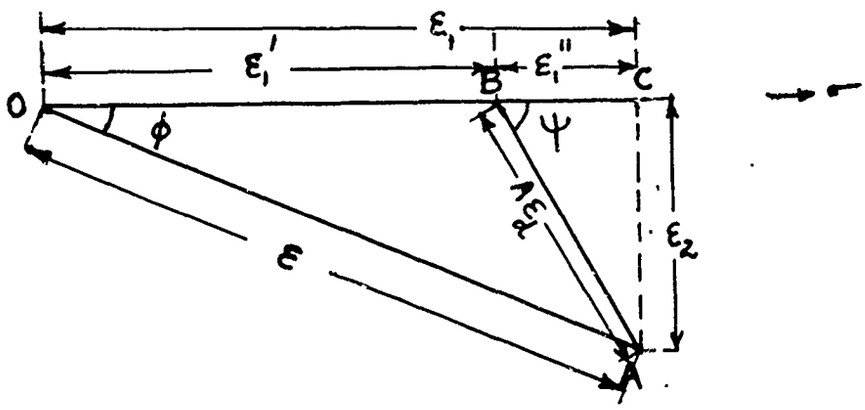

Fig. 37

The stress σ is taken as the reference vector in the direction OC. $\epsilon_1 = \epsilon_1' + \epsilon_1''$ is the strain in phase with σ. ϵ_2 is the strain 90° out of phase with stress σ. OA is strain ϵ which lags behind stress σ by an angle ϕ .

ϵ_1' = elastic strain, entirely in phase with σ

$A\epsilon_d$ = dislocation strain which lags behind σ by an angle ψ which is a function of $\omega\tau$ and independent of crystal orientation.

ϵ_1'' = elastic component of dislocation strain.

Consider ϵ_1:

When $\epsilon_1'' \ll \epsilon_1'$, we can say $\epsilon_1 = \epsilon_1' = \frac{\sigma}{E}$ where E is the Youngs modulus along the axis of the crystal.

Consider ϵ_2:

$\epsilon_2 = A \sin\psi \epsilon_d$ where $\sin\psi$ is a function of $\omega\tau$ and is independent of orientation, A is a factor which converts the dislocation strain ϵ_d caused by dislocation motion on the $\{111\}\langle 110\rangle$ slip system to the direction along σ.

$\epsilon_d = \rho b \bar{x}$ where ρ = dislocation density, b = burger's vector and $\bar{x}$ = the average displacement of a dislocation.

$\bar{x} = \sigma(\sin\chi_o \cos\lambda_o)F$ where F is a factor which depends on the dislocation geometry and the line tension of dislocations.

$\therefore \epsilon_d = (\sigma \cos\lambda_o \sin\chi_o)(F)(\rho b) = \gamma.$

ϵ_d is the engineering shear strain in the slip plane in the slip direction and is represented by $\overset{\approx}{\gamma} = \begin{pmatrix} 0 & 0 & \gamma/2 \\ 0 & 0 & 0 \\ \gamma/2 & 0 & 0 \end{pmatrix}$

To resolve $\overset{\approx}{\gamma}$ in the direction of stress consider Fig. 38.

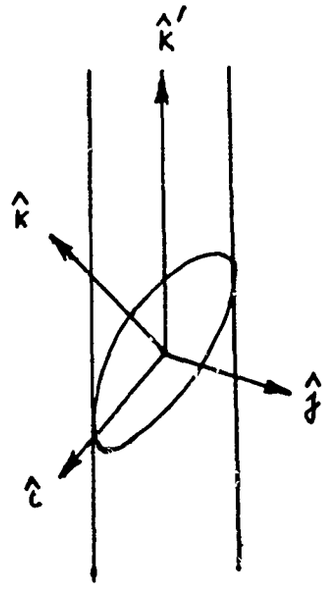

Fig. 38

In Fig. 38, $\hat{i}$ is the direction of slip, $\hat{j}$ the direction normal to $\hat{i}$ and $\hat{k}$; $\hat{k}$ the direction normal to the slip plane and $\hat{k}'$ the direction of stress. The value of $\overset{\approx}{\gamma}$ along $\hat{k}'$ is represented by ϵ_{zz} and given by:

$$\epsilon_{zz} = (\ell_1 \ell_2 \ell_3) \begin{pmatrix} 0 & 0 & \gamma/2 \\ 0 & 0 & 0 \\ \gamma/2 & 0 & 0 \end{pmatrix} \begin{pmatrix} \ell_1 \\ \ell_2 \\ \ell_3 \end{pmatrix}$$

where ℓ_1, ℓ_2 and ℓ_3 are the cosines of angles $\hat{k}'$ makes with $\hat{i}$, $\hat{j}$ and $\hat{k}$ directions.

$$\epsilon_{zz} = (\cos\lambda_o \cos\beta \sin\chi_o) \begin{pmatrix} 0 & 0 & \gamma/2 \\ 0 & 0 & 0 \\ \gamma/2 & 0 & 0 \end{pmatrix} \begin{pmatrix} \cos\lambda_o \\ \cos\beta \\ \sin\chi_o \end{pmatrix}$$

$$= \sin\chi_o \cos\lambda_o \gamma$$

$$= \sin\chi_o \cos\lambda_o \epsilon_d$$

$$\tan\phi \simeq \frac{\epsilon_2}{\epsilon_1} = \frac{\sin\chi_o \cos\lambda_o \epsilon_d \sin\psi}{} \frac{E}{\sigma}$$

Since $\epsilon_d = (\sigma \cos\lambda_o \sin\chi_o) \rho bF$

$$\tan\phi = \rho bF \; E(\cos\lambda_o \sin\chi_o)^2.$$

Therefore to compare measurements at constant ρ on crystals with different orientations, the measured value of $\tan\phi$ has to be divided by $E(\cos\lambda_o \sin\chi_o)^2$.

BIBLIOGRAPHY

1. Bordoni, P.G., La Ric. Scientifica, 19, 851 (1949).
2. Nabarro, F.R.N., Proc. Phys. Soc. (London), 59, 256 (1947).
3. Sommer, A.W., Ph.D. Thesis, Columbia University, 1965
4. Sommer, A.W., and Beshers, D.N., Jour. Appl. Phys., 37, 4063 (1966).
5. Niblett, D.H., Physical Acoustics, Vol. III, Part A (W.P. Mason, editor), chapter 3, Academic Press, New York, 1966.
6. Pare, V.K., Jour. Appl. Phys., 32, 332 (1961).
7. Ameen, D.L., M.S. Thesis, Cornell University, 1962.
8. Okuda, S., Jour. Appl. Phys., 34, 3107 (1963).
9. Routbort, J.L., Ph.D. Thesis, Cornell University, 1965.
10. Mecs, B.M., Ph.D. Thesis, Polytechnic Inst. of Brooklyn, 1966.
11. Chambers, R.H., Private communication.
12. Seeger, A., Phil. Mag., 1, 651 (1956)
13. Guberman, H.D., Ph.D. Thesis, Columbia University, 1963.
14. Wegel, R.L., and Walther, M., Physics, 6, 141 (1935).
15. Pittenger, J., Phys. Rev., 83, 872 (1951).
16. Chambers, R.H., Thesis, Carnegie Institute of Technology, 1957.
17. Kennelly, A.E., Electrical Vibration Measurements, MacMillan Co., New York, 1923.
18. Nowick, A.S., Progress in Metal Physics (ed. B. Chalmers), Vol. 4, p. 1, Interscience, New York, 1953.

19. Wesley, W.A., Jour. Electrochem. Soc., 103, 296 (1956).

20. Schmid, E., and Boas, W., "Kristallplastizitat", Springer, Berlin, 1935.

21. Mader, S., Seeger, A., and Leitz, C., Jour. Appl. Phys., 34, 3368 (1963).

22. Clarebrough, L.M., and Hargreaves, M.E., Progress in Metal Physics, Vol. 8, p. 1, (ed. B. Chalmers), Interscience, New York, 1959.

23. Guth, J.P., M.S. Thesis, Columbia University, 1967.

24. Diehl, J., Mader, S., and Seeger A., Z. Metallkunde, 46, 650 (1955).

25. Mader, S., Z. Physik, 149, 73 (1957).

26. Seeger, A., Diehl, J., Mader, S., and Rebstock, H., Phil. Mag., 2, 323 (1957).

27. Seeger, A., "Dislocations and Mechanical Properties of Crystals" (ed. J.C. Fisher), J. Wiley & sons, Inc., New York, 1957.

28. Haasen, P., Phil. Mag. 3, 384 (1958).

29. Rosi, F.D., Trans. A.I.M.E. 200, 1009 (1954).

30. Diehl, J., Z. Metallkunde 47, 331 (1956).

31. Lange, H., and Lücke, K., Z. Metallkunde, 44 183, 514 (1954).

32. Diehl, J. and Berner, R., Z. Metallkunde 51, 522 (1960)

33. Mecs, B.M. and Nowick, A.S., Acta Met., 13, 771 (1965).

34. Clarebrough, L.M., Hargreaves, M.E., and Loretto, M.H., "Recovery and Recrystallization of Metals" (ed. L. Himmel), J. Wiley & sons, New York, 1963, p. 63.

35. Sosin, A., and Brinkman, J.A., Acta Met., 7,478 (1957).

36. Wuttig, M., and Birnbaum, H.K., Jour. Phys. and Chem. of Solids, 27, 225 (1966).

37. Okuda, S., J. Phys. Soc. Japan, Suppl. 1, 18, 187 (1963).

38. Niblett, D.H., and Wilks, J., Proc. 10th Intern. Congr. Refrig., Copenhagen, 1959, Vol. 1, p. 131, Pergamon Press, New York.

39. Alefeld, G.A., Private Communication.

40. Niblett, D.H., and Wilks, J., Advan. Phys. 9, 1 (1960).

41. Johnston, N.G., and Gilman, J.J., Jour. Appl. Phys., 31, 632 (1960).

42. Fourie, J.T., and Wilsdorf, H.G.F., Jour. Appl. Phys., 31, 2219 (1960).

43. Gilman, J.J., Jour. Phys. Soc. Japan, Suppl. 1, 18, 172 (1963)

44. Alers, G.A., and Zinnerman, J.E., Phys. Rev., 139, No. 2A, 414 (1965).

45. Brailsford, A.D., Phys. Rev. 137, No. 2A, 1562 (1965).

46. Seeger, A., Donth, H., and Pfaff, F., Discuss. of Faraday Society, 23, 19 (1957).

47. Donth, H., Z. Phys., 149, 111 (1957)

48. Mayadas, A.F., Ph.D. Thesis, Cornell University, 1966.

49. Hirsch, P.B., and Steeds, J., Proc. Conf. on Relat. bet. Structure and Mechl. Prop. of Metals, Vol. 1, p. 48, (H.M.S.O.), 1963.

50. Howie, A., Proc. European regional conf. on electron microscopy, Delft, p. 383 (1960).

51. Essmann, U., Acta. Met., 12, 1468 (1964).

52. Price, P.B., Phil. Mag., 5, 873 (1960).

53. Gilman, J.J., Proc. 5th U.S. Natl. Congr. Appl. Mechanics, A.S.M.E., 385 (1966).

54. Van Bueren, H.G., Imperfections in Crystals, North-Holland Publishing Company, Amsterdam, 1960.

55. Low, J.R., and Turkalo, A.M., Acta Met., 10, 215 (1962).

56. Washburn, J., Kelly, A., and Williamson, G.K., Phil. Mag., 5, 1962 (1960).

57. Davidge, R.W., and Whitworth, R.W., Phil. Mag., 6, 217 (1961).

58. Dash, W.C., Jour. Appl. Phys., 29, 705 (1958).

59. Seeger, A., and Schiller, P., Physical Acoustics, Vol. III, Part A, (W.P. Mason, editor), chapter 8, Academic Press, New York, 1966.

60. Schockley, W., Trans. A.I.M.E., 194, 829 (1952).

61. Sack, H.S., Acta Met., 10, 455 (1962).

62. Read, W.T., Dislocations in Crystals, McGraw Hill (1953).

63. Brailsford, A.D., Phys. Rev., 122, 778 (1961).

64. Brailsford, A.D., Phys. Rev., 128, 1033 (1962).

65. Bocek, M., Phys. Stat. Solidii, 3, 2169 (1963).

66. Smallman, R.E., Modern Physical Metallurgy, Butterworths, London (1963).

67. Otte, H.M., and Hren, J.J., Observation of crystalline imperfections and their role in plastic deformation, Report No. OA 3408, Materials Research Lab., Martin Co., Orlando, Florida.

68. Nabarro, F.R.N., Adv. in Physics, 13, 193, (1964).

69. Fourie, J.T., and Murphy, R.J., Phil. Mag., 7, 1617 (1962).

70. Basinski, Z.S., et. al., Phil. Mag., 8, 1989 (1963).

71. Levinstein, H.J., and Robinson, W.H., Proc. conf. on relat. bet. struct. and mechl. prop. metals, Vol. 1, p. 180, (1963).

72. Livingston, J.D., Acta Met., 10, 229 (1962).

73. Basinski, Z.S., and Basinski, S.J., Phil. Mag., 9, 51 (1964).

74. Blewitt, T.H., et al, Defects in Cryst. Solids, Phys. Soc. (London), p. 369, 1955.

75. Gilman, J.J., Technical Report No. 3, Office of Naval Research, Contract Nonr 562(32), July 1962.

76. Howie, A., and Swann, P.R., Phil. Mag., 6, 1215 (1961).

77. Seeger, A., Berner, R., and Wolff, H., Z. Physik, 155, 247 (1959).

78. Seeger, A., Report on conference on defects in crystalline solids, Phys. Soc. (London), 1954, p. 325.

79. Massalski, T.B., and King, H.W., The Fermi Surface (edited by W.A. Harrison and M.B. Webb), p. 290, J. Wiley & sons, Inc., New York, 1960.

ACKNOWLEDGEMENT

The author wishes to express his gratitude to Professor D. N. Beshers for his guidance and continual interest and encouragement throughout the course of this work.

Special thanks are due to International Nickel Company who provided all the polycrystalline rods used in this work and did all the swaging operations.

The author should furthermore like to acknowledge the helpful conversations held with Mr. J. Papazian and Dr. A. Zuckerwar.

This research was conducted under the sponsorship of the Office of Naval Research.

TABLE I

STRAIN HARDENING PARAMETERS IN NICKEL CRYSTALS

Crystal Number	T deg. K	τ_o kg/mm^2	θ_1 kg/mm^2	τ_{11} kg/mm^2	a_{11} %	θ_{11} kg/mm^2	τ_{111} kg/mm^2	a_{111} %
5	298	.7	9.4	1.1	4.2	19.75	4.6	22
11	298	.67	11.45	1.5	6.4	23.7	5.3	22.9
13	298	.43	7	1.4	14.3	13.2	5	44.8
14	298	.53	-	-	-	21	4.0	18.6
16	77	.65	3.0	.85	6.2	13.4	5.3	39.5
17	77	.65	7.4	1.2	5.6	13.3	5.4	37
18	298	.63	3.3	.8	5.4	12.4	3.25	25.2

TABLE II

ORIENTATION DEPENDENT PARAMETERS

	Crystal No 5	Crystal No 11	Crystal No 13	Crystal No 14	Crystal No 18
$E \times 10^{-12}$ dynes/cm^2	1.6	2.7	2.2	1.43	2.25
λ_o degrees	43	37	57	40	47
χ_o degrees	41	34	49	39	44
$\sin \chi_o \cos \lambda_o$	.48	.447	.411	.483	.475
$E \sin \chi_o \cos \lambda_o$	.77	1.2	.907	.69	1.07
$E \sin^2 \chi_o \cos^2 \lambda_o$ (10^{12} dynes/cm^2)	.37	.537	.372	.332	.508

TABLE III

TEMPERATURES OF PEAKS X AND Y FOR VARIOUS VALUES OF τ.

Fig. No.	Crystal No.	Resolved shear stress τ Kg/mm^2	Temp. of Peak X.	Temp. of Peak Y.
5	5	1.1	-18	-
6	5	4.8	-20	-
6	5	6.7	-35	-150
6	5	7.8	-40	-138
6	5	8.8	-30	-135
12	11	1.3	-10	-
13	11	2.28	-10	-
14	11	4.88	-20	-
14	11	7.4	-35	-140
14	11	8.15	-18	-150
26	13	.93	-12	-
26	13	1.8.	-14	-
27	13	2.57	-17	-
27	13	3.08	-24	-
28	13	4.12	-35	-
28	13	5	-51	-138
29	13	6	-52	-135
29	13	7.3	-40	-138

TABLE III (cont'd)

Fig. No.	Crystal No.	Resolved shear stress τ Kg/mm^2	Temp. of Peak X.	Temp. of Peak Y.
31	14	1	-20	-
31	14	2	-20	-
32	14	3	-25	-
32	14	4	-30	-132
33	14	5	-32	-132
33	14	6	-26	-130
34	14	7	-19	-129
34	14	8	-18	-134
34	14	9	-	-134
19	16	5.14	-15	-129
19	16	6.45	-24	-128
19	16	7.81	-30	-130
19	16	9.08	-28	-130
23	18	3.3	-45	-
23	18	4.5	-42	-128
23	18	5.7	-38	-126
23	18	6.7	-38	-131

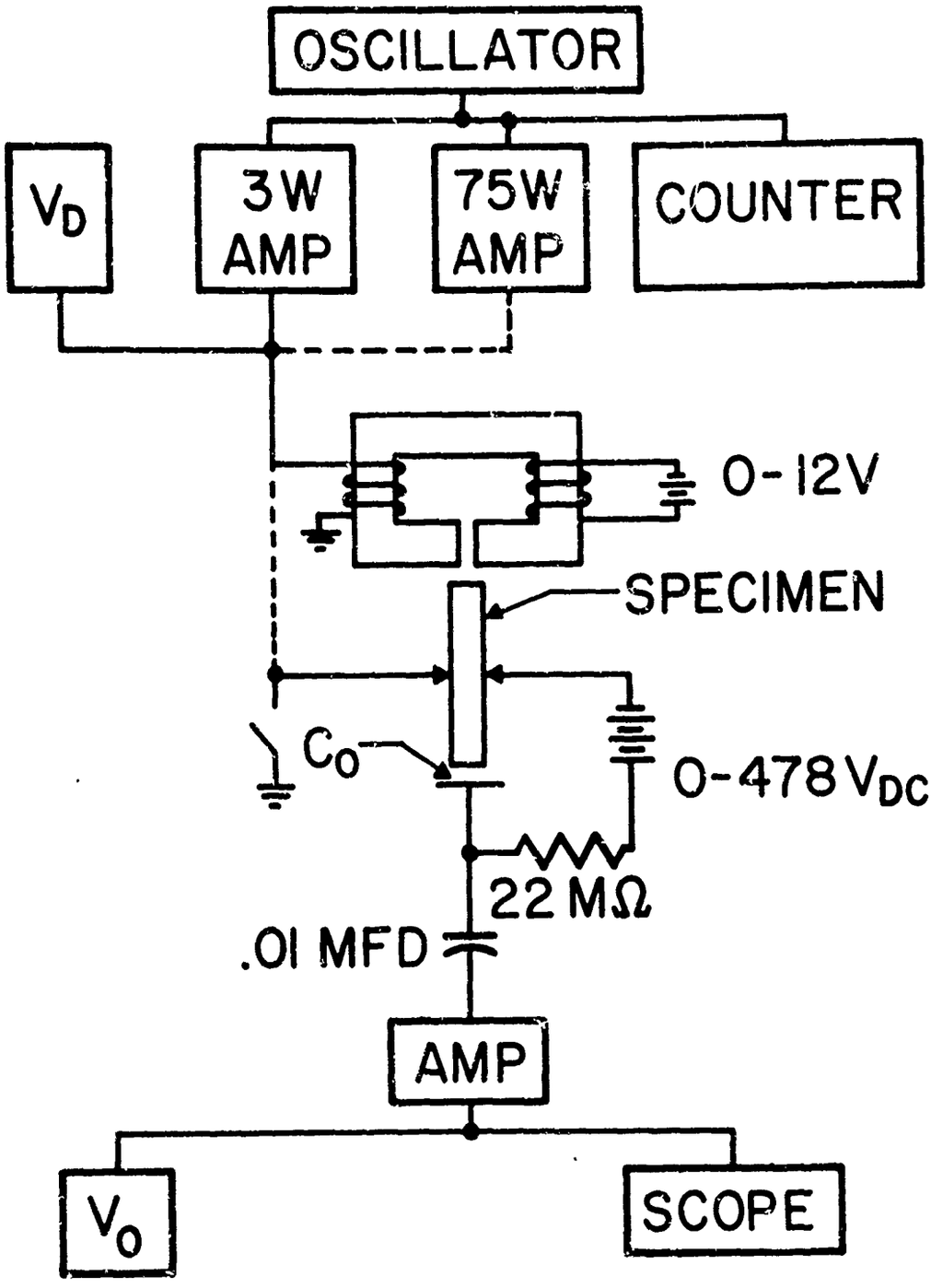

Fig. 1. Schematic layout of internal friction apparatus (after Guberman[13]).

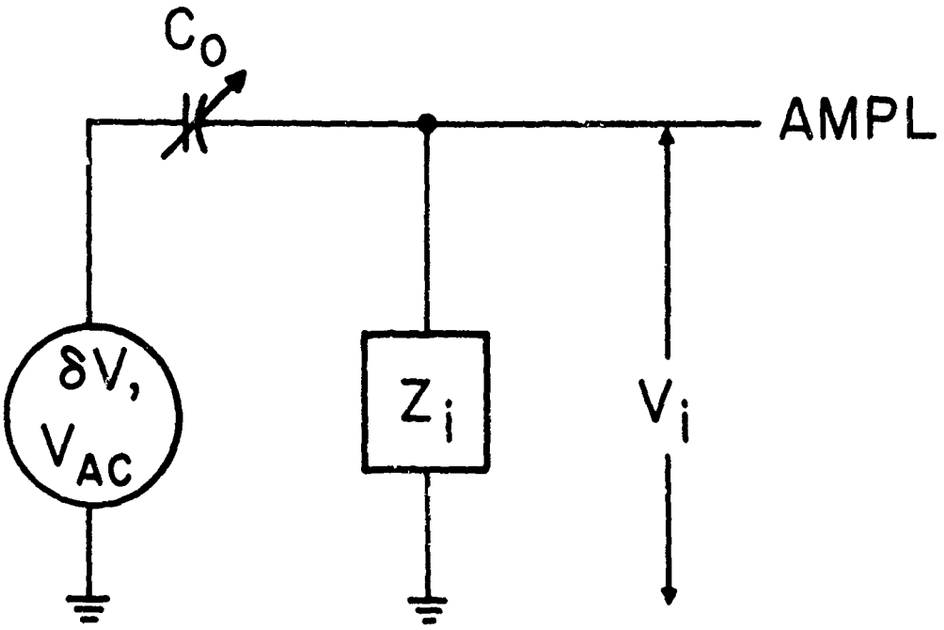

Fig. 2. Equivalent detection circuit. (after Guberman[13]).

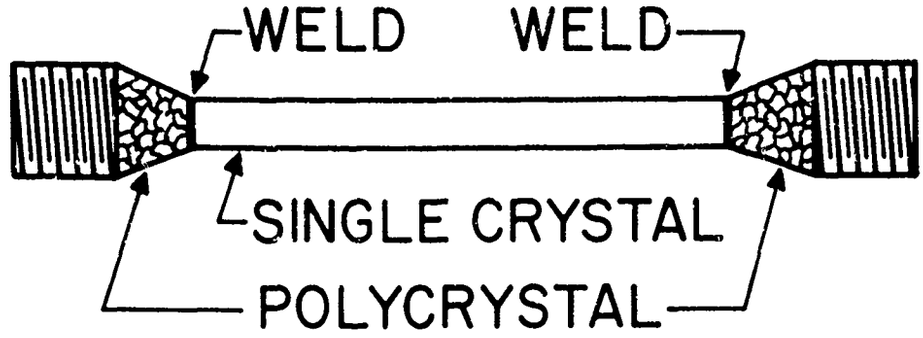

Fig. 3(a). Schematic of the specimen used for deformation and damping studies.

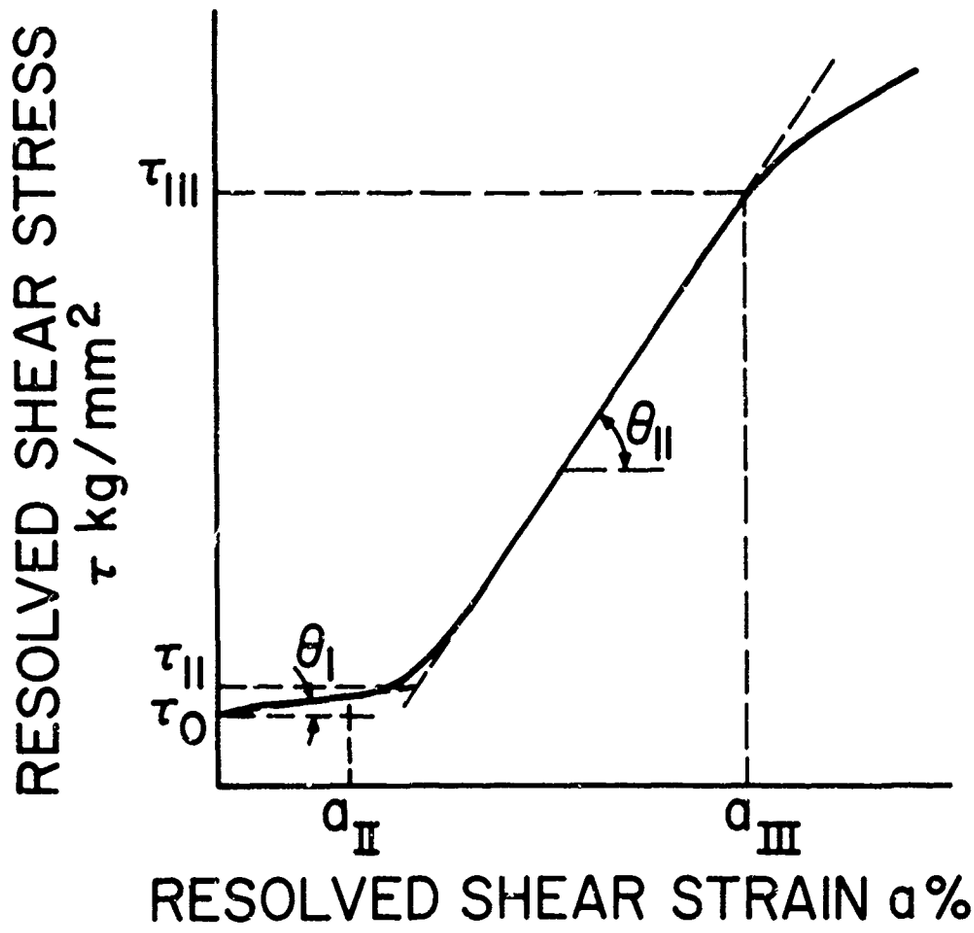

Fig. 3(b). Schematic work hardening curve with the definition of the work hardening parameters.

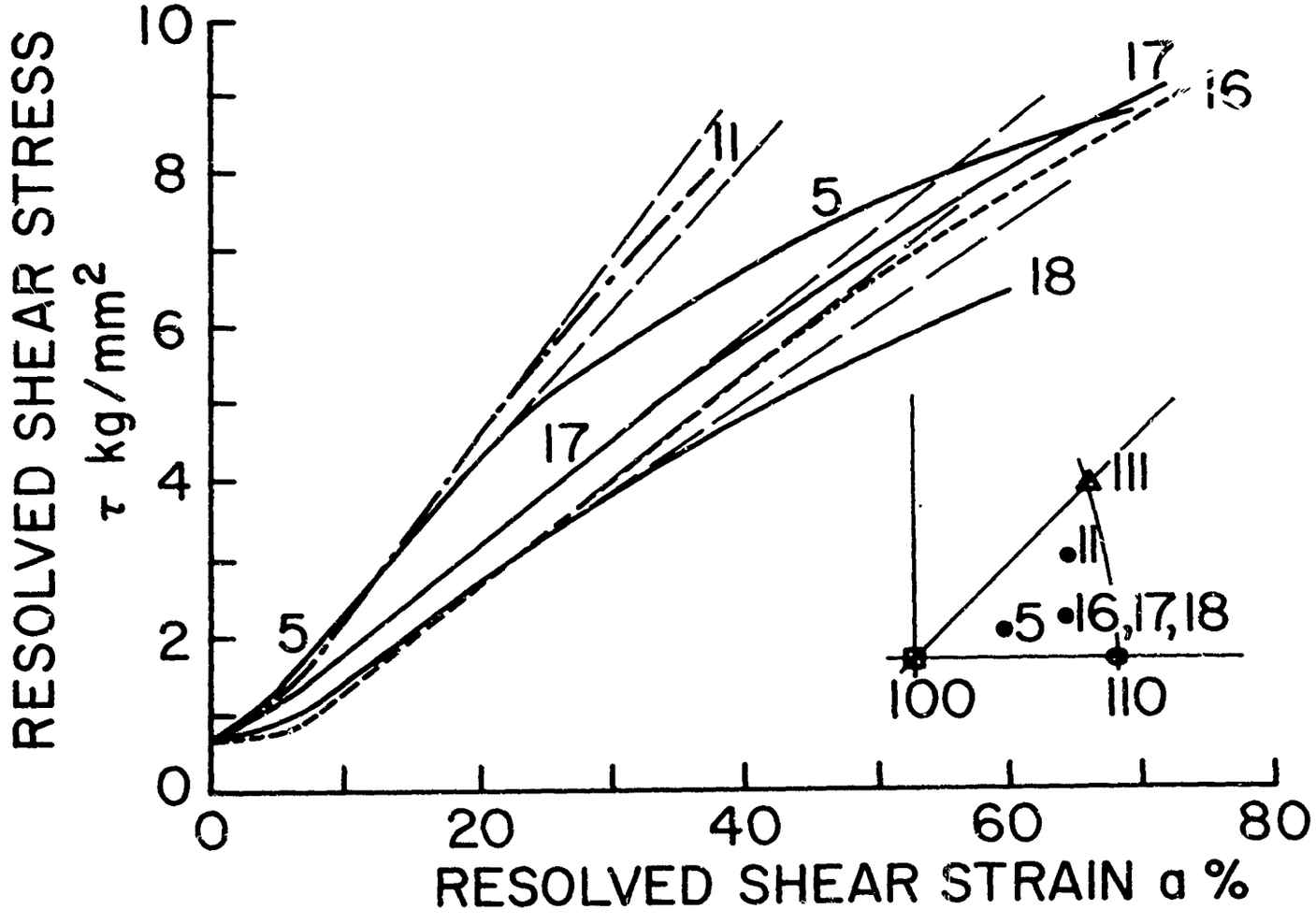

Fig. 4(a). Work hardening curves of crystals and their orientations.

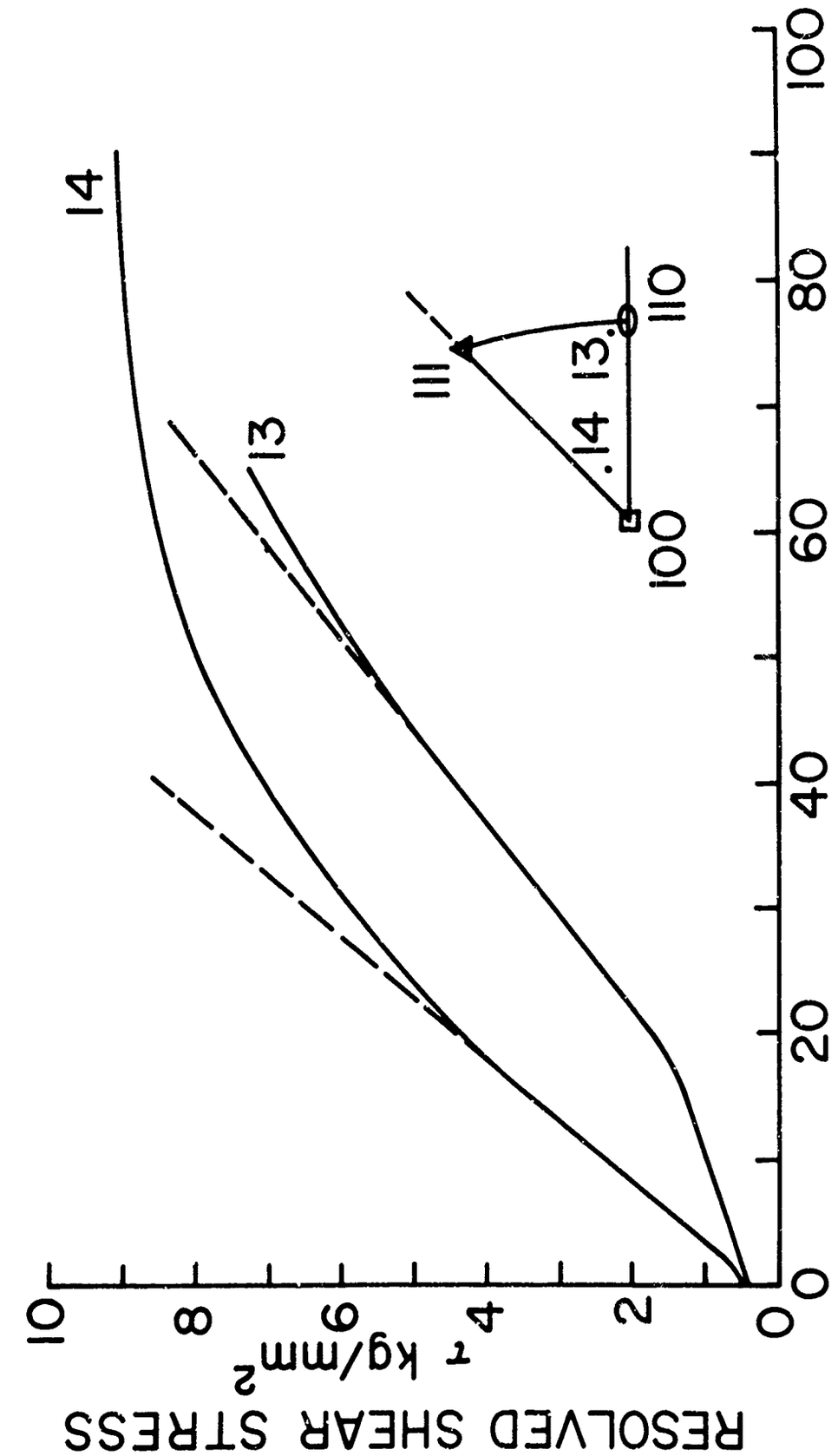

Fig. 4(b). Work hardening curves of crystals and their orientations.

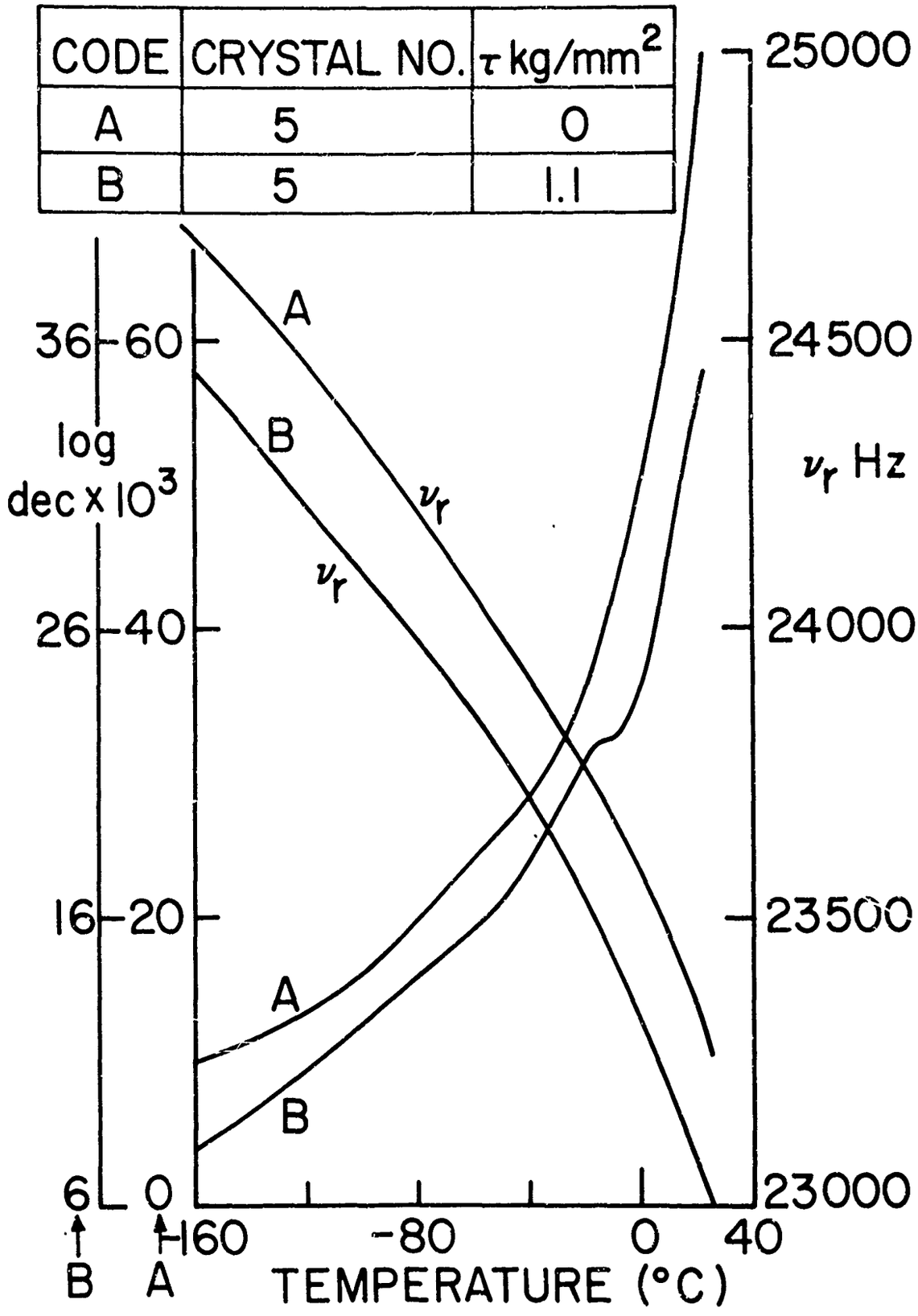

Fig. 5. Log.dec. and ν_r vs T at H = 0 in annealed crystal and after stress τ = 1.1 Kg/mm^2.

CODE	CRYSTAL NO.	τ kg/mm^2
A	5	4.8
B	5	6.7
C	5	7.8
D	5	8.8

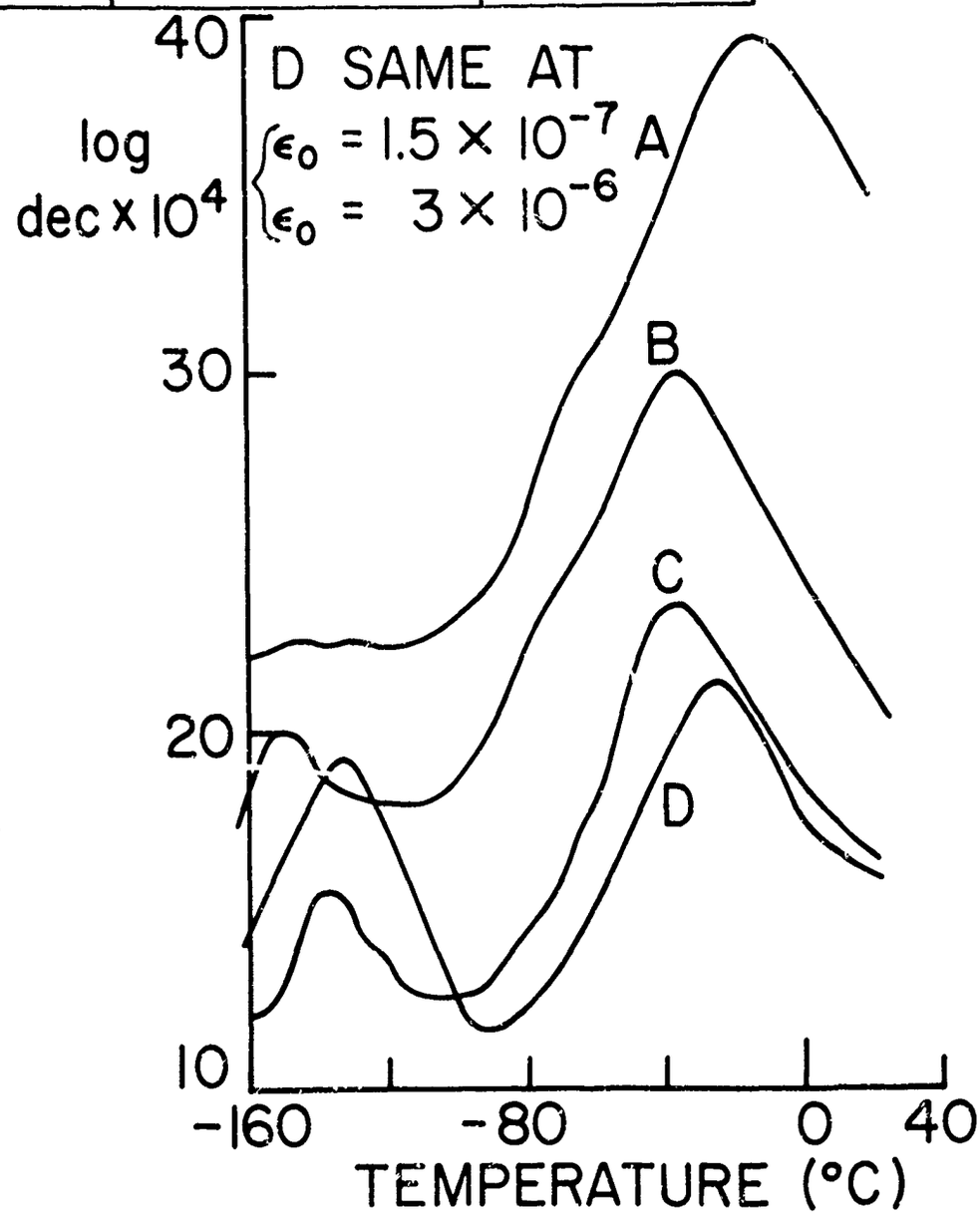

Fig. 6. Log.dec. vs T at H = 0 after deformation to τ = 4.8, 6.7, 7.8 and 8.8 Kg/mm^2.

CODE	CRYSTAL NO.	τ kg/mm^2	ν_c
A	5	4.8	2.5
B	5	6.7	1.5
C	5	7.8	0.3
D	5	8.8	0

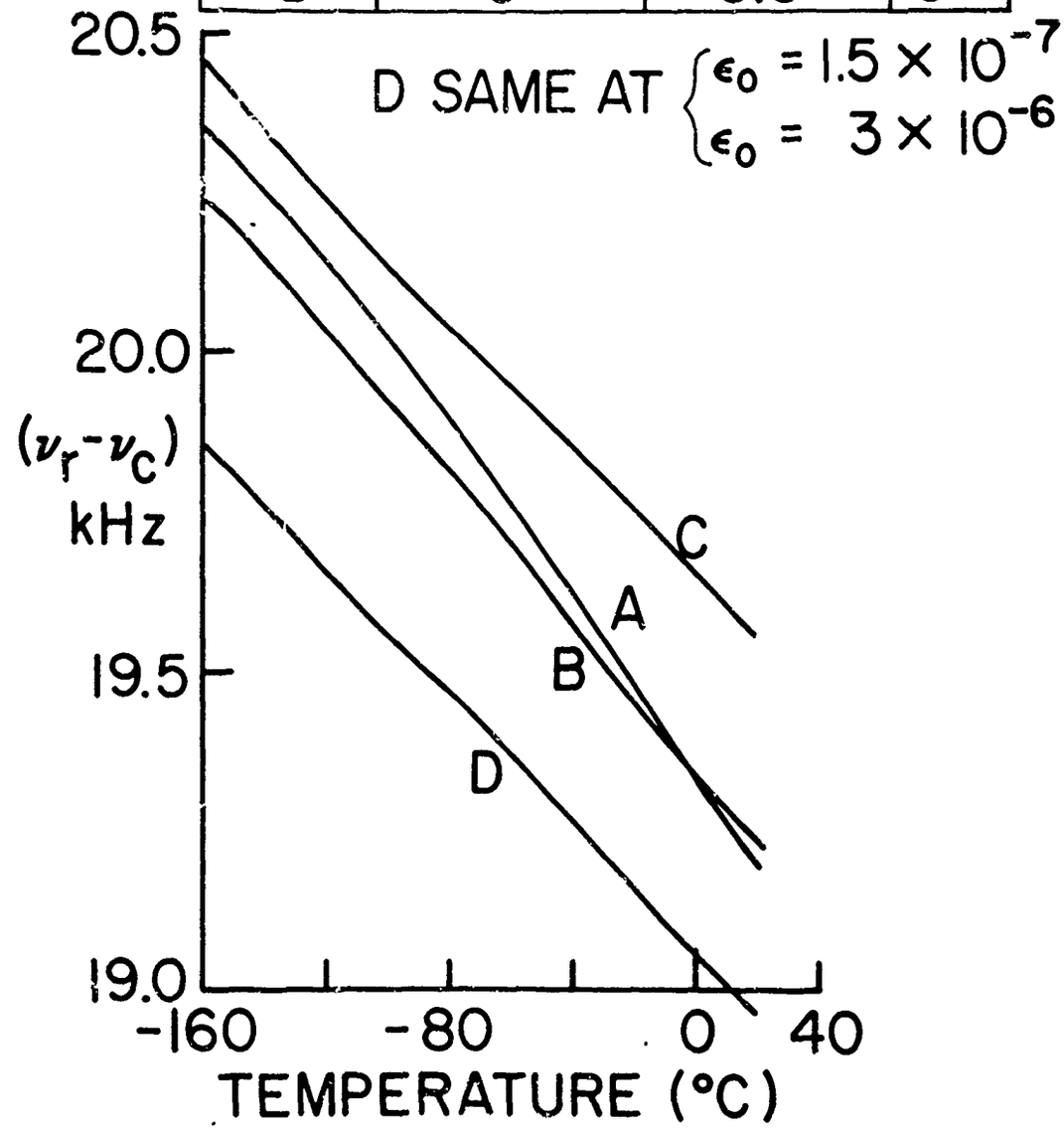

Fig. 7. ν_r vs T at H = 0 after deformation to τ = 4.8, 6.7, 7.8 and 8.8 Kg/mm^2.

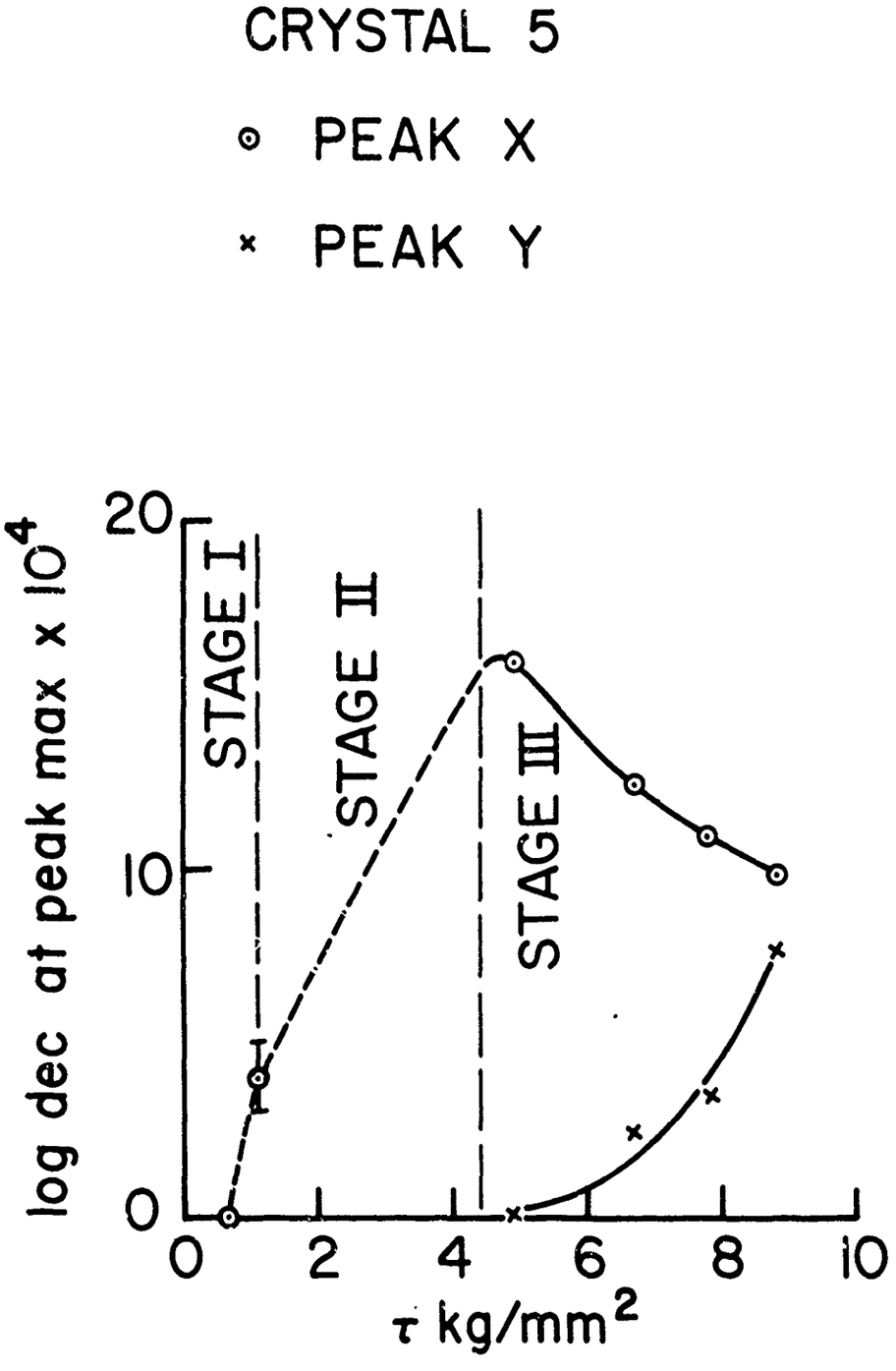

Fig. 8. Correlation of the heights of peaks X and Y with resolved shear stress τ.

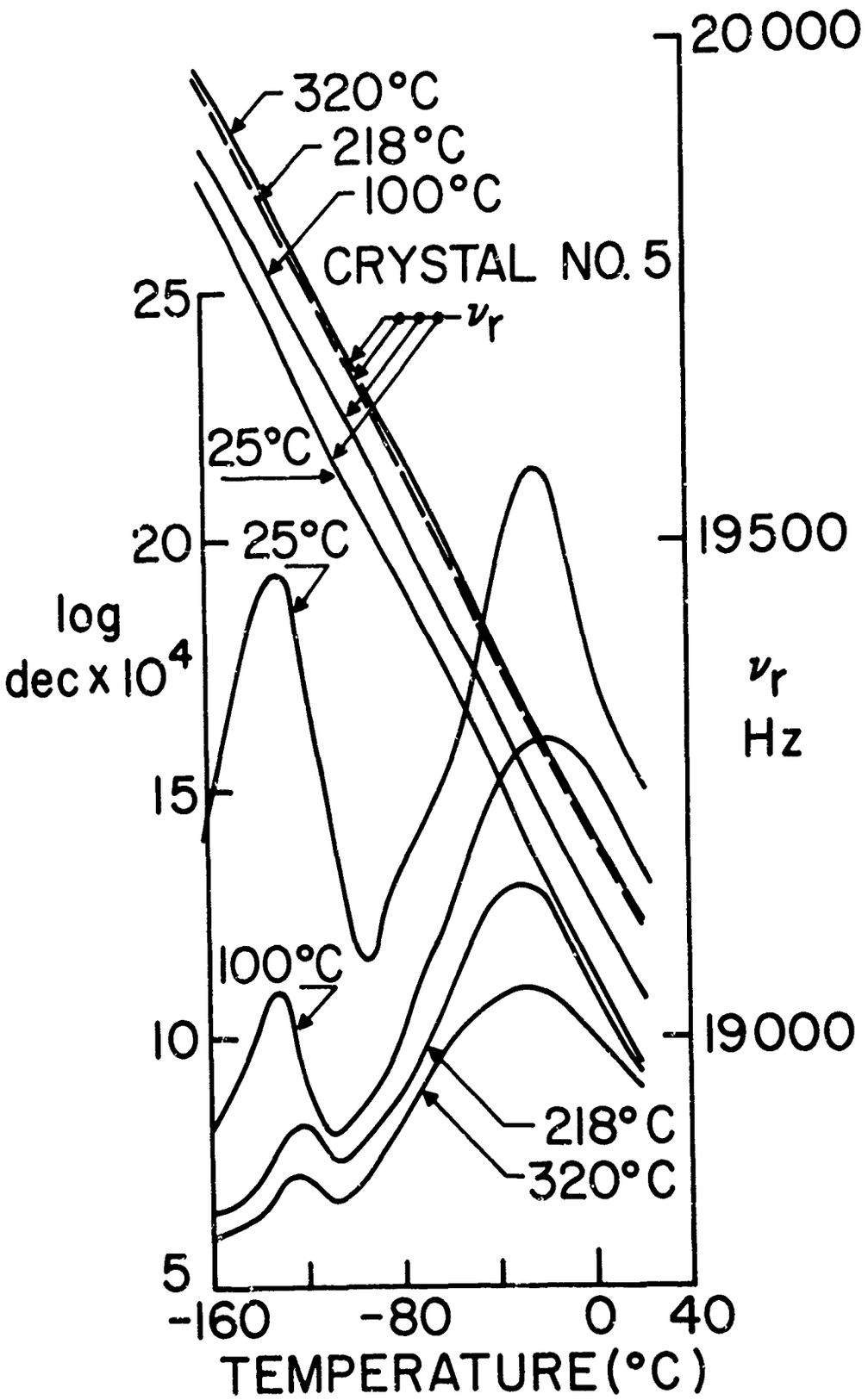

Fig. 9. The response of log.dec. and ν_r vs T at H = 0 to isochronal annealing (30 min at each T). Initially deformed to τ = 8.8 Kg/mm^2.

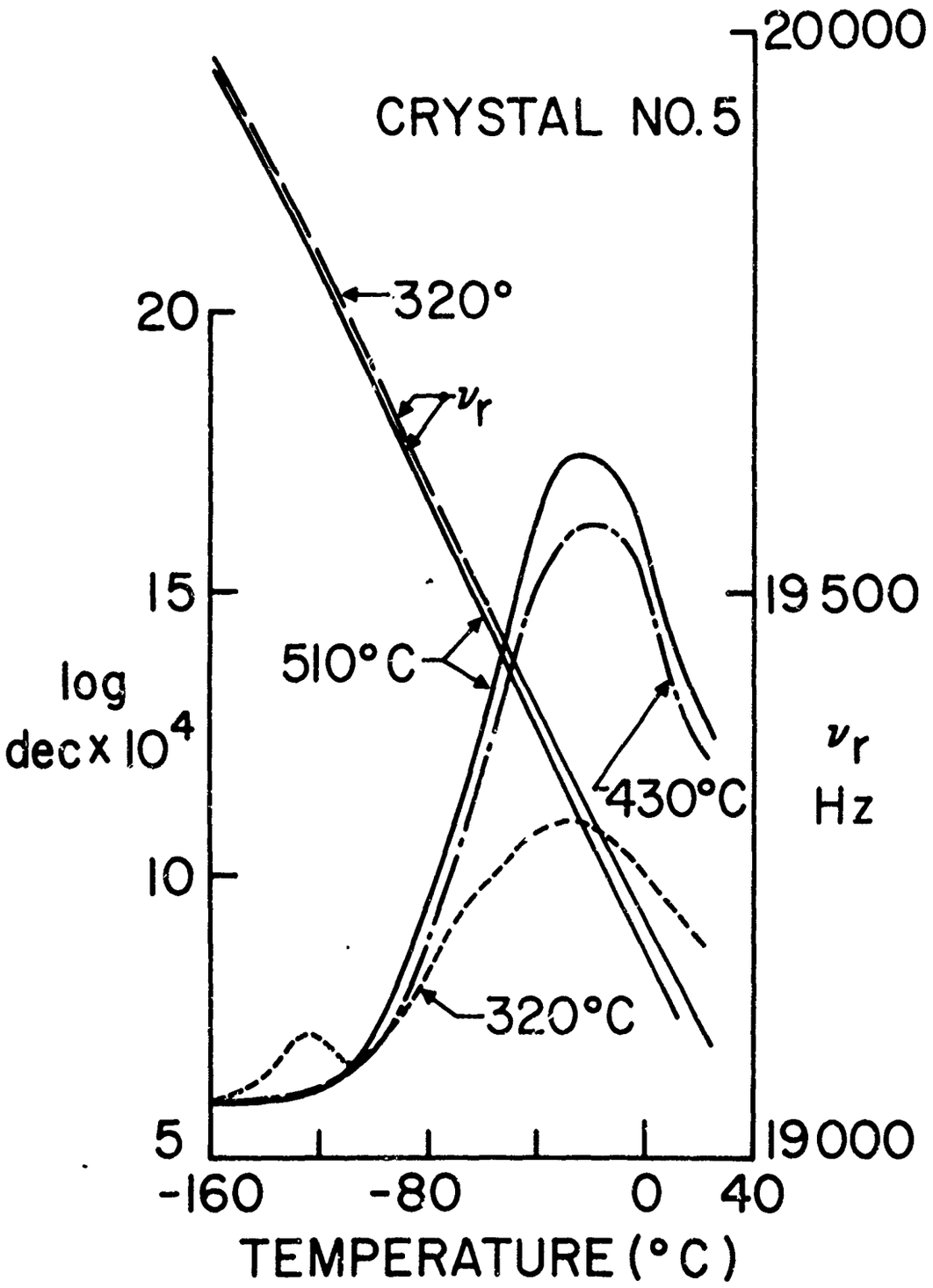

Fig. 10. The response of log.dec. and ν_r vs T at H = 0 to isochronal annealing (30 min. at each T). Initially deformed to τ = 8.8 Kg/mm^2.

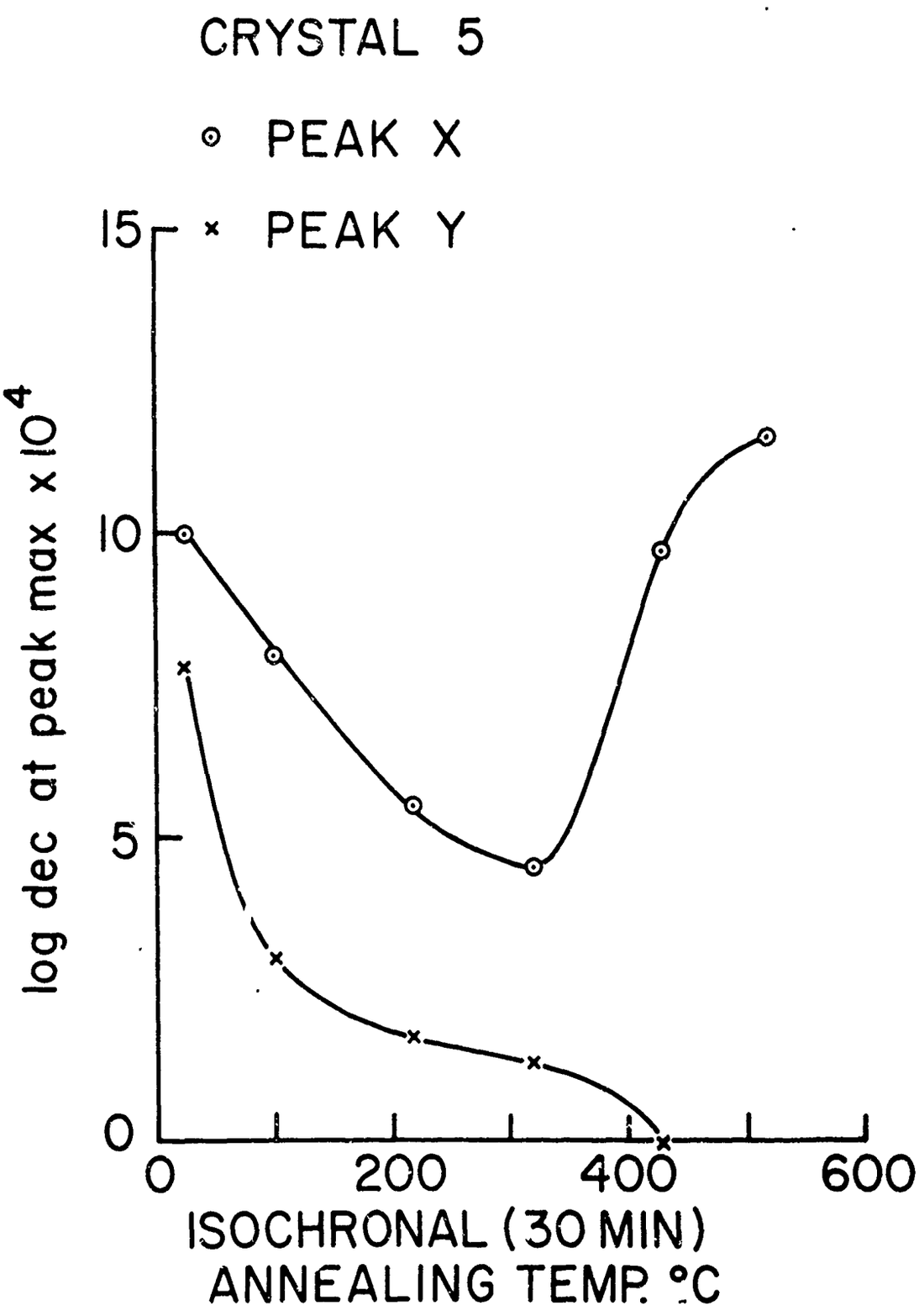

Fig. 11. Variation of damping peak heights with isochronal (30 min) annealing temperature. Initially deformed to $\tau = 8.8$ Kg/mm^2.

CODE	CRYSTAL NO.	MAG. FIELD H	τ kg/mm^2	C
A	II	200 Oe	0	5
A′	II	0	0	5
B	II	0	1.3	1

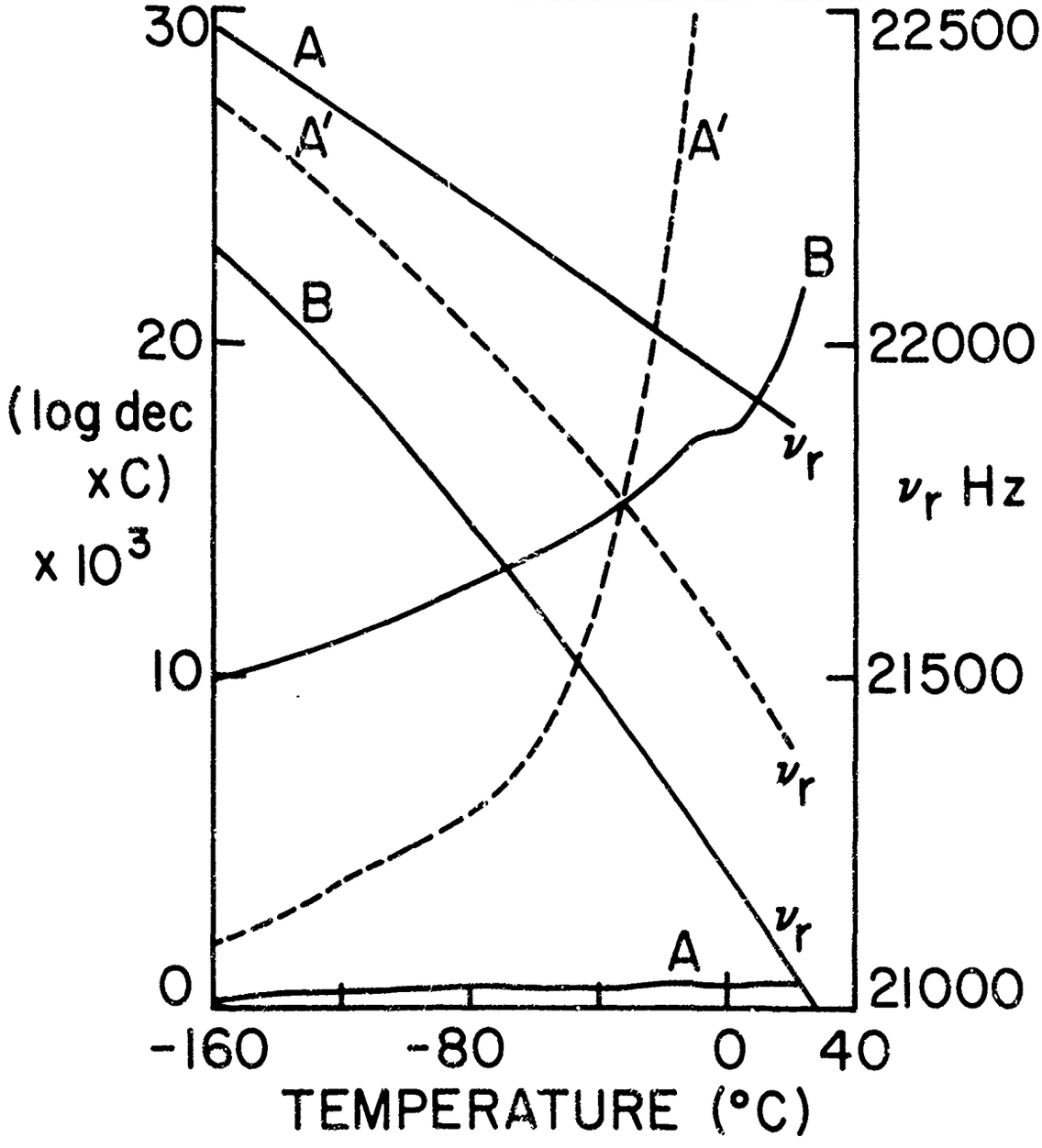

Fig. 12. Log.dec. and ν_r vs T at H = 0 and H = 200 Oe for annealed crystal and at H = 0 after deformation to τ = 1.3 Kg/mm^2.

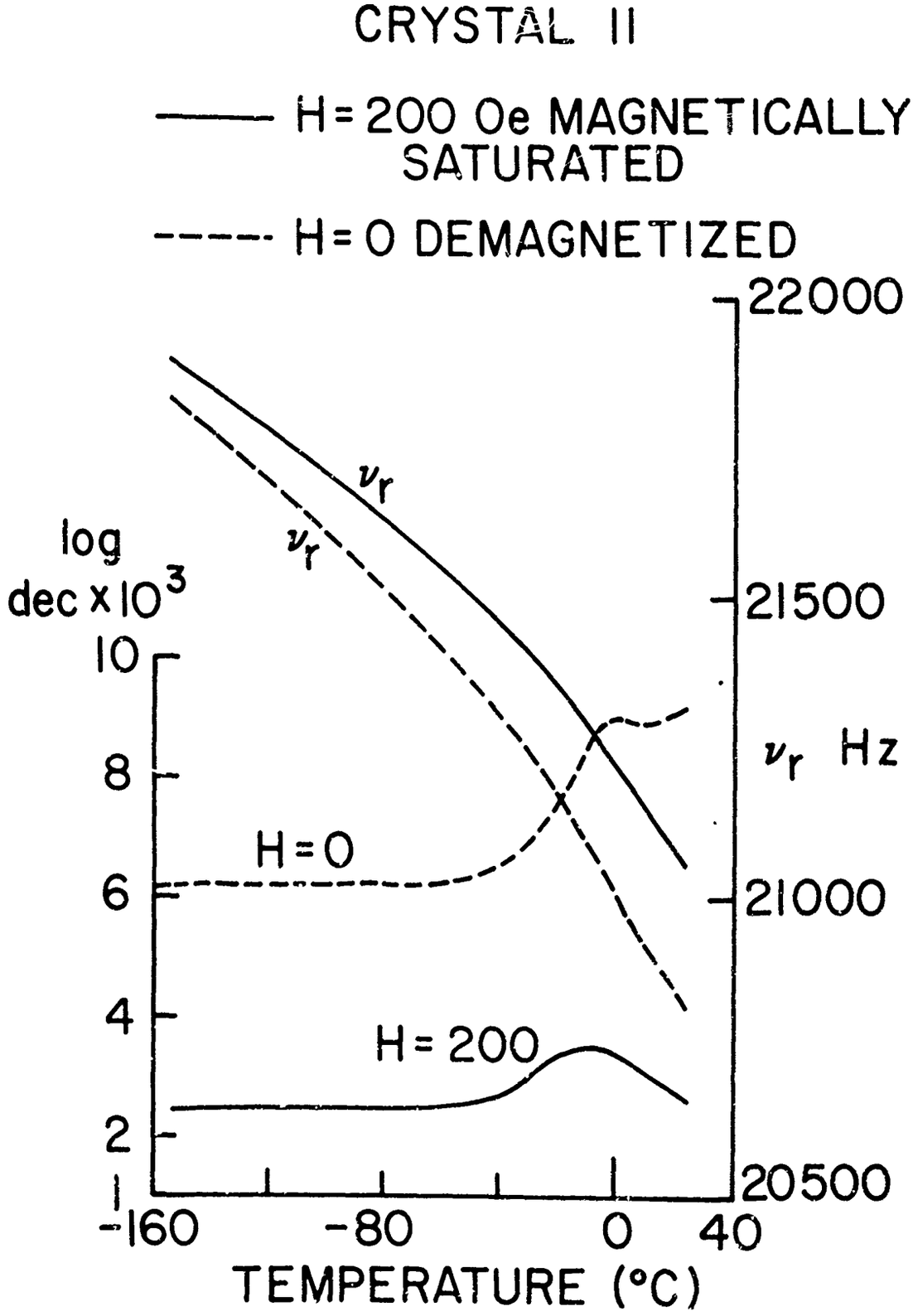

Fig. 13. Log.dec. and ν_r vs T at H = 0 and H = 200 Oe after deformation to τ = 2.28 Kg/mm^2.

CODE	CRYSTAL NO.	τ kg/mm^2	ν_C
A	II	4.88	.8
B	II	7.4	0
C	II	8.15	0

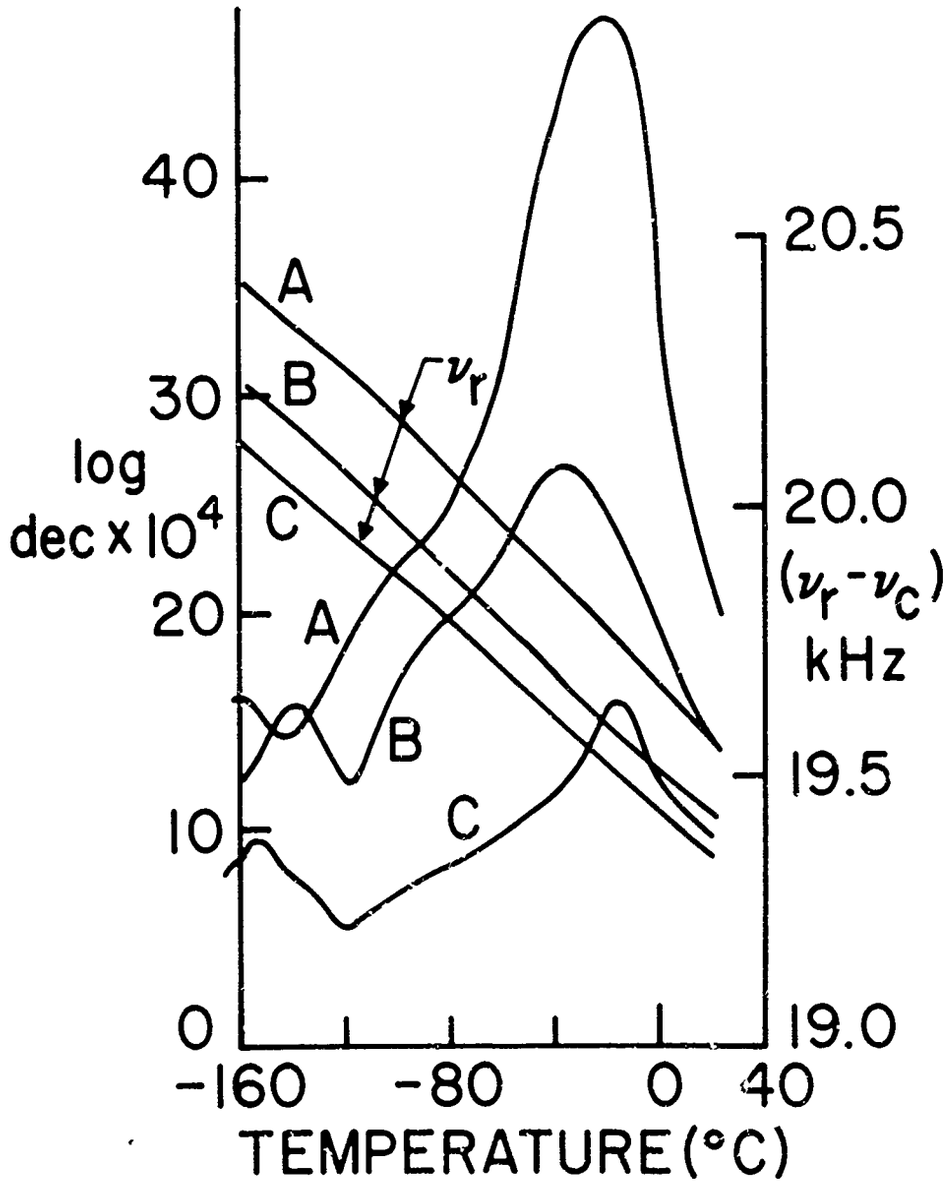

Fig. 14. Log.dec. and ν_r vs T at H = 0 after deformation to τ = 4.88, 7.4 and 8.15 Kg/mm^2.

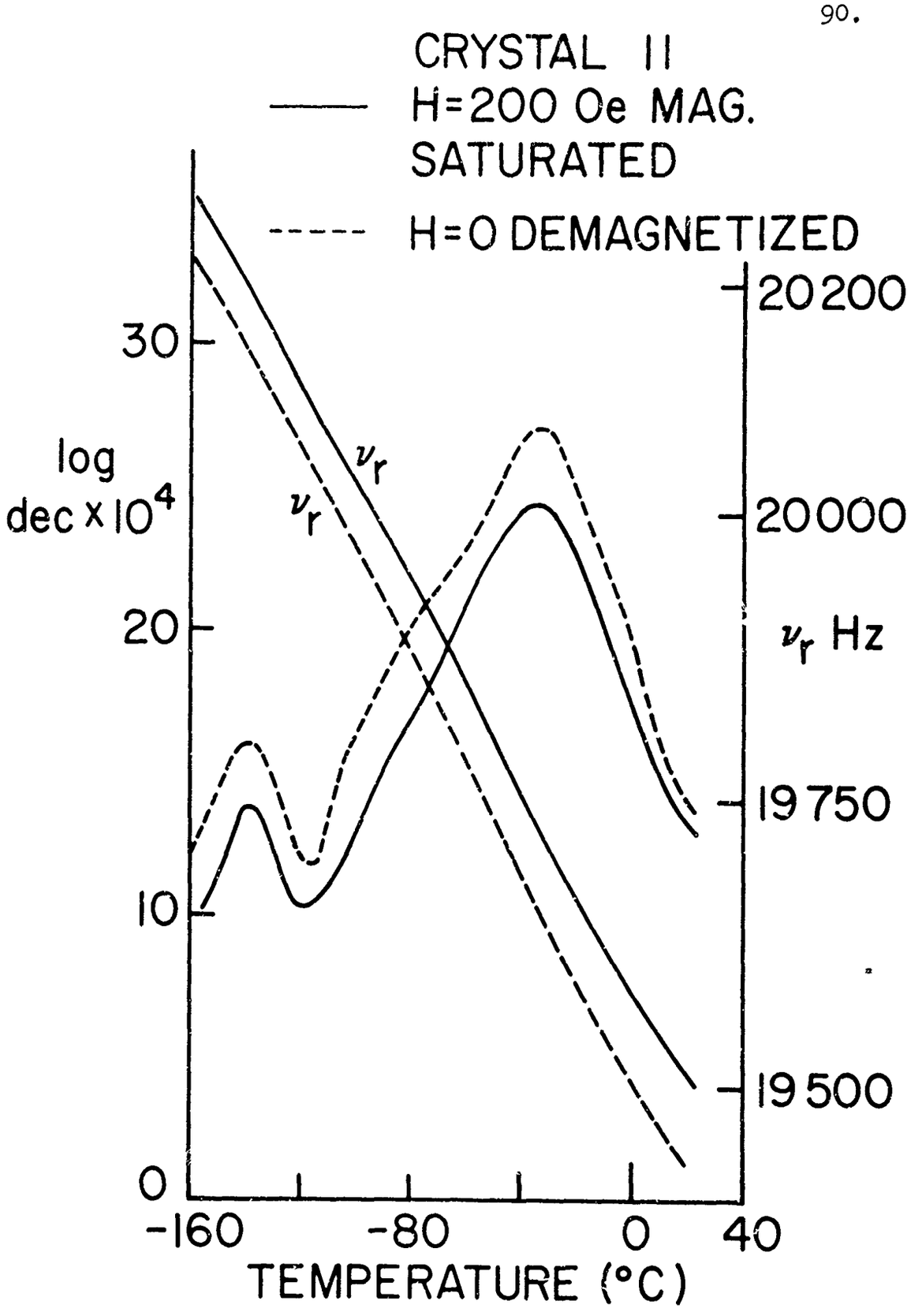

Fig. 15. Log. dec. and ν_r vs T at H = 0 and H = 200 Oe after deformation to τ = 7.4 Kg/mm^2.

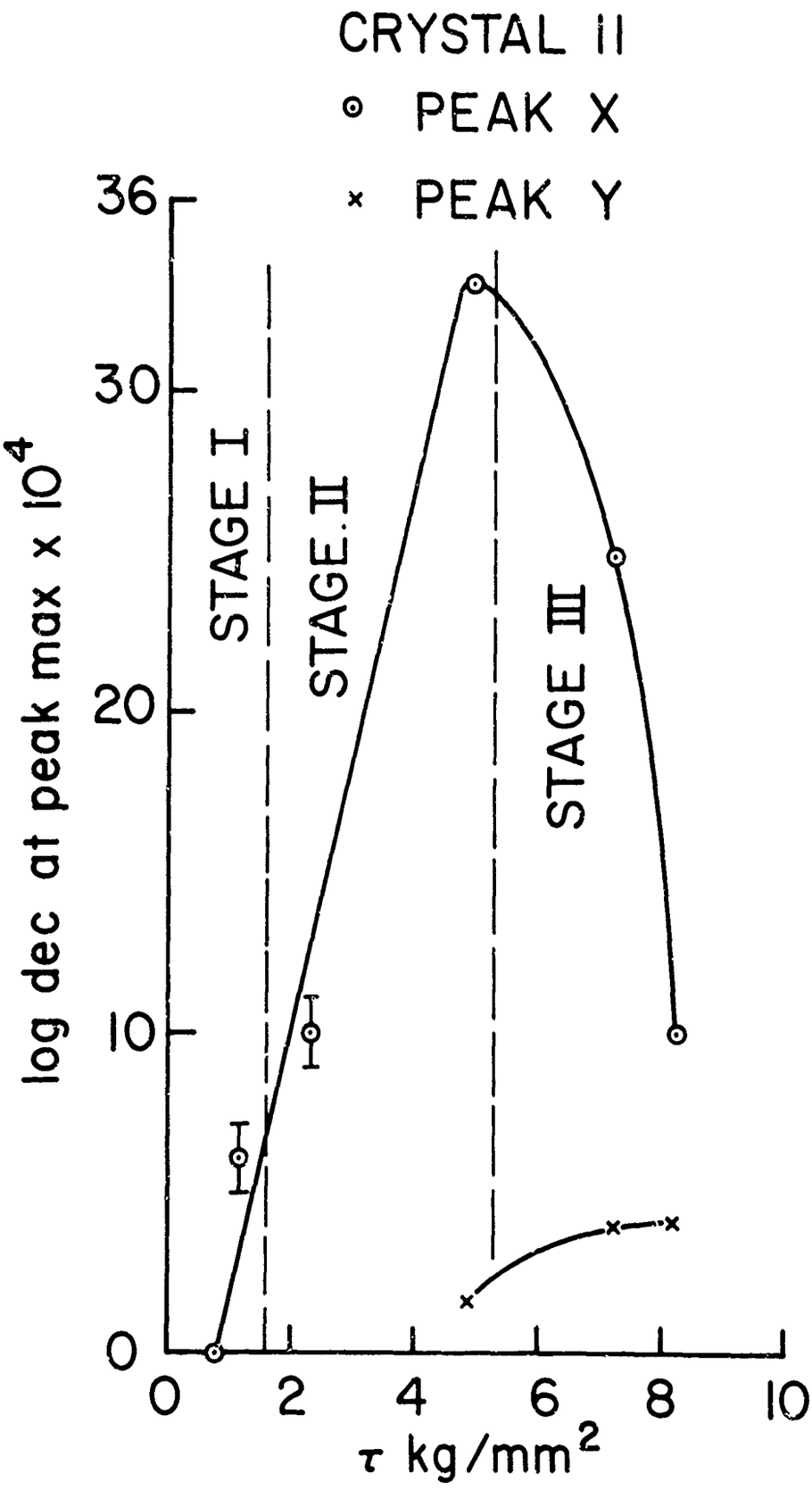

Fig. 16. Correlation of the heights of peaks X and Y with τ.

CODE	CRYSTAL NO.	ν_c	REMARKS
A	11	43.1	GRIPS CUT OFF
B	11	0	WITH GRIPS

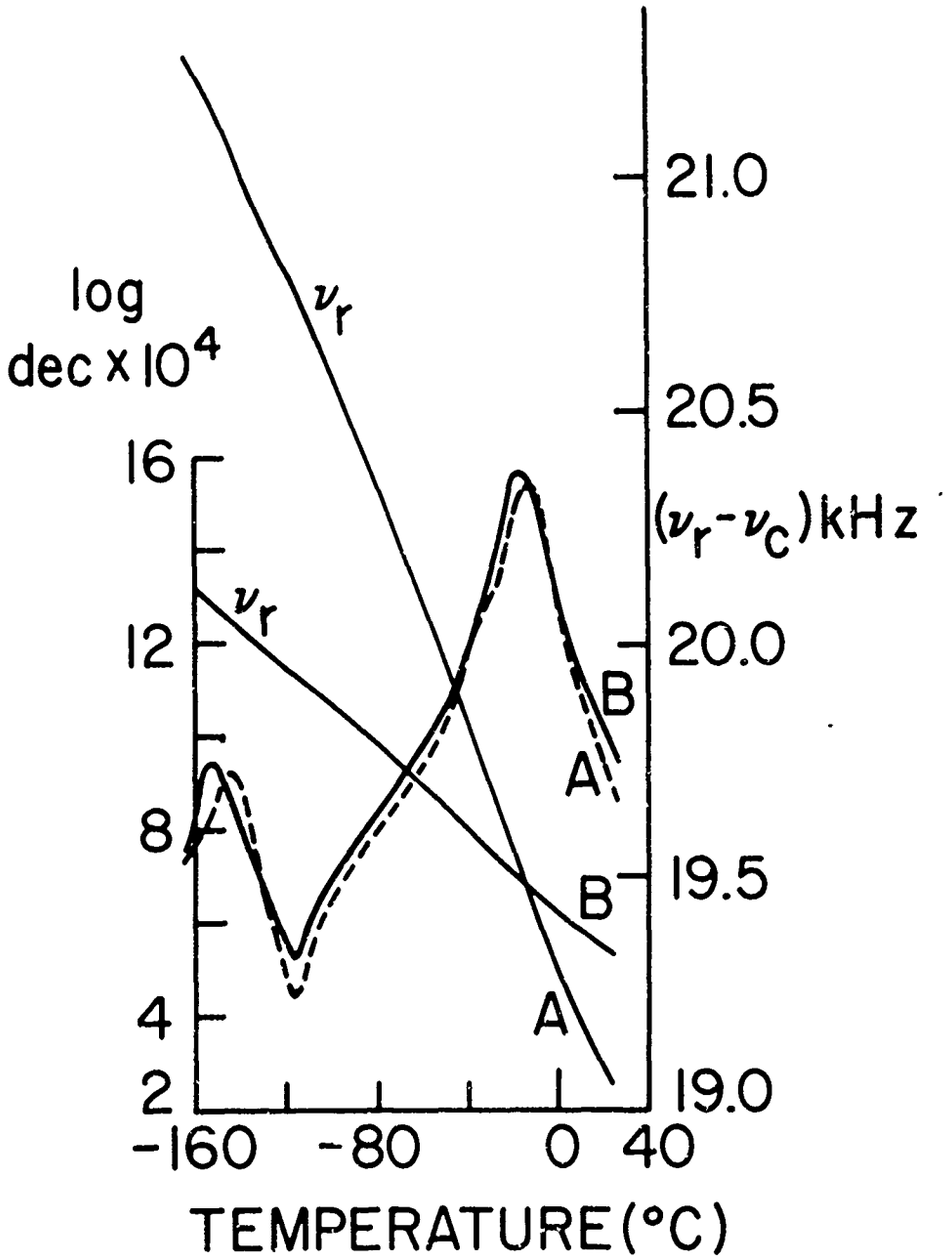

Fig. 17. Log.dec. and ν_r vs T at H = 0 for specimen with and without grips after deformation to τ = 8.15 Kg/mm^2.

CODE	CRYSTAL NO.	τ_{kg/mm^2}	ν_c	C
A	16	0	2	3
B	16	.91	0	4

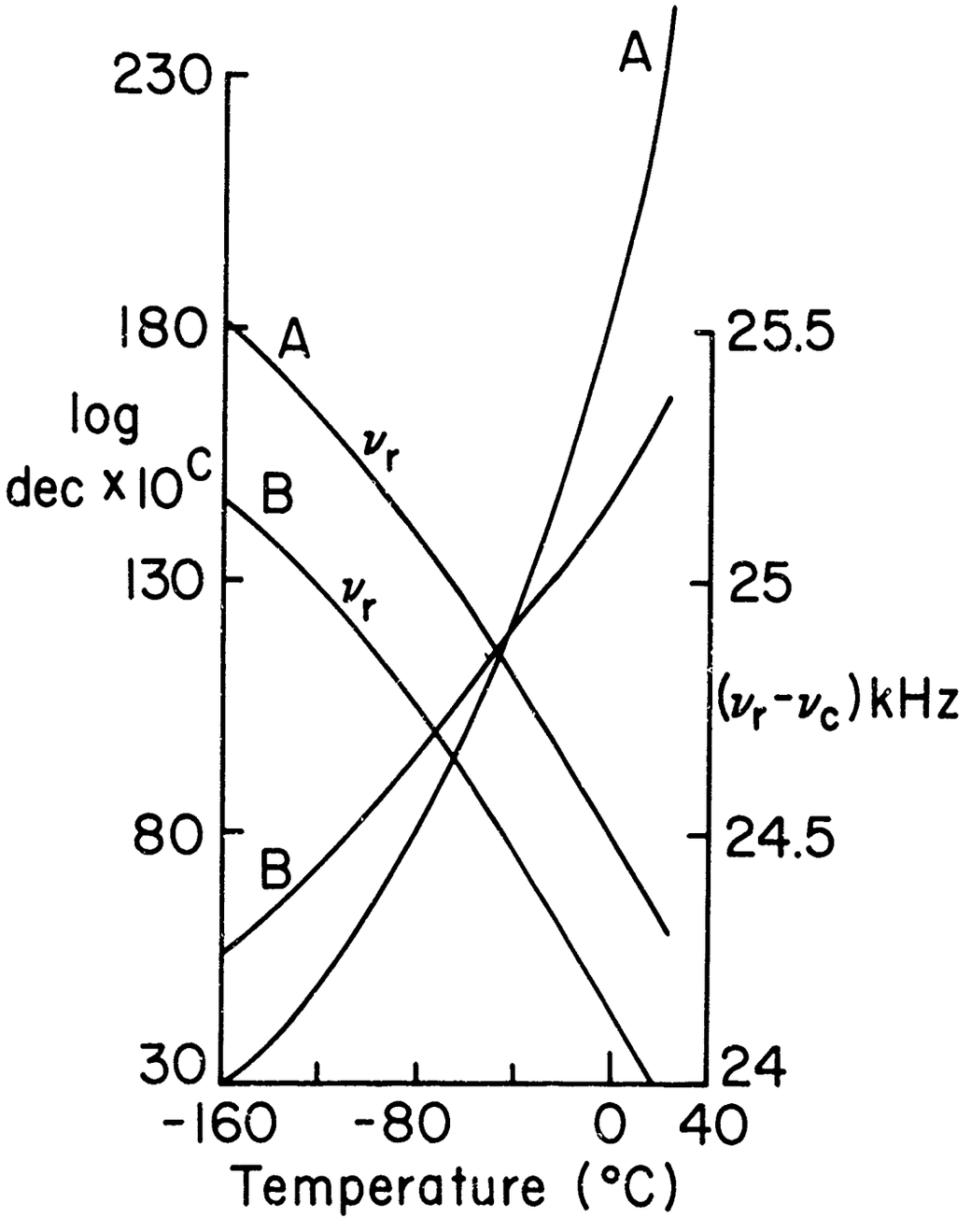

Fig. 18. Log. dec. and ν_r vs T at H = 0 in annealed crystal and after deformation to τ = .91 Kg/mm^2.

CODE	CRYSTAL NO.	τ kg/mm^2
A	16	5.14
B	16	6.45
C	16	7.81
D	16	9.08

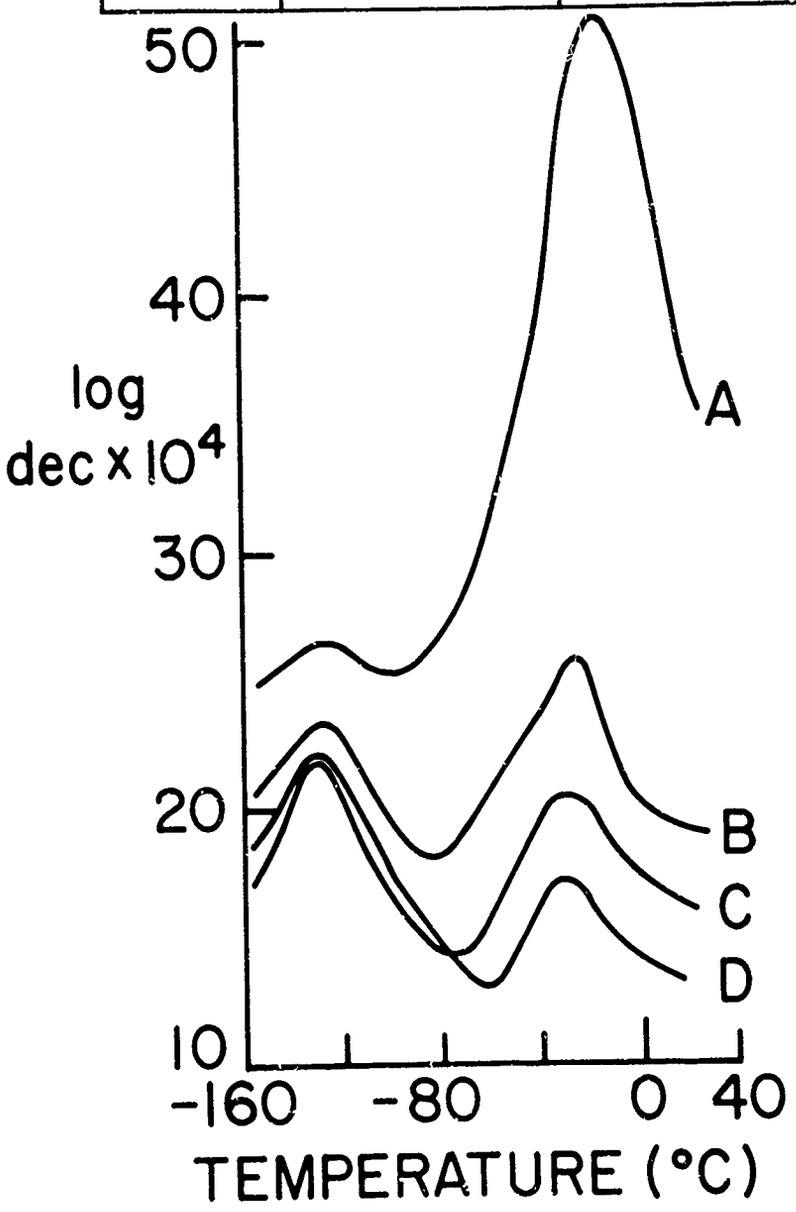

Fig. 19. Log. dec. vs T at H = 0 after deformation to τ = 5.14, 6.45, 7.81 and 9.08 Kg/mm^2.

CODE	CRYSTAL NO.	τ kg/mm^2	ν_c
A	16	5.14	2.0
B	16	6.45	1.5
C	16	7.81	0.9
D	16	9.08	0

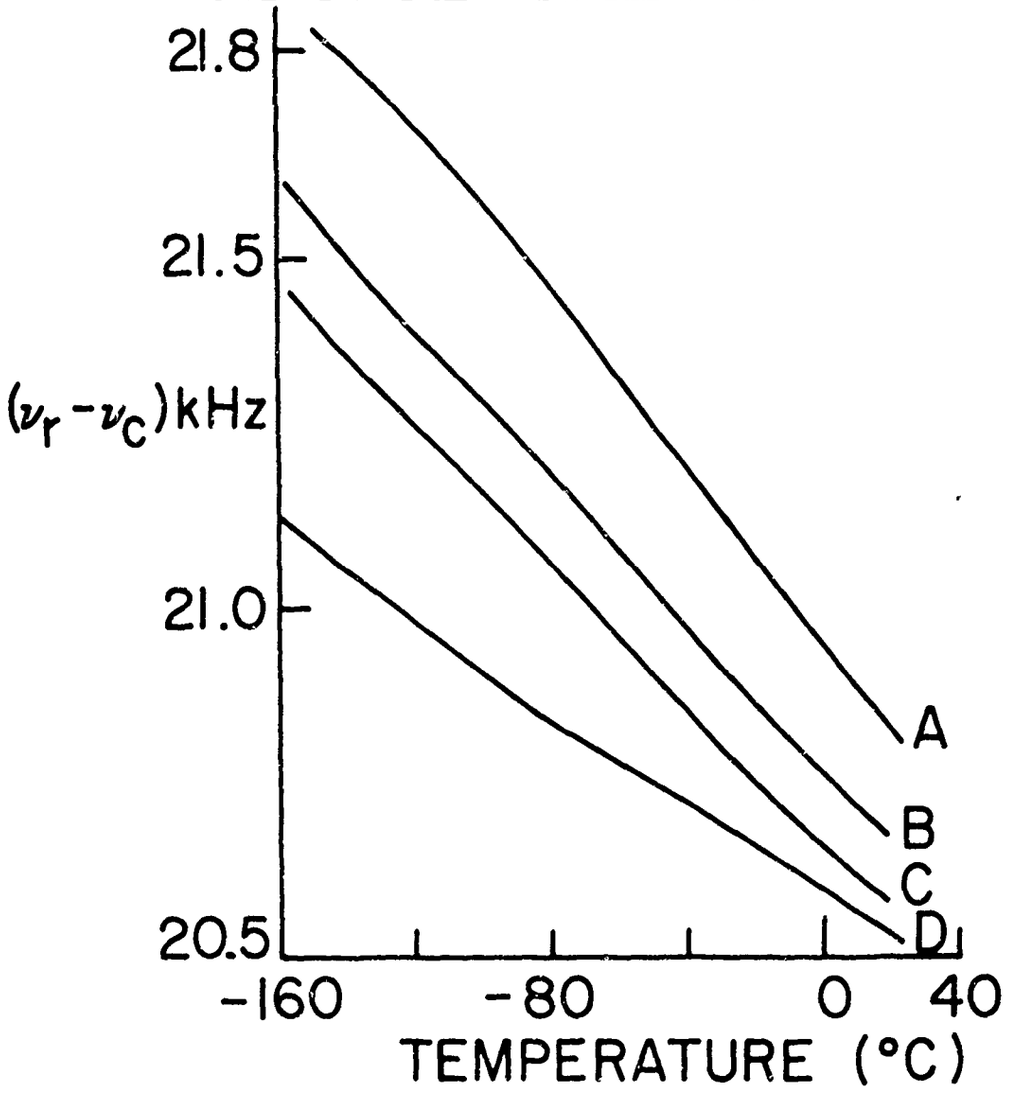

Fig. 20. ν_r vs T at H = 0 after deformation to τ = 5.14, 6.45, 7.81 and 9.08 Kg/mm^2.

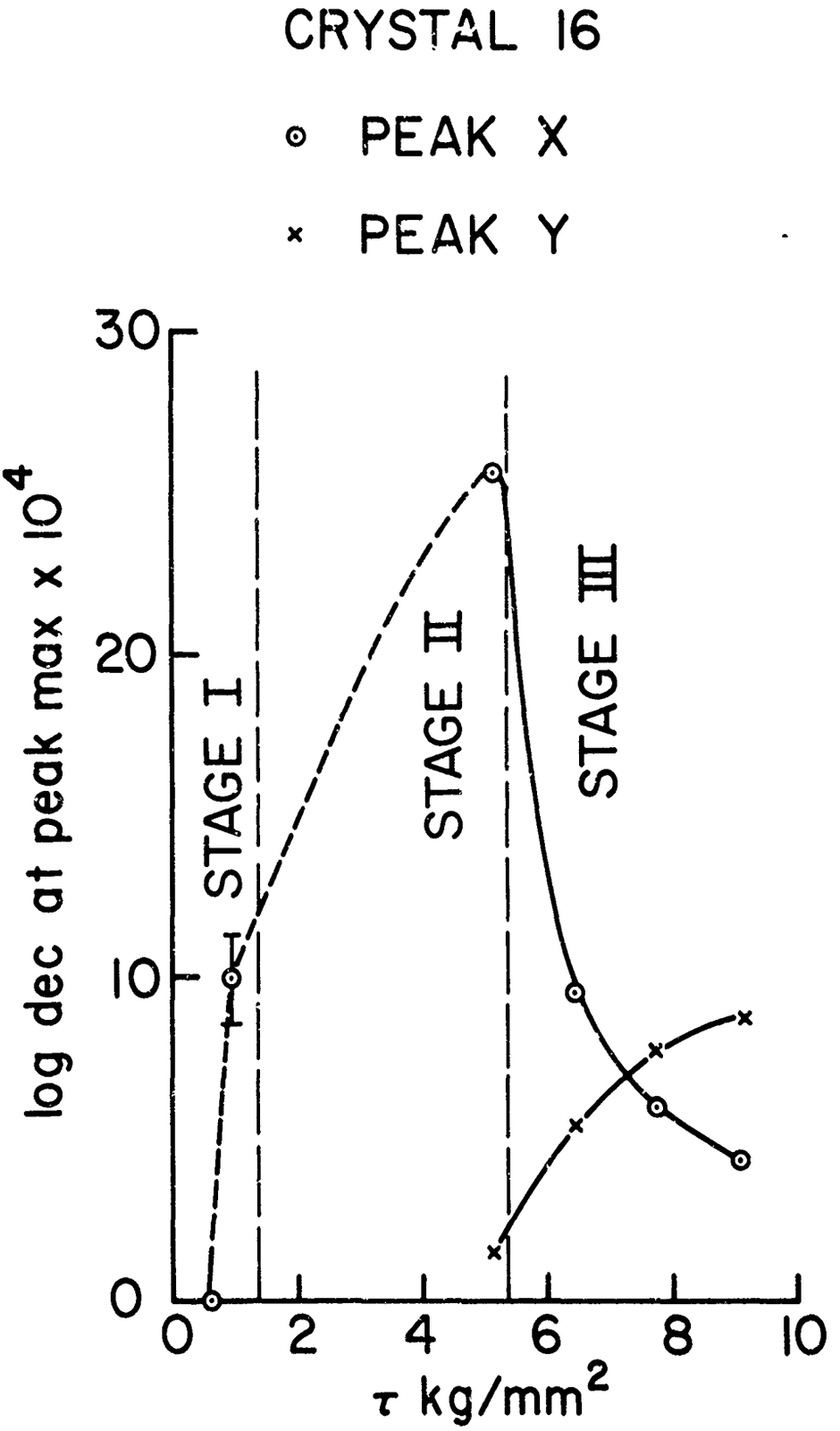

Fig. 21. Correlation of heights of peaks X and Y with τ.

CODE	CRYSTAL NO.	τ kg/mm^2
A	17	9.13
B	16	9.08

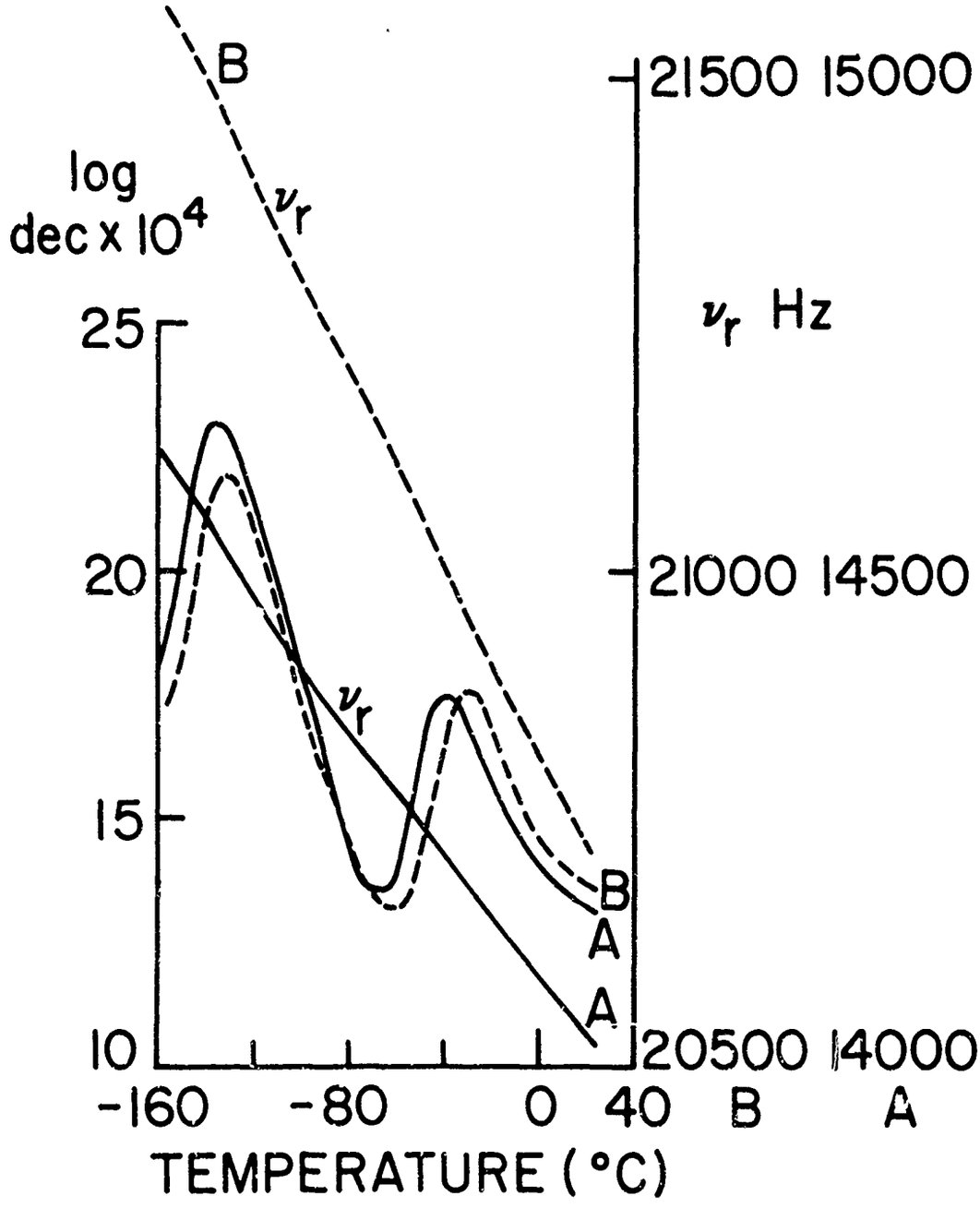

Fig. 22. Log.dec. and ν_r vs T at H = 0 in crystals 16 and 17 after deformation to the same resolved shear stress τ.

CODE	CRYSTAL NO.	τ kg/mm^2
A	18	3.3
B	18	4.5
C	18	5.7
D	18	6.7

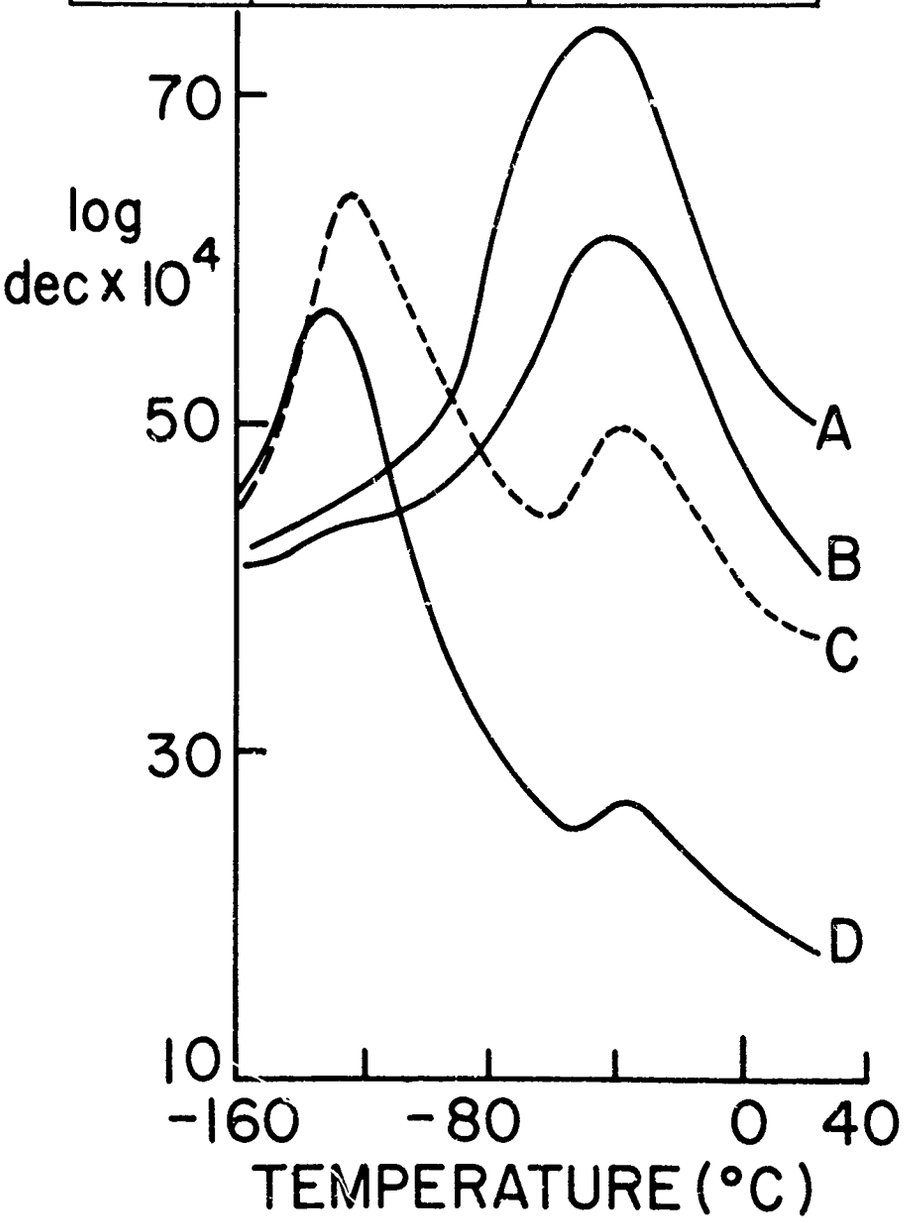

Fig. 23. Log.dec. vs T at H = 0 after deformation to τ = 3.3, 4.5, 5.7 and 6.7 Kg/mm^2.

CODE	CRYSTAL NO.	τ kg/mm^2	ν_c (k Hz)
A	18	3.3	2.6
B	18	4.5	1.8
C	18	5.7	1.9
D	18	6.7	0

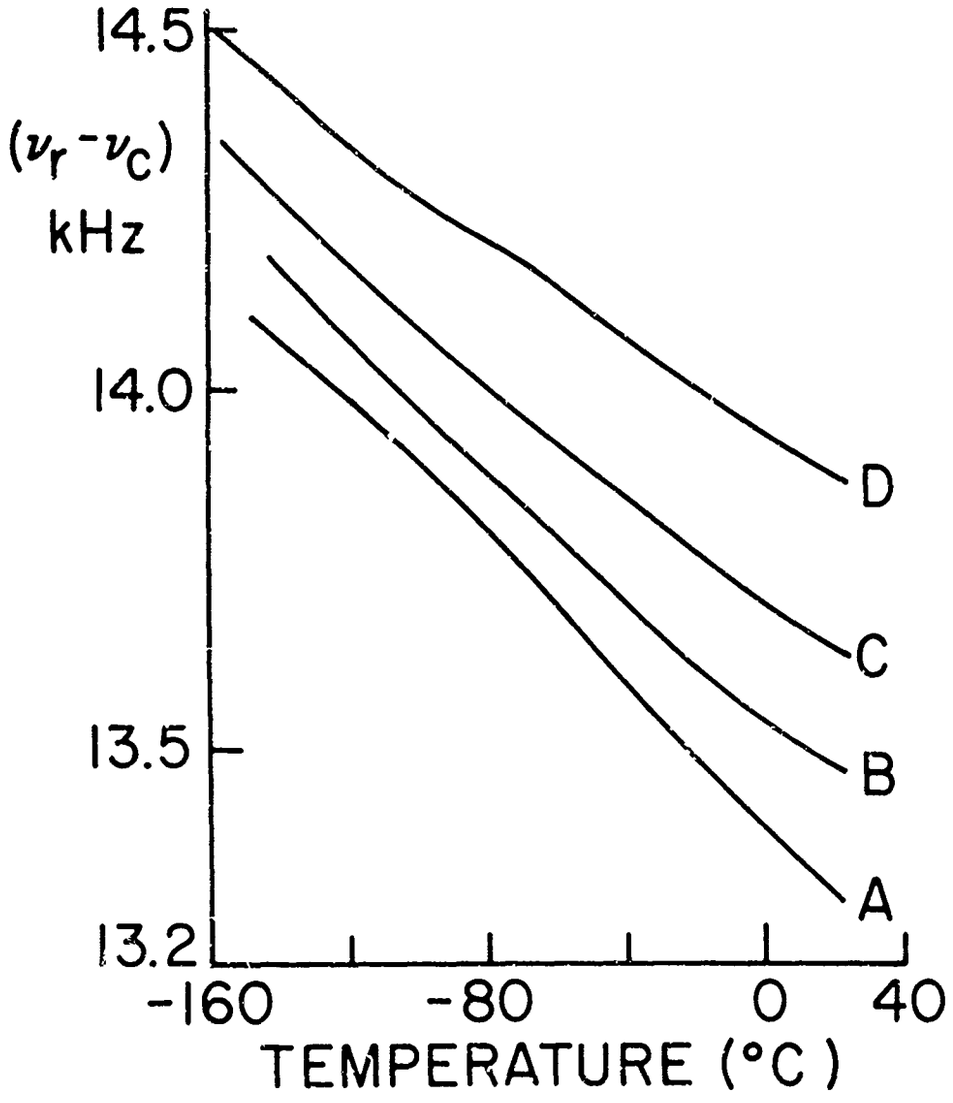

Fig. 24. ν_r vs T at H = 0 after deformation to τ = 3.3, 4.5, 5.7 and 6.7 Kg/mm^2.

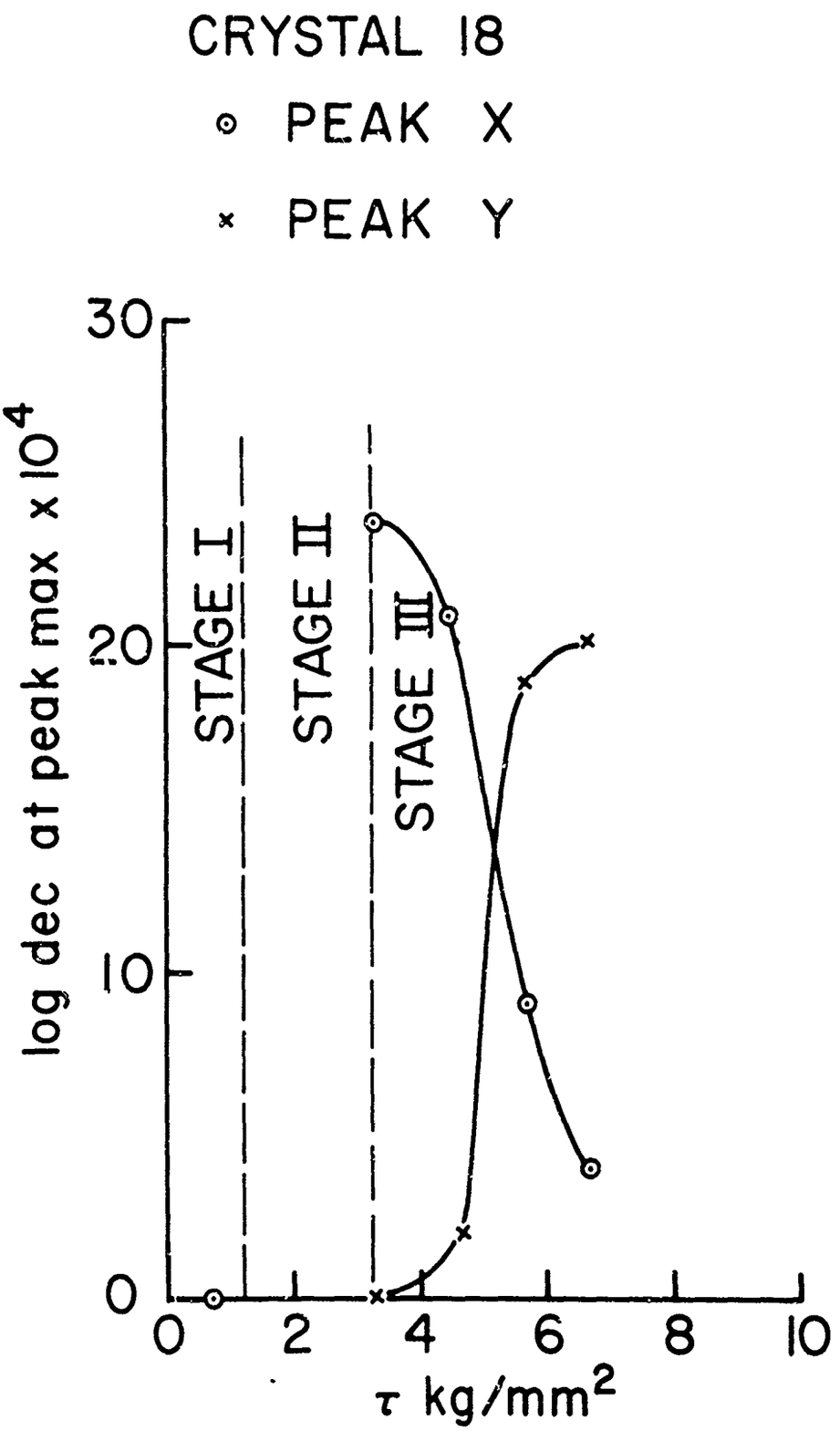

Fig. 25. Correlation of the heights of peaks X and Y with τ.

CODE	CRYSTAL NO.	τ kg/mm^2
A	13	.93
B	13	1.8

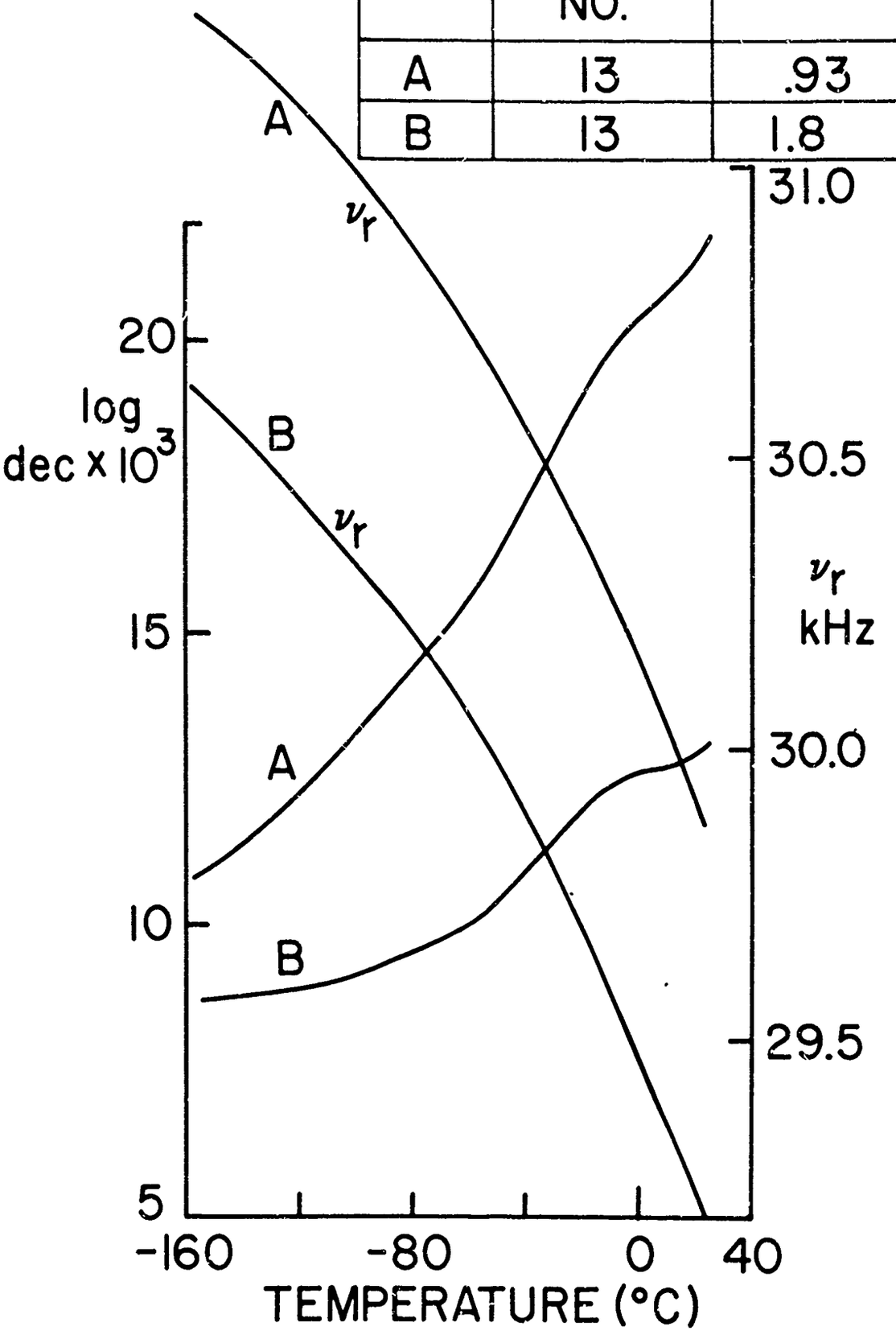

Fig. 26. Log.dec. and ν_r vs T at H = 0 after deformation to τ = .93 and 1.8 Kg/mm^2.

CODE	CRYSTAL NO.	τ kg/mm^2
A	13	2.57
B	13	3.08

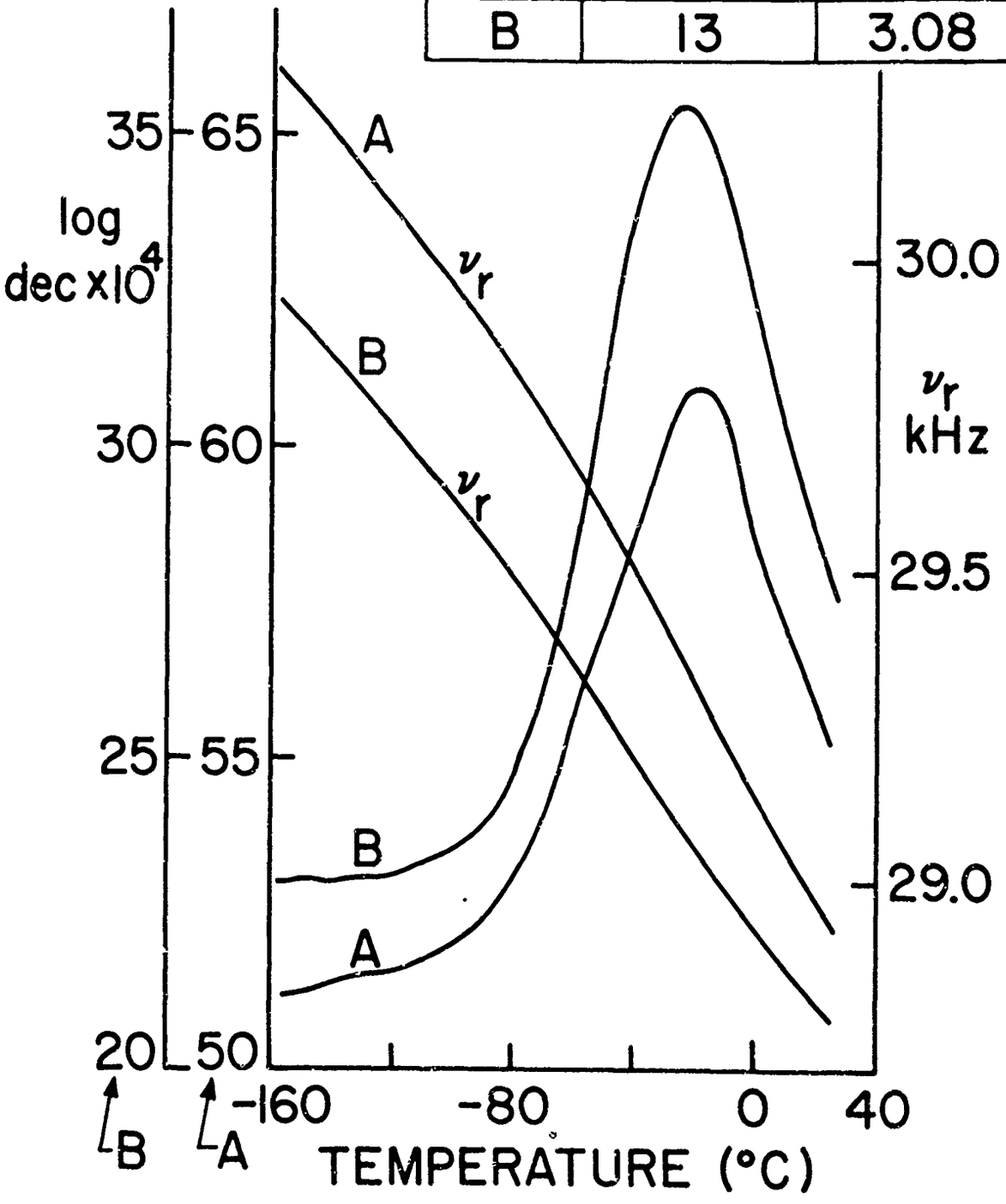

Fig. 27. Log.dec. and ν_r vs T at H = 0 after deformation to τ = 2.57 and 3.08 Kg/mm^2.

CODE	CRYSTAL NO.	τ kg/mm^2	ν_c
A	13	4.12	.8
B	13	5	0

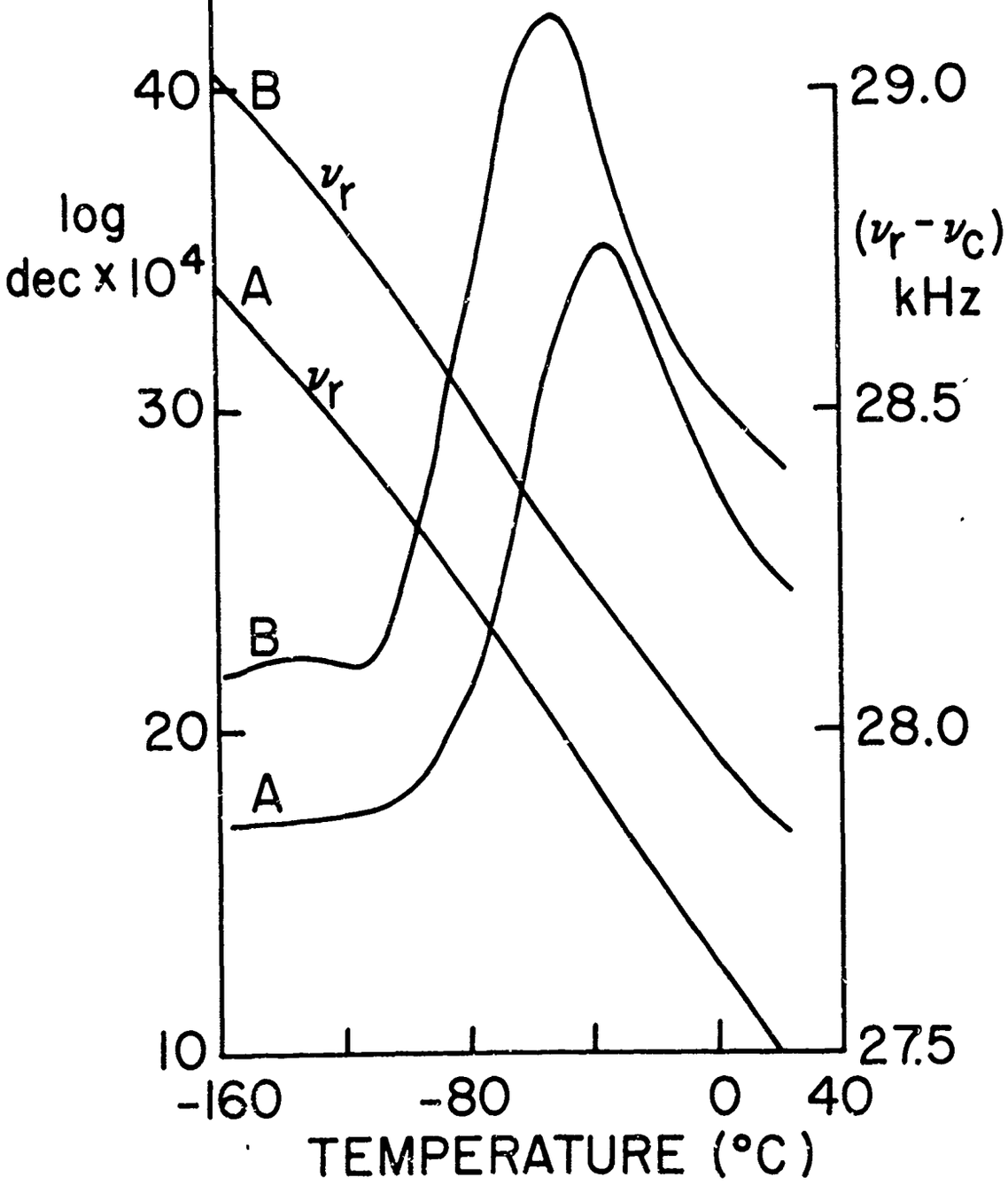

Fig. 28. Log.dec. and ν_r vs T at H = 0 after deformation to τ = 4.12 and 5 Kg/mm^2.

CODE	CRYSTAL NO.	τ kg/mm^2	ν_c
A	13	6.0	.5
B	13	7.3	0

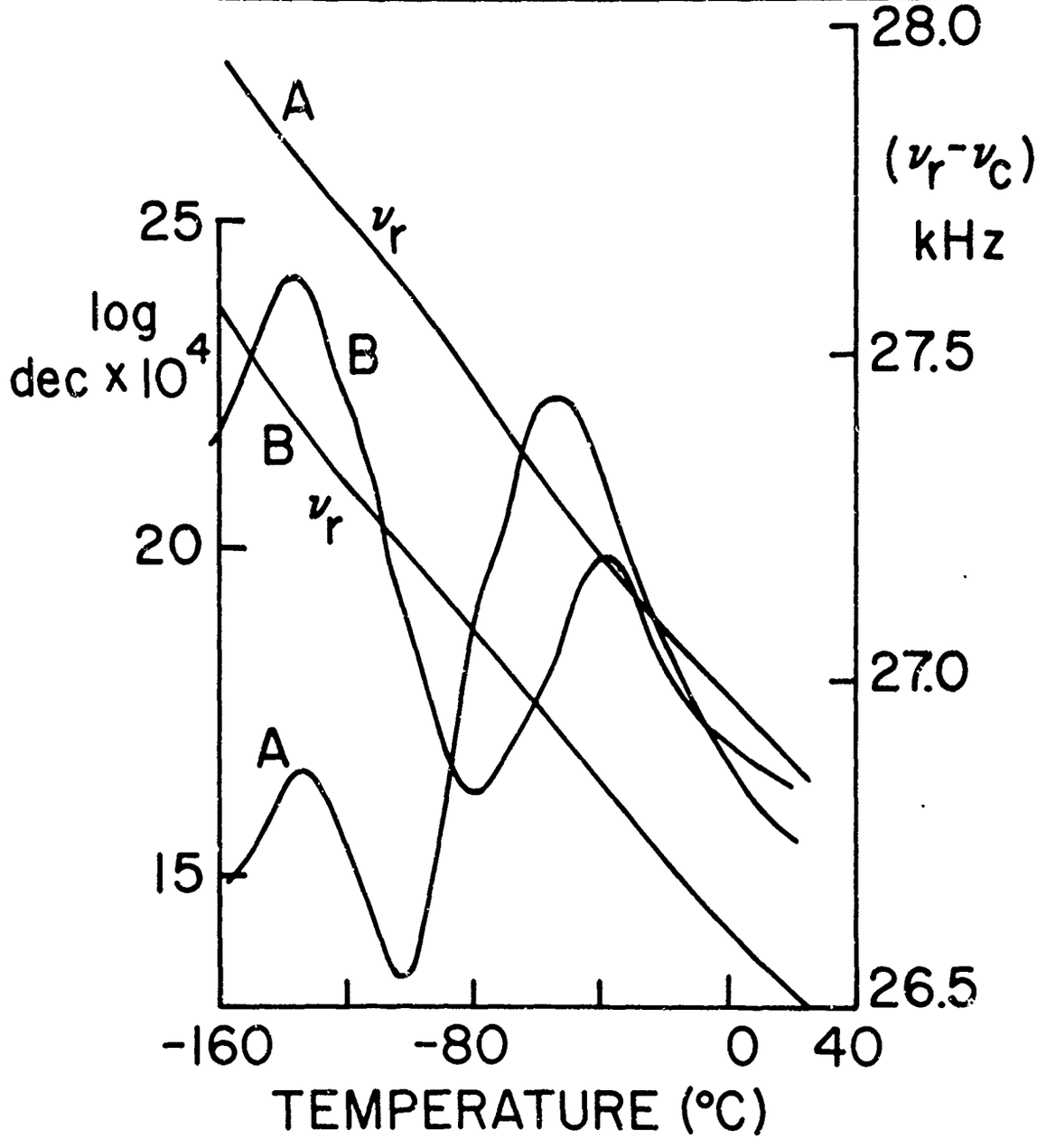

Fig. 29. Log.dec. and ν_r vs T at H = 0 after deformation to τ = 6 and 7.3 Kg/mm^2.

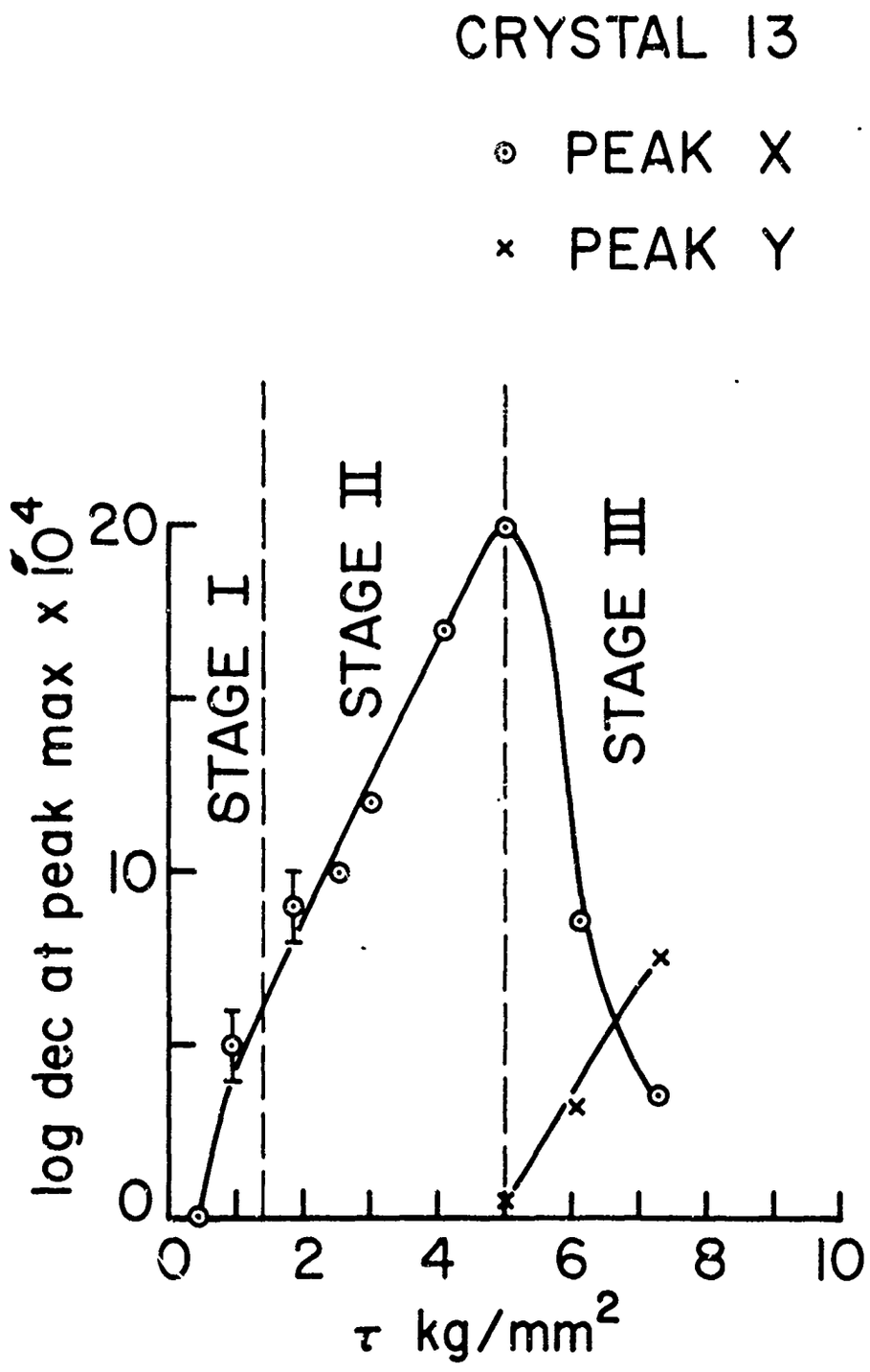

Fig. 30. Correlation of the heights of peaks X and Y with τ.

CODE	CRYSTAL NO.	τ kg/mm^2	ν_c
A	14	1	.7
B	14	2	0

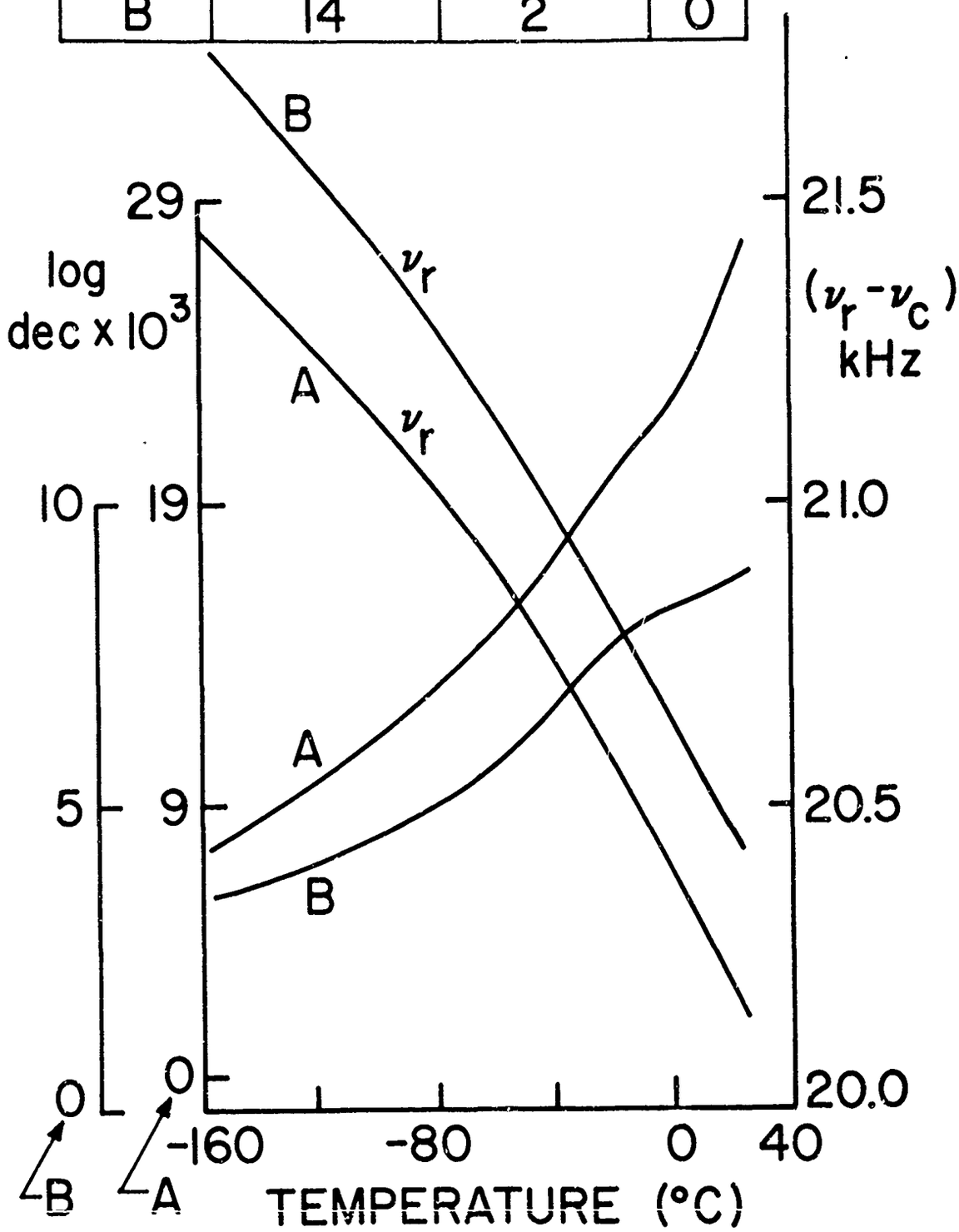

Fig. 31. Log.dec. and ν_r vs T_2 at H = 0 after deformation to τ = 1 and 2 Kg/mm^2.

CODE	CRYSTAL NO.	τ kg/mm^2
A	14	3
B	14	4

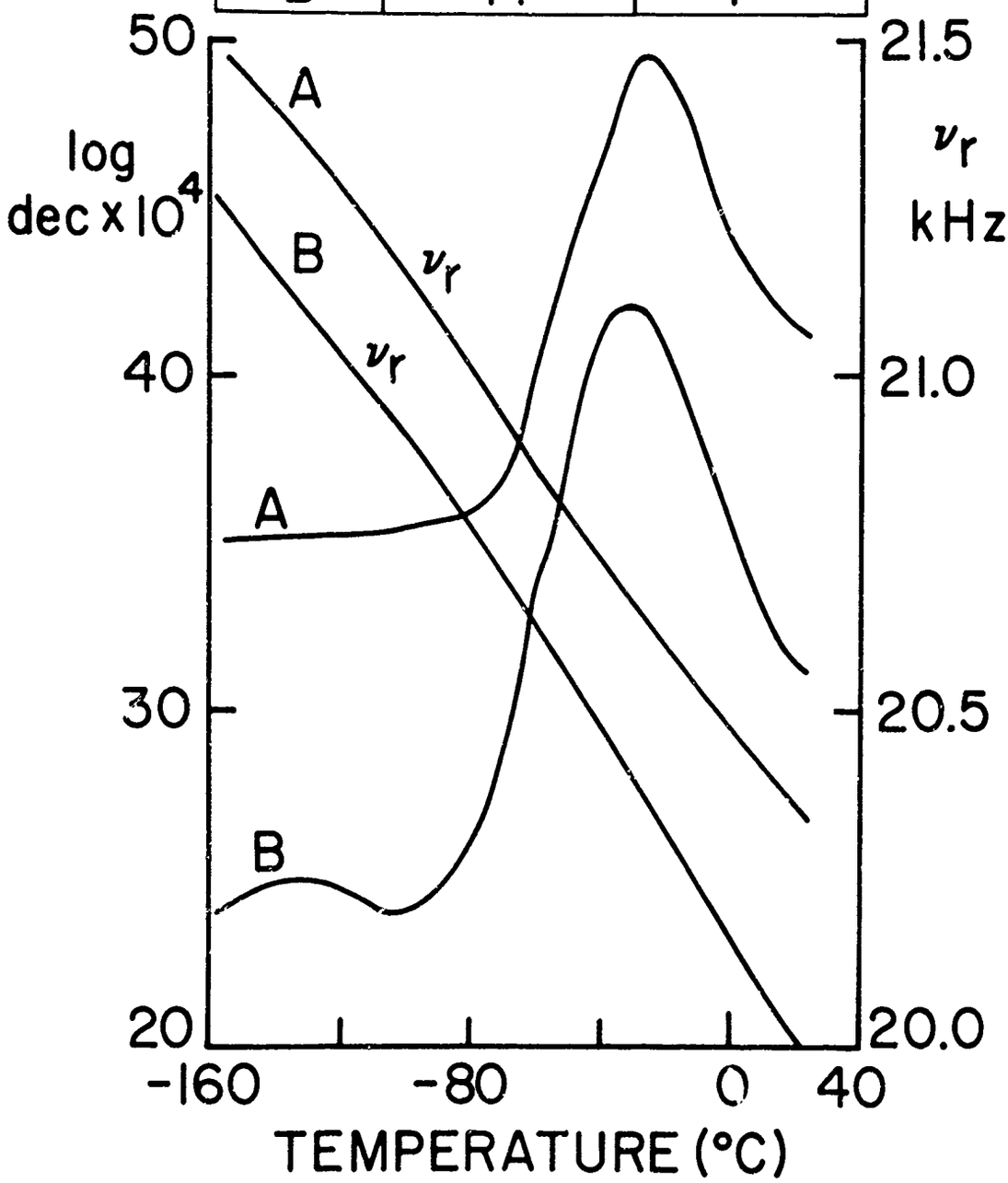

Fig. 32. Log.dec. and ν_r vs T_2 at H = 0 after deformation to τ = 3 and 4 Kg/mm^2.

CODE	CRYSTAL NO.	τ kg/mm^2
A	14	5
B	14	6

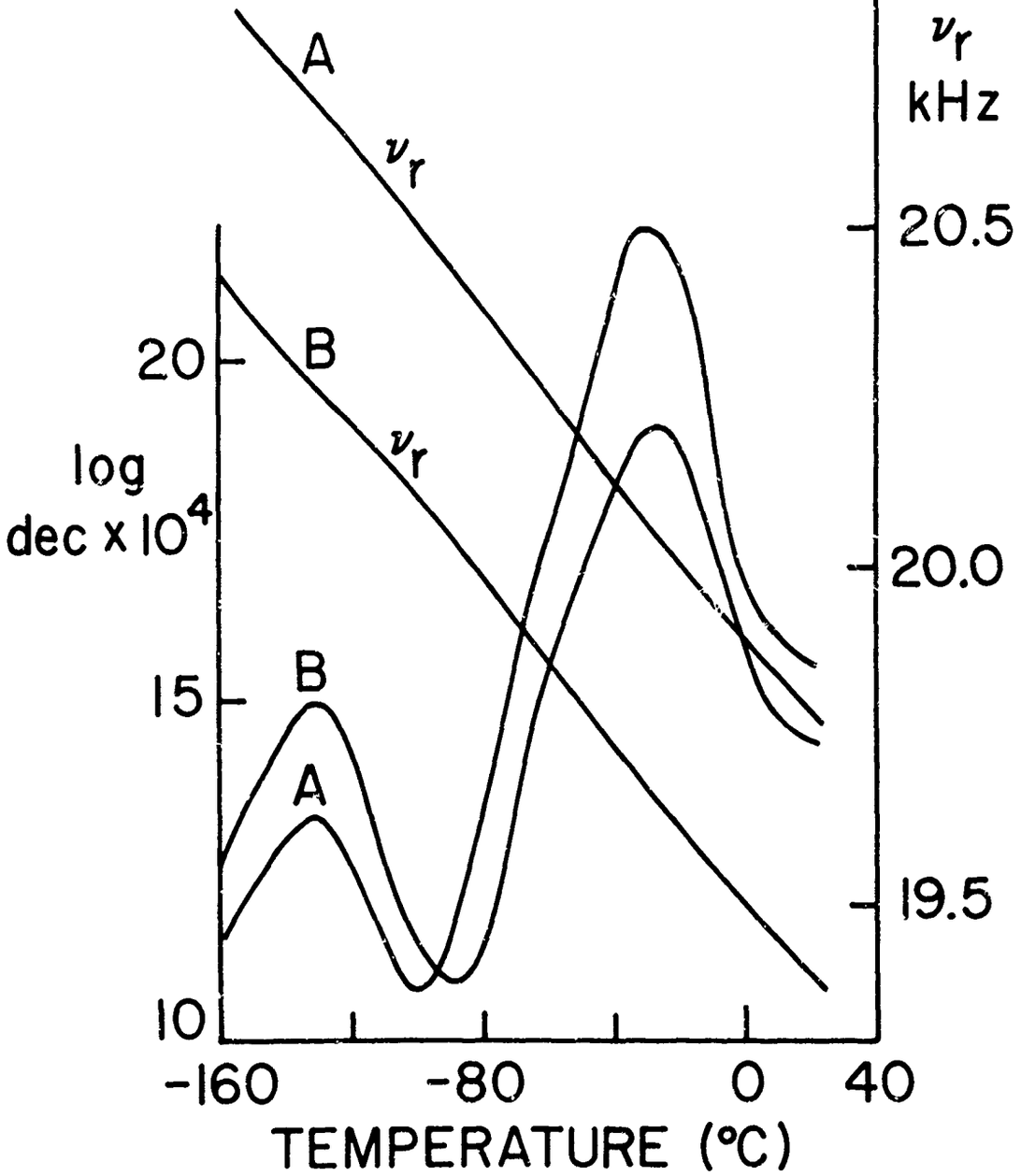

Fig. 33. Log.dec. and ν_r vs T_2 at H = 0 after deformation to τ = 5 and 6 Kg/mm^2.

E290-MS-2006-4

CODE	CRYSTAL NO.	τ kg/mm^2	ν_c
A	14	7	2.5
B	14	8	2
C	14	9	0

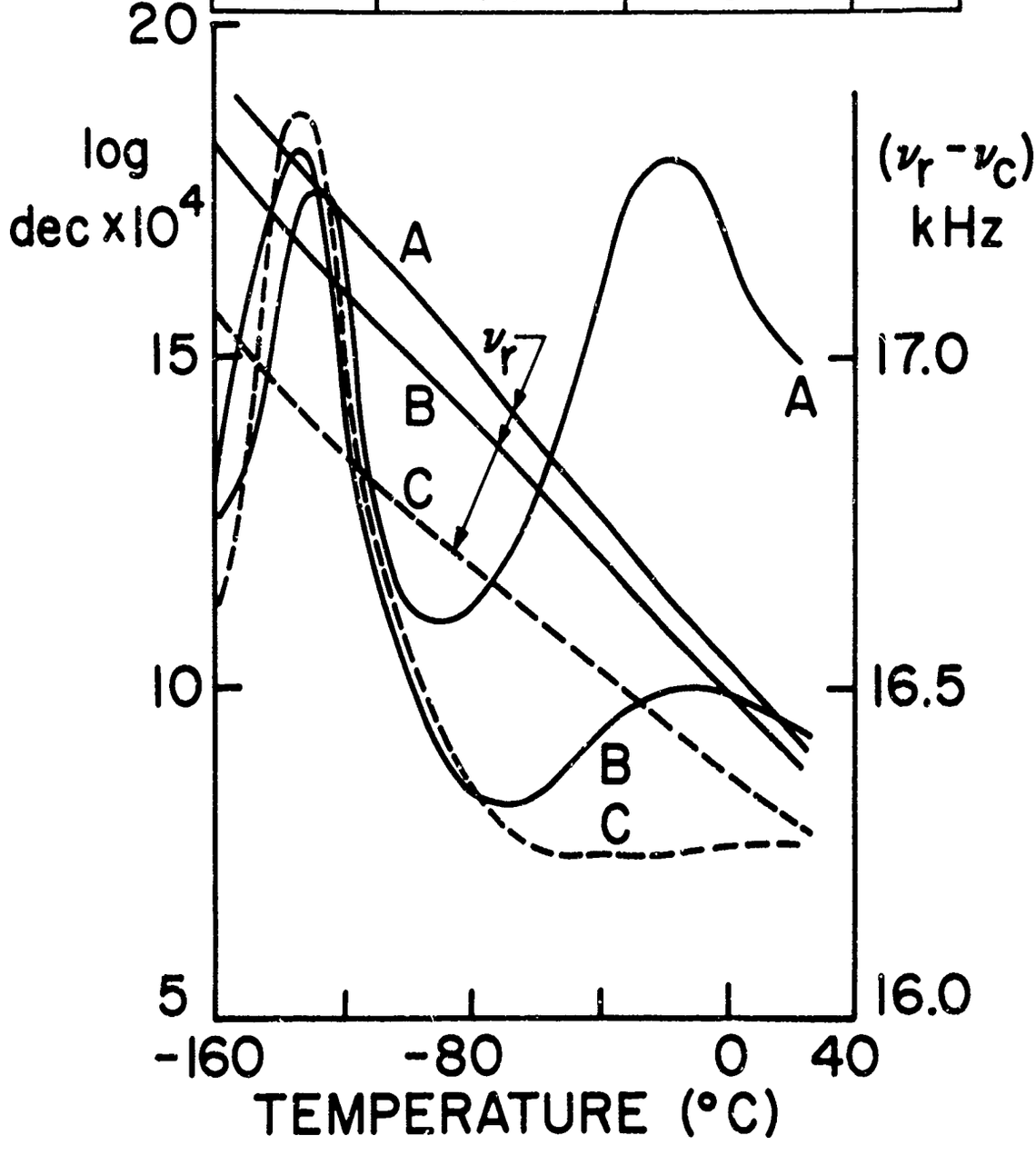

Fig. 34. Log.dec. and ν_r vs T at H = 0 after deformation to τ = 7, 8 and 9 Kg/mm^2.

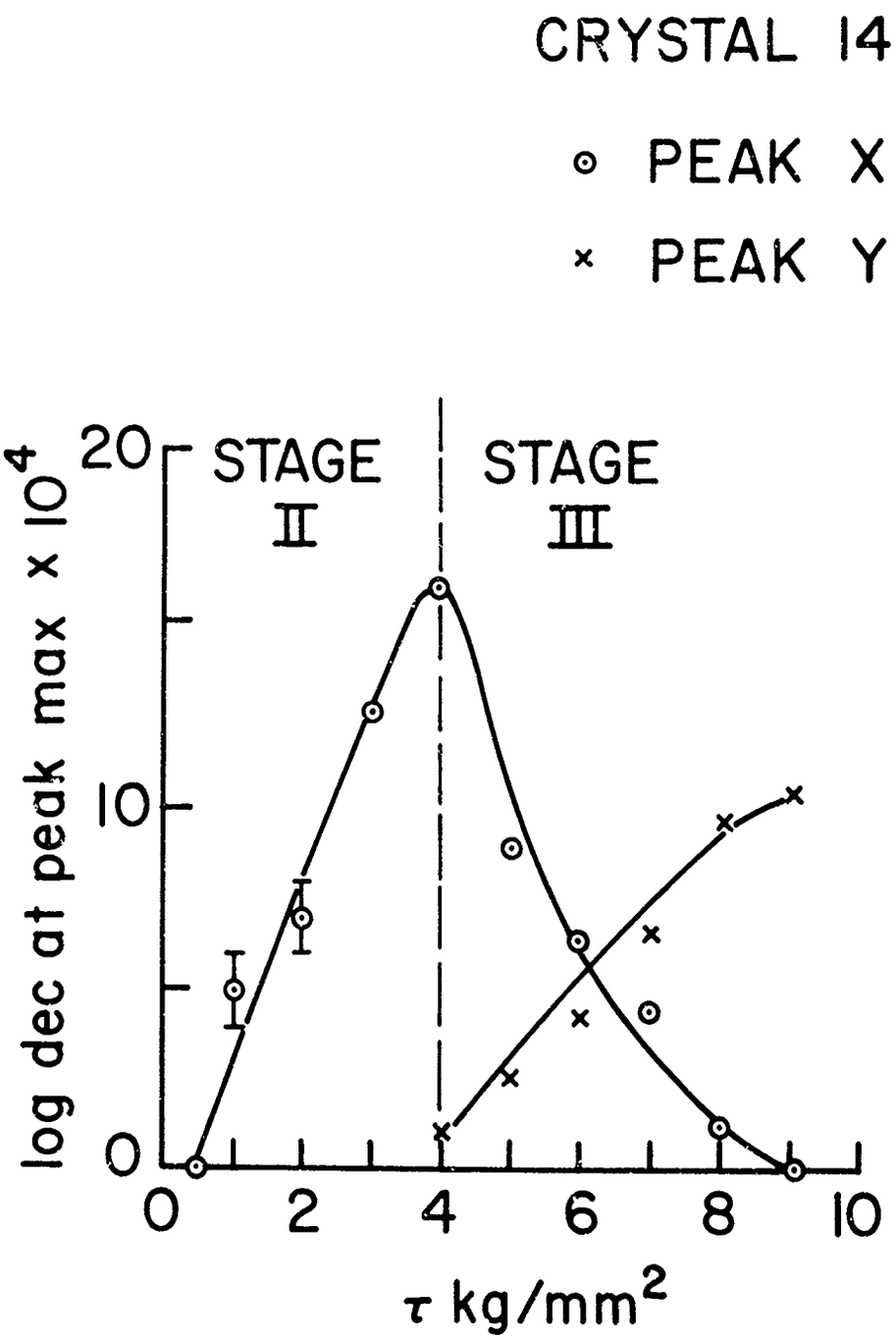

Fig. 35. Correlation of the heights of peaks X and Y with τ.

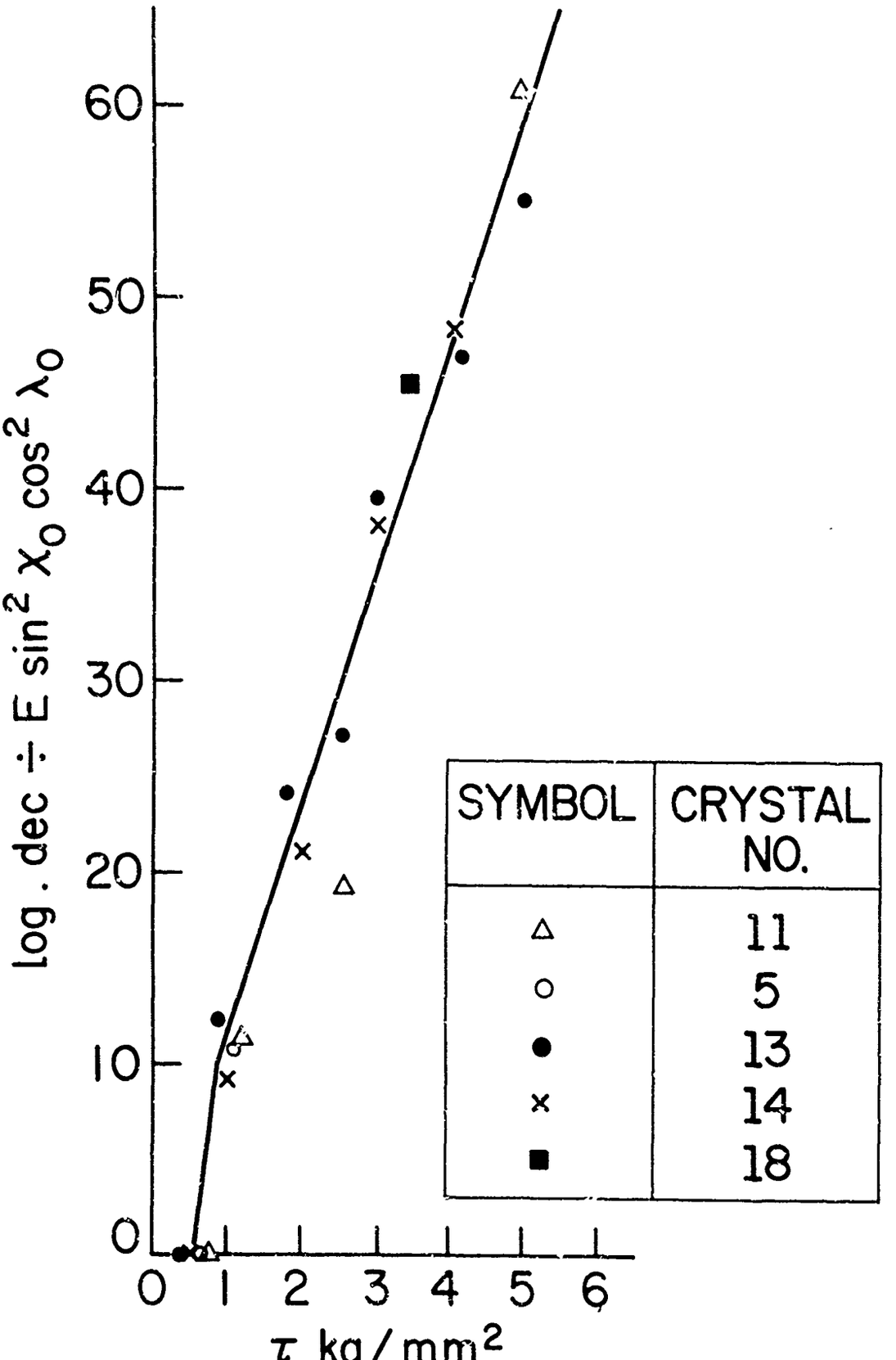

Fig. 36. Correlation of log.dec.÷ E $\sin^2 \chi_o \cos^2 \lambda_o$. with τ for stages of deformation I and II for crystals of different orientations.

UNCLASSIFIED

Security Classification

DOCUMENT CONTROL DATA - R&D

(Security classification of title, body of abstract and indexing annotation must be entered when the overall report is classified)

1. ORIGINATING ACTIVITY *(Corporate author)*

Columbia University

2a. REPORT SECURITY CLASSIFICATION

Unclassified

2b. GROUP

3. REPORT TITLE

Internal Friction Studies in Nickel Crystals from 77°K - 298°K.

4. DESCRIPTIVE NOTES *(Type of report and inclusive dates)*

Technical Report

5. AUTHOR(S) *(Last name, first name, initial)*

Venkatesan, Peruvemba S.

6. REPORT DATE	7a. TOTAL NO. OF PAGES	7b. NO. OF REFS
January 10, 1968	111.	79

8a. CONTRACT OR GRANT NO.	9a. ORIGINATOR'S REPORT NUMBER(S)
NONR 266(61)	Technical Report No. 9
b. PROJECT NO.	
c.	9b. OTHER REPORT NO(S) *(Any other numbers that may be assigned this report)*
d.	

10. AVAILABILITY/LIMITATION NOTICES

Distribution of this Document is unlimited.

11. SUPPLEMENTARY NOTES	12. SPONSORING MILITARY ACTIVITY
None	Office of Naval Research, Code 423 Washington, D.C. 20360

13. ABSTRACT

The internal friction spectrum in nickel single crystals has been studied near 20 kHz from 77°K to 298°K as a function of the stages of deformation, crystal orientation, temperature of deformation, magnetic field and state of annealing. Plastic deformation produces two major peaks centered at 230°K (peak X) and 130°K (peak Y). Peak X grows throughout stages I and II and falls in stage III. Peak Y occurs only in stage III. The height of peak X when plotted against the flow stress resolved on the primary glide system is approximately a straight line in each of stages I and II, with the slope in stage I probably higher than the slope in stage II. The variation in the height of peak X with crystal orientation is consistent with the hypothesis that dislocations in the primary glide system are responsible for it. Peak Y shows a different dependence, for which there is no immediate explanation. Isochronal annealing (1/2 hour) in steps of 100°C showed two recovery stages, one between 25°C and 100°C, and the other between 320°C and 430°C. Peak X is not removed till recrystallization and peak Y is removed between 320°C and 430°C.

DD FORM 1 JAN 64 1473

Security Classification

Security Classification

14. KEY WORDS	LINK A		LINK B		LINK C	
	ROLE	WT	ROLE	WT	ROLE	WT
Damping Internal Friction Nickel Deformed (cold-worked) Dislocation Motion Bordoni Peaks Peierls Stress						

INSTRUCTIONS

1. ORIGINATING ACTIVITY: Enter the name and address of the contractor, subcontractor, grantee, Department of Defense activity or other organization *(corporate author)* issuing the report.

2a. REPORT SECURITY CLASSIFICATION: Enter the overall security classification of the report. Indicate whether "Restricted Data" is included. Marking is to be in accordance with appropriate security regulations.

2b. GROUP: Automatic downgrading is specified in DoD Directive 5200.10 and Armed Forces Industrial Manual. Enter the group number. Also, when applicable, show that optional markings have been used for Group 3 and Group 4 as authorized.

3. REPORT TITLE: Enter the complete report title in all capital letters. Titles in all cases should be unclassified. If a meaningful title cannot be selected without classification, show title classification in all capitals in parenthesis immediately following the title.

4. DESCRIPTIVE NOTES: If appropriate, enter the type of report, e.g., interim, progress, summary, annual, or final. Give the inclusive dates when a specific reporting period is covered.

5. AUTHOR(S). Enter the name(s) of author(s) as shown on or in the report. Enter last name, first name, middle initial. If military, show rank and branch of service. The name of the principal author is an absolute minimum requirement.

6. REPORT DATE: Enter the date of the report as day, month, year, or month, year. If more than one date appears on the report, use date of publication.

7a. TOTAL NUMBER OF PAGES: The total page count should follow normal pagination procedures, i.e., enter the number of pages containing information.

7b. NUMBER OF REFERENCES: Enter the total number of references cited in the report.

8a CONTRACT OR GRANT NUMBER: If appropriate, enter the applicable number of the contract or grant under which the report was written.

8b, 8c, & 8d. PROJECT NUMBER: Enter the appropriate military department identification, such as project number, subproject number, system numbers, task number, etc.

9a. ORIGINATOR'S REPORT NUMBER(S): Enter the official report number by which the document will be identified and controlled by the originating activity. This number must be unique to this report.

9b. OTHER REPORT NUMBER(S). If the report has been assigned any other report numbers *(either by the originator or by the sponsor)*, also enter this number(s).

10. AVAILABILITY/LIMITATION NOTICES: Enter any limitations on further dissemination of the report, other than those imposed by security classification, using standard statements such as:

(1) "Qualified requesters may obtain copies of this report from DDC."

(2) "Foreign announcement and dissemination of this report by DDC is not authorized."

(3) "U. S. Government agencies may obtain copies of this report directly from DDC. Other qualified DDC users shall request through _____."

(4) "U. S. military agencies may obtain copies of this report directly from DDC. Other qualified users shall request through _____."

(5) "All distribution of this report is controlled. Qualified DDC users shall request through _____."

If the report has been furnished to the Office of Technical Services, Department of Commerce, for sale to the public, indicate this fact and enter the price, if known.

11. SUPPLEMENTARY NOTES: Use for additional explanatory notes.

12. SPONSORING MILITARY ACTIVITY: Enter the name of the departmental project office or laboratory sponsoring *(paying for)* the research and development. Include address.

13. ABSTRACT: Enter an abstract giving a brief and factual summary of the document indicative of the report, even though it may also appear elsewhere in the body of the technical report. If additional space is required, a continuation sheet shall be attached.

It is highly desirable that the abstract of classified reports be unclassified. Each paragraph of the abstract shall end with an indication of the military security classification of the information in the paragraph, represented as *(TS)*, *(S)*, *(C)*, or *(U)*.

There is no limitation on the length of the abstract. However, the suggested length is from 150 to 225 words.

14. KEY WORDS. Key words are technically meaningful terms or short phrases that characterize a report and may be used as index entries for cataloging the report. Key words must be selected so that no security classification is required. Identifiers, such as equipment model designation, trade name, military project code name, geographic location, may be used as key words but will be followed by an indication of technical context. The assignment of links, roles, and weights is optional.

DD FORM 1 JAN 64 1473 (BACK)

UNCLASSIFIED

Security Classification